

Magnetic fields of accreting pulsars

Dissertation

der Mathematisch-Naturwissenschaftlichen Fakultät
der Eberhard Karls Universität Tübingen
zur Erlangung des Grades eines
Doktors der Naturwissenschaften

vorgelegt von

Victor Doroshenko

aus Stavropol, Russland

Tübingen
2011

Tag der mündlichen Qualifikation: 24. Mai 2011
Dekan: Prof. Dr. Wolfgang Rosenstiel
1. Berichterstatter: Prof. Dr. Andrea Santangelo
2. Berichterstatter: Prof. Dr. Klaus Werner

Zusammenfassung

Akkretierende Pulsare sind rotierende Neutronensterne mit einem starken Magnetfeld, die sich in einem Doppelsternsystem befinden. Solche Systeme geben gepulste Röntgenstrahlung ab. Diese Emission wird durch die Gravitationsenergie gespeist, die freigesetzt wird, wenn Plasma von einem nicht entarteten Begleitstern durch das Magnetfeld auf die Pole des Neutronensterns geleitet wird. Das Plasma wird durch den Aufprall auf die Oberfläche des Neutronensterns oder in der sogenannten Akkretionssäule zu Röntgenstrahlung thermalisiert. Selbst vierzig Jahre nach der Entdeckung ist die Strahlungsemission von akkretierenden Pulsaren weiterhin rätselhaft. Eine der offenen Fragen ist das Magnetfeld der Neutronensterne in diesen Systemen an sich und wie man jenes messen kann.

Das Röntgenspektrum dieser Systeme ist gekennzeichnet durch ein Potenzgesetz mit einem Abbruch. Das Potenzgesetz wird als das Ergebnis aus der Comptonisierung der Bremsstrahlung und der Zyklotronstrahlung angesehen. Sowohl die Brems-, als auch die Zyklotronstrahlung entstehen durch das einfallende heiße Plasma in das hoch-magnetisierte Plasma in der Nähe der Polkappen. Die theoretische Beschreibung des Spektrums ist jedoch bei weitem noch nicht vollständig. Die Anwesenheit eines starken Magnetfeldes ($B \sim 10^{12} G$) beschränkt die Bewegung der Elektronen senkrecht zum Magnetfeld in Landau-Niveaus. Diese sind quantisierte Energiezustände in denen sich die Elektronen befinden können. Der Wirkungsquerschnitt der Compton-Streuung verändert sich dadurch, da dieser von dem Photonenimpuls und dem Magnetfeld abhängt. Diese Abhängigkeit zeigt sich in Zyklotronresonanzlinien (engl. cyclotron resonance scattering features, im folgenden CRSFs), welche als linienförmige Absorptionsmerkmale in einigen Spektren von Pulsaren beobachtet werden. Die Schwerpunktsenergie dieser Linien steht über $E_{cyc} [keV] \approx 11.57 \times 10^{-12} B G$ in direkter Beziehung zu dem Magnetfeld im Entstehungsbereich der Linien. Diese Relation bietet die Möglichkeit das Magnetfeld des Neutronensterns direkt zu bestimmen.

Die temporalen Eigenschaften von Neutronensternen, speziell die Änderung der Spinpuls Frequenz, dienen ebenfalls zur Abschätzung des Magnetfeldes. Da Neu-

tronensterne sehr kompakte Objekte mit einem geringen intrinsischen Trägheitsmoment sind, wird der Spin komplett von den äußeren Drehmomenten beherrscht. Diese hängen von der Wechselwirkung zwischen der, von dem Magnetfeld bestimmten, Magnetosphäre und der akkretierten Materie ab. Die Studie dieser Drehmomente und der Spinentwicklung kann daher ebenfalls eine Abschätzung des Magnetfeldes liefern. In dieser Arbeit wird die Rolle der Drehmomente bei der Spinentwicklung für eine Auswahl von langsam rotierenden Pulsaren untersucht. Desweiteren werden die Rückschlüsse betrachtet, die man aus der Theorie der Drehmomente auf die Magnetfelder ziehen kann.

Ich stelle eine detaillierte Studie des spektralen und zeitlichen Verhaltens dreier langsam rotierender, akkretierender Pulsare vor. Namentlich sind dies 1A 1118-61, GX 301-2 und Vela X-1.

Basierend auf RXTE Daten gehe ich zuerst auf die Entdeckung einer Zyklotronresonanzlinie im Spektrum von 1A 1118-61 ein. Ebenfalls führe ich eine genaue Betrachtung der temporalen Parameter von 1A 1118-61 durch und zeige eine Möglichkeit auf um die bisher unbekannte Umlaufdauer dieses Systems zu bestimmen.

Darauf folgend präsentiere ich die Analyse der Beobachtungen der bekannten High Mass X-ray Binaries GX 301-2 und Vela X-1, die mit INTEGRAL und RXTE durchgeführt wurden. Da die Beobachtungen eine gute Statistik bieten, können die bekannten spektralen Eigenschaften (inklusive einer Beobachtung von CRSFs) der Quellen bestätigt werden. Desweiteren berichte ich von der Entdeckung, basierend auf Suzaku Daten, gepulster Röntgenstrahlung im “off-state” von Vela X-1. Dies ist ein überraschendes Ergebnis, da bisher angenommen wurde, dass die Röntgenstrahlung im “off-state” komplett unterdrückt wird. Ich diskutiere diese Resultate im Zusammenhang mit aktuellen Theorien der “gated” Akkretion.

Anschließend lege ich das Hauptaugenmerk auf die zentrale Frage dieser Arbeit, wie die temporalen Eigenschaften von GX 301-2 und Vela X-1 möglicherweise helfen, den Einfluss der Drehmomente auf den Neutronstern einzugrenzen und eine Abschätzung für das Magnetfeld des Neutronensterns zu liefern. Die Vorhersagen von mehreren bestehenden Modellen des Drehmoments für die Spinentwicklung dieser Quellen werden mit Beobachtungen von CGRO BATSE verglichen. Zum ersten Mal kann eine Korrelation zwischen der Ableitung der Spinfrequenz und der Akkretionsrate gezeigt werden, die in allen Modellen vorausgesagt wird. Mit Hilfe dieser Korrelation können wir eine gesicherte untere Grenze $B \geq 10^{13}$ G für die Magnetfeldstärke der Neutronensterne in GX 301-2 und Vela X-1 angeben. Dieses Ergebnis widersprechen den Abschätzungen des Magnetfeldes, die mit den Energien der CRSFs der Quellen gemacht wurden.

Dieser Widerspruch bringt erneut das alte Probleme der Existenz von leuchtkräftigen lang-periodischen akkretierenden Pulsaren mit moderatem Magnetfeld ins Spiel. Möglichkeiten diese Widersprüche in Einklang zu bringen werden diskutiert.

Zuerst zeige ich die Möglichkeit auf, dass CRSFs hoch oberhalb des Neutronsterns in der Akkretionssäule oder in dem Akkretionsstrom oberhalb der Polkappen entstehen, in einem Bereich, in dem sich das Magnetfeld erheblich abschwächt. Zusätzlich überprüfe ich kritisch mögliche Abwandlungen bestehender Theorien der Drehmomente und folgere auf Grund von grundlegenden Erhaltungsargumenten, dass man durch die Verwendung gängiger Drehmoment-Modelle möglicherweise die Magnetfeldstärke nur unwesentlich zu hoch ansetzt. Schließlich diskutiere ich wie die Ergebnisse für GX 301–2 und Vela X-1 zusätzlich bestätigt werden können und warum ähnliche Überlegungen auch auf andere akkretierende Pulsare angewendet werden könnten.

Abstract

Accreting pulsars are rotating, highly magnetized neutron stars in binary systems which emit pulsed X-rays. This emission is powered by the gravitational energy of the plasma accreted from a non degenerate companion funneled onto the polar caps of the neutron star by the magnetic field, and thermalized to X-rays either in the impact with the surface of the neutron star, or in the so-called accretion column. Although discovered more than forty years ago many aspects of the emission from accreting pulsars remain puzzling. One of the key open issues is the magnetic field of the neutron stars in these systems and how we can measure it.

The X-ray spectrum of these systems is characterized by a cut-off power-law, interpreted as the result of the comptonization of the bremsstrahlung and cyclotron emission produced in the highly magnetized accreted plasma in the vicinity of the polar caps by the hot in-falling plasma. The theoretical description of the spectra is, however, far from complete. The presence of a strong magnetic field ($B \sim 10^{12}$ G) constrains and quantizes the motion of the electrons perpendicularly to the field in the Landau levels, thus modifying the cross-section for Compton scatterings. The scattering cross-section strongly depends on the photon momentum and the magnetic field which manifests as the so-called cyclotron resonance scattering features (CRSFs), observed as line-like absorption features in the spectra of some pulsars. The centroid energy of these features is directly related to the magnetic field in the line-forming region via $E_{\text{cyc}}[\text{keV}] \simeq 11.57 \times 10^{-12} B \text{ G}$, providing a way to directly measure the magnetic field of a neutron star.

The timing properties of a neutron star, and more specifically the changes of the pulse spin frequency, can be also used to estimate its magnetic field. Neutron stars are very compact objects with a low intrinsic moment of inertia and therefore their spin is completely governed by the external torques. These torques depend on the interaction between the magnetosphere, determined by the strength of the field, and the accreted matter. Therefore the study of these torques and the spin history can provide an estimate of the magnetic field.

In this thesis the role of these torques in the spin history of a sample of slow-

rotating pulsars and the magnetic fields inferred from the torque theory has been studied.

More specifically, I present a detailed study of the spectral and timing behavior of three slow-rotating accreting pulsars, namely 1A 1118-61, GX 301-2 and Vela X-1.

Based on *RXTE* data, I first report on the discovery of a cyclotron scattering feature in the spectrum of 1A 1118-61. I also perform a detailed study of the timing parameters of 1A 1118-61 and suggest a possible measurement of the previously unknown orbital period of the source.

Using the data from *INTEGRAL* and *RXTE*, I present an analysis of the well known High Mass X-ray Binaries GX 301-2 and Vela X-1 confirming with high statistics the already known spectral properties (including the observation of CRSFs) of the sources. Based on *Suzaku* data, I then report on the discovery of pulsed emission in the “off-states” of Vela X-1. This was a surprising result considering that until now it was thought that the X-ray emission was totally suppressed in the “off-states”. I discuss these findings in the context of recent theories for “gated” accretion.

I then focus on the central question of this work, i.e. on how the timing properties of GX 301-2 and Vela X-1 may help to constrain the torques affecting the neutron star and to estimate its magnetic field. The predictions of several existing torque models on the spin history of the sources are compared with *CGRO BATSE* observations. These observations reveal, for the first time, a correlation between the pulse frequency derivative and the accretion rate, as predicted in all torque models. Using this correlation, we can put a strong lower limit $B \geq 10^{13}$ G on the magnetic field strength of the neutron stars in Vela X-1 and GX 301-2.

This result contradicts the estimates of the magnetic field obtained from the observed energies of the CRSFs in these sources, which once again brings onto the stage the long-standing problem of the existence of luminous long-periodic accreting pulsars with moderate magnetic field. Possible ways to reconcile this contradiction are discussed.

First I suggest that CRSFs may form high above the neutron star in the accretion column or the accretion stream above the polar caps where the magnetic field considerably weakens. Second, I critically revise possible modifications of the existing torque theory and from basic conservation arguments conclude that the magnetic field obtained on the basis of current torque models is probably not significantly overestimated. Finally I discuss how the result on GX 301-2 and Vela X-1 can be further verified, and why similar considerations might apply to other accreting pulsars.

Contents

Zusammenfassung	3
Abstract	6
I Introduction and thesis outline	13
1 X-ray binaries	17
1.0.1 Stellar evolution of single stars	18
1.0.2 Stellar evolution of stars in binaries	19
1.1 Phenomenology and Classification	20
1.1.1 Classification	20
1.1.2 Accretion processes	23
1.2 Accretion powered pulsars	24
2 Magnetic fields of neutron stars	31
2.1 Rotation powered neutron stars	31
2.1.1 Radio pulsars	31
2.1.2 Magnetars	33
2.2 Accretion powered pulsars	36
2.2.1 Accretion torques	37
2.2.2 Cyclotron Resonance Scattering Feature (CRSF)	40
3 Instrumentation	47
3.1 Rossi X-Ray Timing Explorer	47
3.1.1 Overview	47
3.1.2 PCA: proportional counter array	48
3.1.3 HEXTE: High Energy X-ray Timing Experiment	50
3.2 International Gamma-Ray Astrophysics Laboratory	50
3.2.1 Overview	50
3.2.2 IBIS	51

3.2.3	SPI	53
3.2.4	JEM-X	53
3.3	Compton Gamma-Ray Observatory	55
3.4	Suzaku (ASTRO-EII)	56
3.4.1	Overview	56
3.4.2	X-ray Imaging spectrometer (XIS)	58
3.4.3	Hard X-ray detector (HXD)	58
 II Observational study of a sample of galactic HMXBs		61
4	1A 1118–61	63
4.1	Introduction	63
4.2	Observations	64
4.3	Results	65
4.3.1	Timing analysis	65
4.3.2	A hint on orbital period from timing	67
4.3.3	Spectral analysis	71
4.4	Conclusions	73
5	GX 301–2	75
5.1	Introduction	75
5.2	Observations and data selection	77
5.3	Results	77
5.3.1	Timing analysis	77
5.3.2	Spectral analysis	80
5.4	Discussion	83
5.4.1	Orbital period evolution	83
5.4.2	Torque balance and magnetic moment of the neutron star	85
5.5	Conclusions	91
6	Vela X-1	92
6.1	Introduction	92
6.2	The torque models and the data	92
6.3	Discussion	95
6.3.1	Other evidence for a strong magnetic field	97
6.3.2	Observation of the “off-states” with <i>Suzaku</i>	100
6.4	Interpretation and discussion	103
6.5	The “off-states” in GX 301–2	106
6.6	Conclusion	107

III Problems and prospects	113
7 The magnetic field and the CRSF energy	115
8 Generalizing the torque model	124
9 Summary and outlook	129
Bibliography	135
Acknowledgements	141
Curriculum vitae (Lebenslauf)	142
List of publications (Publikationsliste)	143

Part I

Introduction and thesis outline

Since their discovery, neutron stars have been understood to be strongly magnetized objects. In fact, if the magnetic moment of a typical progenitor with $B \sim 1 - 100$ G is conserved during the collapse, the magnetic field of a new born neutron star is expected to be $B \sim 10^{12}$ G.

This thesis focuses on estimation of the magnetic field strengths of one class of neutron star systems, the accretion-powered pulsars. These are neutron stars in binary systems luminous in X-rays and powered by gravitational energy. In these systems, the plasma accreted from a non-degenerate companion is funneled by the strong magnetic field onto the polar caps of the neutron star where the energy is thermalized mainly in X-rays. The observed pulsations require that a strong magnetic field, misaligned with respect to the rotation axis, overcomes the enormous drag of the gravitational field.

In accreting X-ray binary pulsars the long term timing behavior of the neutron star, in particular the pulse frequency change, is a result of the complex interplay between mainly two physical components: the angular momentum transfer from the non degenerate companion, determined by how the accretion process proceeds; and the braking torques, which depend on the size of the magnetosphere and therefore on the strength of the field.

In my research work I try to provide an answer to an old question, “which is the magnetic field of accreting pulsars characterized by a slow rotational spin frequency?” To answer this question I have analyzed in detail the timing and spectral properties of two well known and studied accreting X-ray pulsars: GX 301–2 and Vela X-1. This proved to be a very interesting journey which forced me to address the details of the accretion processes in accreting pulsars, the ways matter can leak through the magnetosphere, the morphology of the accretion structures close to the polar caps of the neutron stars, the emission from these accretion structures, and eventually the meaning of the so called cyclotron resonance scattering features observed in the spectra of accreting pulsars which are universally considered the standard probe for the estimate of the magnetic field. The first step of the journey that is this thesis concludes with a key question, “are the high magnetic field neutron stars with magnetar-like star magnetic fields of $B \sim 10^{13} - 10^{14}$ G hosted in GX 301–2 and Vela X-1?”

In Chapter 1 I summarize the origin and the emission mechanisms of neutron star systems, discussing X-ray binaries in greater detail. I then review the distinctions between the rotation and accretion powered neutron stars in Chapter 2, giving emphasis on to how we estimate the magnetic fields of these systems.

In Chapter 3 I give an overview of the missions whose data I used in the observational part of my thesis, namely *Rossi X-ray Timing Explorer (RXTE)*, *International Gamma-Ray Laboratory (INTEGRAL)*, *Suzaku* and the *Compton Gamma-Ray Observatory (CGRO)*.

In the second part of my thesis I discuss the observational findings I have obtained on the three systems studied: 1A 1118–61, GX 301-2 and Vela X-1. This part is largely based on the papers published or submitted during my doctoral project. In Chapter 4 I report on the *RXTE* observations and on the discovery of a Cyclotron Resonance Scattering Feature in the Jan 2009 outburst of the X-ray binary 1A 1118–61 (Doroshenko et al. 2010b). In Chapter 5, I present an extended study of the High Mass X-ray Binary (HMXB) GX 301–2 with *INTEGRAL* and *BATSE* (Doroshenko et al. 2010a). Finally, in Chapter 6, I discuss some observational properties of the HMXB Vela X-1, particularly during the so-called “off-states”. I present an unprecedented study of several “off-states” found in a long *Suzaku* observation of Vela X-1, where the source, contrary to expectations, was found to pulsate and where we were able to study the spectral properties for the first time. These results are being presented in Doroshenko et al. (2011b) and Doroshenko et al. (2011a).

The interpretation of the observed properties of GX 301–2 and Vela X-1 led me to the intriguing conclusion that the neutron stars in these systems must have a very strong magnetic fields ($B \sim 10^{13} - 10^{14}$ G). This is an order of magnitude stronger than the field estimated from the energy of the cyclotron lines observed in these systems. I therefore devoted part of my work to explain this inconsistencies.

In Chapter 7, I try to explain qualitatively how the observed cyclotron lines with energy of 20-50 keV may form in X-ray pulsars with surface magnetic field of $B \sim 10^{14}$ G.

In Chapter 8, I attempt to reconcile the observed cyclotron line energy and the magnetic field estimated with the accretion torque models by deeply exploring torque theory. In the last Chapter I describe the possible future steps of my investigation.

CHAPTER 1

X-ray binaries

A significant fraction of known stars are members of so-called “binary” or “multiple” stellar systems (Tokovinin 1997). Members of a binary system are gravitationally bound and rotate around a common center of mass just like the planets in the Solar system rotate around the Sun. The more massive star of the binary system is usually called the *primary* while the less massive is referred to as the *secondary*. X-ray binaries (XRBs) are simply binary systems luminous in X-rays with X-ray luminosity $\sim 10^{32} - 10^{40} \text{ergs s}^{-1}$. When speaking of X-ray binaries one typically refers to systems in which a compact object, a black hole, a neutron star or a white dwarf (Lipunov 1987), rotates around a normal star. Ordinary stars are dim in X-rays (up to $\sim 10^{32} \text{ergs s}^{-1}$ Güdel 2004). The X-ray emission of these systems is powered by the *accretion of matter* from the normal onto the degenerate component.

The compact objects in X-ray binaries are the final stages in evolution of normal stars. Stars are believed to form from the initially homogenous gas of the interstellar medium which condense into more compact clouds due to Rayleigh-Taylor instabilities. If a gas cloud is sufficiently cold to satisfy the Jeans criterion

$$M \geq M_J \propto T^{3/2} n^{-1/2} \sim 10^3 M_\odot \quad (1.1)$$

it will eventually collapse and form a star or a star system depending on the initial angular momentum. Here T is the gas temperature and n is the number density of particles in the cloud.

The subsequent evolution of the star is defined by the initial cloud mass, its chemical composition and the angular momentum (Schwarzschild 1958). In binary/multiple systems the evolution of each companion is also strongly affected by the exchange of mass and angular momentum between the system members. In the next section I will give a very brief and mainly qualitative overview of the evolution of an isolated star showing how it differs from the evolution of stars in a binary system.

1.0.1 Stellar evolution of single stars

Stellar evolution is the change of physical properties, chemical composition and internal structure of stars with time (Clayton 1968). These changes are driven by the loss of energy of the star as it evolves. The star is basically a self-gravitating ball of hot plasma where the pressure of the plasma is balanced by gravity. The most striking feature of such a system is that it has negative heat-capacity. The loss of energy leads to contraction and heating of the star. Indeed, according to the virial theorem the average potential energy must be twice the average kinetic energy ($U_p = -2U_k$) and the total energy ($U = U_p + U_k = -U_k$) decreases due to the radiative losses, while the average kinetic energy, and hence the temperature, increases.

This is the essential feature for the formation and evolution of the star. As the primordial gas clouds contract, the temperature and density in the core increase until the hydrogen starts fusing into helium. At this point the protostar becomes a star and the equilibrium between the internal gas pressure and the gravity is reached. This is the so-called Main Sequence (MS) stage. The main sequence is a continuous and distinctive band that appears on plots of stellar color versus brightness, also called Hertzsprung–Russell diagrams (Hertzsprung 1911). In the MS stage the star burns hydrogen into helium slowly radiating the energy away and contracting until all hydrogen in the core of the star is consumed. Since the star consists mostly of hydrogen, the MS stage is where the star spends most of its life. The lifetime on the MS is determined by the *nuclear* timescale (Lipunov 1987)

$$\tau_n \simeq \frac{0.1M\epsilon}{L} \simeq 10^{10} \frac{M}{M_\odot} \frac{L_\odot}{L} \text{ yr}, \quad (1.2)$$

where M and L are the mass and luminosity of the star respectively, and $\epsilon \sim 7 \times 10^{-3} c^2$ (Lipunov 1987). This timescale is set by the ratio between the total amount of available nuclear energy and the rate of energy loss (i.e. the luminosity). The total amount of energy is proportional to the fraction of mass available for fusion ($\sim 10\%$ in the case of hydrogen burning) of the total mass of the star.

As the hydrogen in the core runs out, the rate of energy release and the pressure decrease and the core starts to contract. The temperature and the density in the core increase and eventually reach values sufficiently high to trigger the fusion of helium into carbon and oxygen. The hydrogen continues to burn in the outer layers of the star providing sufficient energy to balance the gravitational forces. The excess of energy supplied by the core leads to the expansion of the outer layers. At this stage the star leaves the MS and moves towards the giant (red giant or supergiant) branch.

This happens on a much shorter *thermal* timescale:

$$\tau_t \simeq \frac{GM^2}{RL} \simeq 3 \times 10^7 \left(\frac{M}{M_\odot} \right)^2 \frac{R_\odot}{R} \frac{L_\odot}{L} \text{ yr}, \quad (1.3)$$

Here R is the radius of the star and G is the gravitational constant.

Cycles of nuclear burning and gravitational contraction continue providing that the mass of the star (and hence temperature and density in the stellar core) is sufficient each time to start the next fusion cycle. If the stellar mass exceeds $\sim 10M_\odot$ this cycle continues until the core consists mainly of iron and further fusion provides no energy (Lipunov 1987). Depending on the mass and metallicity of the progenitor, the core will collapse into a black-hole or a neutron star through the spectacular *supernova* explosion.

In a less massive star the pressure of degenerate electrons may be sufficient to prevent further contraction at one of the burning stages. In this case the outer layers continue to burn until the bare core remains. The core gradually cools, leaving a degenerate *white dwarf*.

The final product of the stellar evolution is, therefore, a compact object unless the star is completely destroyed in a type Ia supernova explosion (Hillebrandt & Niemeyer 2000) or has insufficient mass to start fusion at all. The nuclear timescale in this case may exceed the age of the universe as in the case of *brown-dwarfs*. The type of remnant compact object mainly depends on the initial mass and chemical composition of the progenitor star (Lewin et al. 1995). Stars with initial mass $\lesssim 11M_\odot$ form white dwarfs (final mass $\leq 1.4M_\odot$) while stars with mass $\lesssim 40M_\odot$ form neutron stars (final mass $\sim 1.4 - 3M_\odot$ depending on the assumed equation of state of the neutron star). If the mass of compact remnant exceeds $\sim 3M_\odot$ (the Oppenheimer-Volkoff limit, Oppenheimer & Volkoff 1939) a black-hole will form. This may happen for instance if the progenitor star is very massive ($\sim 40M_\odot$, van den Heuvel & Habets 1984). Note that these boundaries are only approximate as there remains much uncertainty in stellar evolution, especially for massive stars.

1.0.2 Stellar evolution of stars in binaries

The transfer of mass, tidal interactions, angular momentum and heat transfer complicate the stellar evolution process in binary systems. However the main outcome is basically the same: one or two compact objects, possibly gravitationally bound, remain as end stage of the binary system evolution.

Mass transfer in a binary system may occur either via stellar winds or via the so-called Roche-Lobe overflow through the *Lagrangian* points. Each star is still a self-gravitating body but the gravitational influence of the other component, in particular the centripetal forces generated by the spin of the star and its orbital

motion, must also be taken into account. In the *Roche* approximation (Hilditch 2001) the gravitational field can be approximated as that of two co-orbiting point masses M_1 and M_2 corresponding to the masses of the stars and located at their centers. In the reference frame co-rotating with the binary revolution the *Roche* potential is given by

$$\Phi = -\frac{GM_1}{r_1} - \frac{GM_2}{r_2} - \frac{\omega^2 r_3^2}{2}, \quad (1.4)$$

where r_1 and r_2 are the distances to the center of the stars, ω is the orbital angular velocity and r_3 is the distance to the axis of rotation of the binary (Fig. 1.1). In this approximation several equipotential surfaces exist that intersect themselves in the so-called *Lagrangian* points. The matter can flow freely through these points since the gravitational and the centripetal forces cancel here. The equipotential with critical point (usually called L_1) between the two stars forms a two lobed figure with one of the stars at the center of each lobe (usually called the *Roche* lobe).

If at some stage of the evolution one of the stars fills its *Roche* lobe (solid eight-shaped line Fig. 1.1), the matter will flow onto the companion at a significant rate on a thermal timescale. This obviously affects the evolution of the companion and, for instance, may lead to ignition of previously non burning material. It also affects the orbital separation: typically the more massive star fills the *Roche* lobe first which leads to a decrease of the orbital separation and hence the orbital period. Eventually the stars may merge due to this process.

Several mass transfer episodes may take place during the evolution of a binary system with different evolutionary paths depending on the system parameters (van den Heuvel & Habets 1984). An example of such a path is summarized for a massive system in Figure 1.2.

1.1 Phenomenology and Classification

1.1.1 Classification

X-ray binaries are usually classified by the nature of the compact object and/or by the donor star type. The compact object may be a neutron star (Neutron Star X-ray Binaries, NS-XRBs), a black hole (Black Hole X-ray Binaries, BH-XRBs or BHBs) or an accreting white dwarf (Cataclysmic Variables, CVs). The type of the donor star is usually defined by its mass. In Low Mass X-ray Binaries (LMXBs) the donor companion, a late-type star of spectral type A or later or a white dwarf has a mass of $M \leq 1.2M_\odot$, whereas in High Mass X-ray Binaries (HMXBs) the donor is an early type (O,B) star with mass $M \geq 10M_\odot$ (Levine et al. 1996). We observe that this classification usually applies only to NS-XRBs and BHBs.

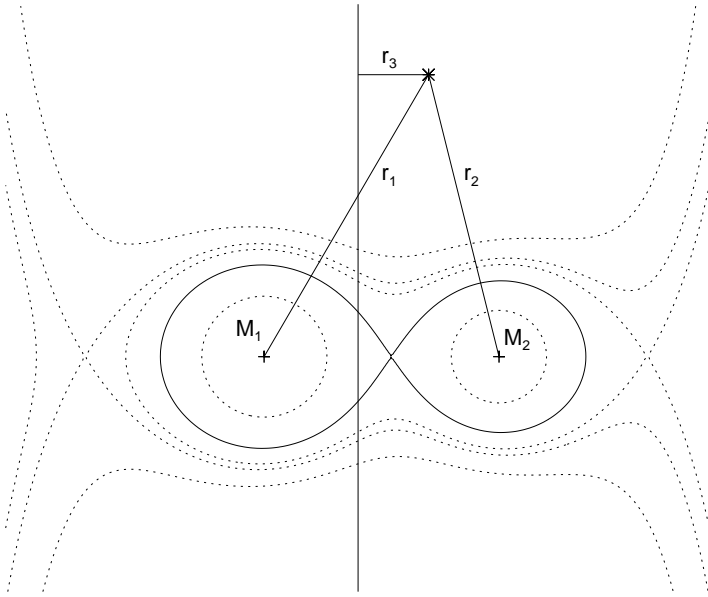


Figure 1.1: Equipotential lines of the *Roche* potential in a co-rotating frame parallel to the rotational axis, indicated with the vertical line. Note self-intersections of equipotential lines which correspond to Lagrangian points. Image credit: D. Klochkov

Since the nuclear timescale, which determines how fast a normal star evolves, is much longer for low-mass stars than for high-mass stars (see equation 1.2), LMXBs are typically very old systems (evolution timescale is Gyrs) belonging to the galactic bulge population while the HMXBs are young and are typically associated with star-formation regions in the galactic disk (see Figure 1.3 and Grimm et al. 2003). The difference in age has two important consequences. First, the highly luminous early type donor stars of HMXBs have powerful stellar winds that can sustain accretion. This is not the case for old systems where the mass transfer can only occur via Roche lobe overflow and the accretion always proceeds from a disk (Hilditch 2001).

Second, if the compact object of the old LMXRB system is a neutron star, one expects it to have a relatively low magnetic field since there has been enough time for the field to decay. One does not expect therefore to generally observe X-ray pulsations. Indeed most LMXBs usually do not exhibit pulsations. However this is by far an over-simplification. The observed phenomenology of LMXBs is very rich

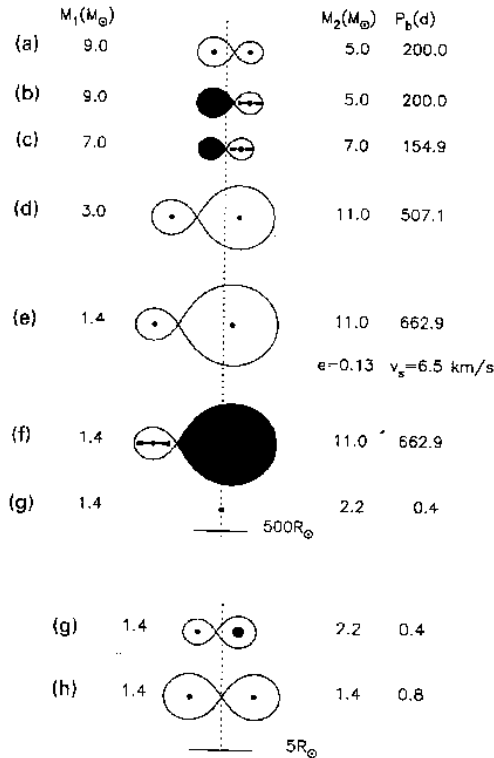


Figure 1.2: Evolution of a massive binary system in the case of conservative mass transfer. The more massive component evolves first and a first mass transfer episode takes place in (b). Both stars continue to evolve (d) and eventually the more evolved component forms a neutron star in an eccentric orbit after a supernova explosion event (e). As the second star continues to evolve a second mass transfer episode takes place making the neutron star appear as a bright X-ray pulsar (f). The mass transfer stops at some point possibly shutting the X-ray pulsar down (g) and finally a second supernova explosion takes place disrupting the system and leaving two isolated neutron stars (possibly observed as radio pulsars). Figure after van den Heuvel & Habets (1984)

and is determined mainly by geometry of the system, its orientation with respect to observer and the accretion rate. Most interesting observational features of binaries in this class include thermonuclear bursts, quasi-periodic oscillations in the KHz regime, pulsed emission during outbursts and relativistic iron lines formed in the

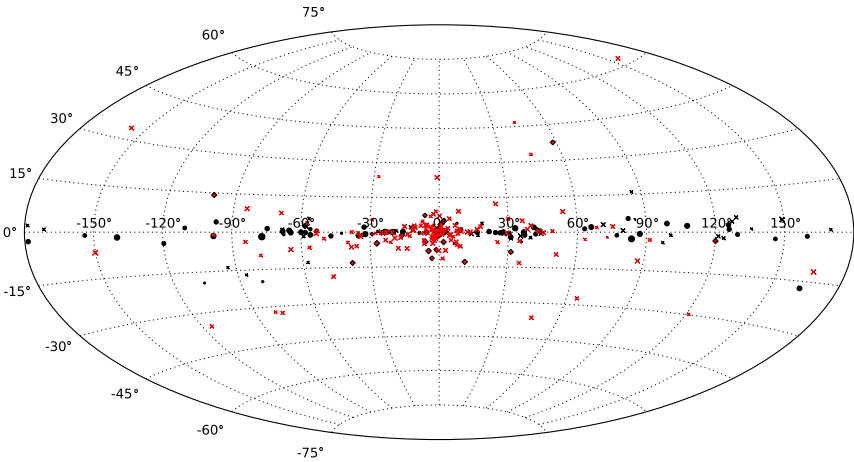


Figure 1.3: Distribution of X-ray binaries in galaxy in galactic coordinates. Black and red dots show pulsating HMXBs and LMXBs, crosses show non pulsating HMXBs and LMXBs. Note that most LMXBs are not pulsating. Symbol size represents average X-ray flux (2-10 keV) from the source. Figure based on catalogue data from Liu et al. (2006, 2007).

boundary layer close to the surface of the neutron stars. It is widely discussed in literature how all these phenomena if combined could allow not only to distinguish between neutron stars and black-holes in XRBs, but also could potentially constrain the equation of state of the neutron star. These topics are however out of the scope of this thesis so I suggest the reader to refer to Lewin et al. (1997); Strohmayer (1999); Lattimer & Prakash (2007) for more details.

CVs, and in particularly the magnetized ones (so-called polars and intermediate polars), also exhibit a variety of interesting observational features. More details on this class of X-ray binaries can be found in Warner (2003).

1.1.2 Accretion processes

As we already said, the X-ray emission of XRBs is powered by the accretion of matter from the donor onto the degenerate component. Accretion can occur through the capture of winds or through Roche lobe overflow. The gravitational energy of the accreted matter is thermally radiated either following the impact with the surface of the compact object, like in systems containing neutron stars or white dwarfs, or

in the so-called accretion disk.

The amount of energy released depends on the accretion rate and on the compactness parameter M/R :

$$L \sim GM \frac{\dot{M}}{R} \quad (1.5)$$

here L is the luminosity, M is the mass of the compact object, R its typical radius and \dot{M} is the accretion rate of the mass inflow (Lipunov 1987). If emitted thermally from a relatively small area (a few times the size of the object), the radiation predominantly falls in the X-ray range (~ 1 keV). In XRBs containing a neutron star or a black hole, L_x can reach up to $0.2\dot{M}c^2 \sim 10^{39}$ ergs s^{-1} .

For white dwarf systems the compactness parameter is much lower. In many cases the X-ray emission is mainly powered by nuclear fusion when the accreted plasma burns on the surface of the white dwarf. Such emission may be persistent (at high accretion rates) or burst-like (Warner 2003).

Since the angular momentum of the in-falling matter (which is not negligible due to the orbital motion) is conserved, the angular velocity of the matter increases as it approaches the compact object. Eventually it may exceed the local Keplerian velocity preventing the matter from falling directly onto the compact object. In this case an accretion disk (Shakura & Syunyaev 1973) is formed which transports the excess of angular momentum outwards. At the same time some fraction of the gravitational energy is dissipated via viscous friction in the accretion disk, predominantly in X-rays (Shakura & Syunyaev 1973). Due to this, black holes which have no surface and are otherwise invisible can be observed. The accretion disk may obviously form around a compact object of any type provided the angular momentum of the accreting matter is sufficient.

If the compact object is strongly magnetized (with $B \geq 10^8$ G for neutron star), the magnetic pressure exceeds the ram-pressure of the in-falling matter ($B^2/8\pi \geq \rho v^2$) which is funneled onto the magnetic poles. If the compact object rotates and the spin axis is misaligned with respect to the magnetic field axis, we will observe the pulsations of the X-ray flux. Accreting magnetized neutron stars are known as accreting pulsars and magnetized dwarfs as polars or intermediate polars (Lewin et al. 1997).

1.2 Accretion powered pulsars

This thesis is dedicated to the study of accretion-powered pulsars so in this section I will review their properties. More details can be found, for instance, in Nagase (1989); Lipunov (1987); Rose (1998).

Accreting X-ray pulsars are relatively young, strongly magnetized neutron stars mainly found in HMXB systems. Their pulsed X-ray emission is powered by accretion. At some radius the strong magnetic field overcomes the gravitational drag and the plasma is confined along the field lines and funneled to the polar caps. Within this radius the motion of plasma is governed by the magnetic field so this area is usually called the magnetosphere.

We know that the accretion pulsars are young because the nuclear timescale is rather short for stars with mass exceeding $10 M_{\odot}$ so the donor star evolves fast and the lifetime of the HMXB system is short (tens of Myrs according to (1.2), see also Rose 1998). In fact, many HMXBs are clearly associated with star formation regions (Levine et al. 1996, see also Figure 1.3).

The optical companion is usually a (super)giant star or a *Be*-star. There are however numerous exceptions such as Her X-1, which has a MS companion. Other examples include GRO J1655–40, 4U 1543–47, and LMC X–3. HMXBs with neutron stars are therefore generally classified in three groups according to the donor star type: Super Giant X-ray Binaries (SgXRB) with giant and super-giant optical companions, *Be* X-ray binaries (BeXRB) with *Be* stars as optical companion and the so-called “intermediate mass X-ray binaries” like Her X-1 with a MS companion.

The groups differ mainly in how accretion proceeds. In SgXRBs and BeXRBs the matter is accreted from the optical companion onto the neutron star via stellar winds, which is enhanced along the spin-equator plane in BeXRBs. Systems with intermediate mass accrete through Roche Lobe overflow. In the latter case an accretion disk (see above) always forms (Frank et al. 1992; Pringle 1981) due to the angular momentum of the orbiting plasma.

In my thesis I will focus on systems in which accretion mainly occurs from the wind of an optical companion. More details on disk accretion may be found in Lipunov (1987); Frank et al. (1992).

In SgXRBs and BeXRBs the neutron star has an eccentric orbit. The main reason for this being that the orbit disturbed by the natal kick to the neutron star in the supernova explosion does not have enough time to circularize via tidal interactions (Frank et al. 1992). The accretion in most cases proceeds either from the circumstellar disk of the *Be* companion or from the powerful radiationally-driven wind of a supergiant companion which does not fill its Roche-lobe (Frank et al. 1992)¹. Note however that SgXRBs (including GX 301–2) have very dense winds which effectively fill the Roche Lobe. While accretion still proceeds from wind, it becomes “focused” forming an accretion stream (Leahy & Kostka 2008).

¹to be more precise the probability to observe a HMXB at this stage is low since Roche lobe overflow takes place on thermal timescales which are very short for massive stars

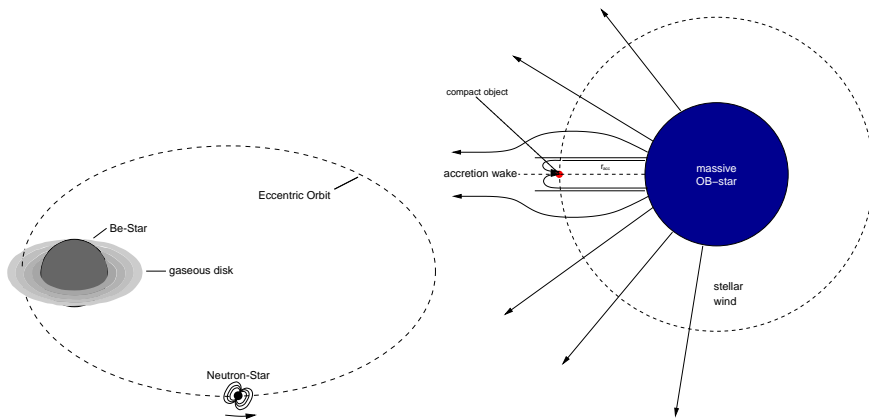


Figure 1.4: Accretion in BeXRB and SgXRB (i.e. directly from stellar wind, see Bondi & Hoyle 1944). Image credit: Kretschmar (2004); Kreykenbohm (2004)

The orbital periods of HMXBs are in the range 1-1000 d, so taking into account the high eccentricity of the orbit, it is not surprising that a significant fraction of accreting pulsars are transients, characterized by periodical outbursts close to the periastron passage. Particularly this is the case for BeXRBs where the fast rotation of the *Be* stars is responsible for the enhancement of the wind in the equatorial direction forming a circumstellar “disk” around the star. Most of the mass loss of *Be* stars occurs through this disk. When the neutron star passes through this disk the accretion rate strongly increases resulting in particularly powerful outbursts. During the outbursts the luminosity can reach $10^{36} - 10^{39} \text{ erg s}^{-1}$ and an accretion disk often forms. The formation of the disk is associated with rapid spin-up episodes observed in many sources (Bildsten et al. 1997). Outside of the outbursts the neutron stars of the BeXRBs are usually dim and spin-down steadily.

In SgXRBs the situation is somewhat different and the luminous optical companion loses most of the mass via radiatively driven wind (see Figure 1.6 for comparison). The wind is almost spherically symmetric and variations of the X-ray flux with the orbital phase are less dramatic than in the case of the BeXRBs. In fact, most of SgXRBs may be considered persistent sources (Liu et al. 2006), although wind focusing may lead to significant enhancement of the X-ray flux at certain orbital phases (Leahy & Kostka 2008). The radiatively driven wind is intrinsically unstable (Runacres & Owocki 2005) and the accretion of denser clumps leads to X-ray flares when the matter is accreted onto the neutron star (Walter & Zurita Heras 2007). Due to the dense wind, SgXRBs are strongly absorbed and are difficult

to detect in soft X-rays despite the relatively high luminosity ($10^{36} - 10^{38} \text{ erg s}^{-1}$). The boom of discoveries of these systems began with the launch of missions with imaging capabilities in hard X-rays like *INTEGRAL* and *Swift* (Walter & Zurita Heras 2007).

The pulse period usually changes erratically in these sources, although as I show in my thesis, a correlation with flux is observed at least in some cases. I further discuss this topic in Chapter 2.

As already discussed, depending on the angular momentum of the captured matter accretion may proceed either directly from a wind or from an accretion disk (Shakura & Sunyaev 1973) as summarized in Figure 1.5. The fact that the accretion disk of accreting pulsars (if any) is disrupted by the magnetosphere at large inner radii implies that the disk luminosity is low which makes it difficult to observe directly in accretion-powered pulsars. A steady and rapid spin-up or the observation of quasi periodic oscillations may indicate the presence of an accretion disk in the system (Bildsten et al. 1997).

The magnetic field funnels the plasma onto the polar caps where the energy is released. At low luminosities (below $\sim 5 \times 10^{36} \text{ ergs s}^{-1}$, Basko & Sunyaev 1976) the matter is stopped at the neutron star surface via Coulomb interactions producing a hotspot. At higher luminosities the radiation pressure of the emission coming from the small polar caps ($\sim 1 \text{ km}$ size Lipunov 1987) starts to slow down the accretion flow and an *accretion column* arises.

The concept of the accretion column was introduced by Basko & Sunyaev (1976) to explain the observed luminosity of X-ray pulsars which exceeds the Eddington luminosity limit even assuming spherically symmetric accretion:

$$L_{\text{Edd}} = 4\pi GM \frac{m_p c}{\sigma_T} \sim 5 \times 10^{37} \text{ erg s}^{-1} \quad (1.6)$$

This limit becomes an order of magnitude less if one considers that the plasma is funneled onto polar caps with much smaller area, as suggested by the observation of pulsations. To explain the existence of pulsars with luminosities above the critical one, Basko & Sunyaev (1976) suggested that the plasma is significantly slowed down by the radiation pressure at some height and then slowly sinks down as the excess energy is emitted through the side walls of the column. The column must be optically thick otherwise it would not form at all as the photons which support it would immediately escape. The geometry of the column is defined by the magnetic field structure and by the ways in which the plasma enters the magnetosphere. Usually two cases are considered: “solid” and “hollow” columns, see Fig. 1.6 (Basko & Sunyaev 1976).

All X-ray pulsars in HMXBs exhibit similar spectra: typically a cut-off power-law modified at lower energies by photoelectric absorption. Fluorescent emission

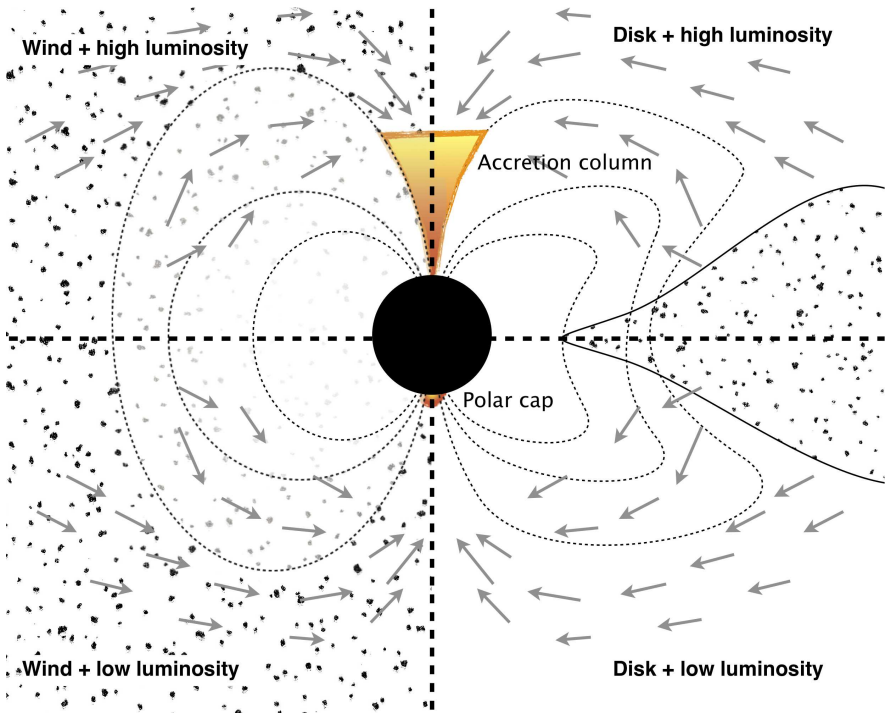


Figure 1.5: Sketch of an accreting pulsar for various accretion regimes.

lines of iron, nickel and other elements originating in the surrounding plasma heated by X-ray emission from the pulsar are often observed. In some sources Cyclotron Resonance Scattering Features (CRSF) are observed in absorption. These are discussed in greater detail in Chapter 2. The continuum part of the spectrum is believed to be the result of comptonization of thermal, bremsstrahlung and cyclotron emission originating close to the polar cap and in the accretion column by the hot plasma which falls onto the neutron star. An sample spectrum calculated by Becker & Wolff (2007) is presented in Figure 1.7.

It was suggested by Basko & Sunyaev (1976) that the spectrum of such a column will have a characteristic cut-off power law shape, which is indeed observed in accreting pulsars. More detailed calculations of the spectrum emerging from the accretion columns of accreting pulsars were performed recently by Becker & Wolff (2005) with similar results.

It is important to note however that both Basko & Sunyaev (1976) and Becker &

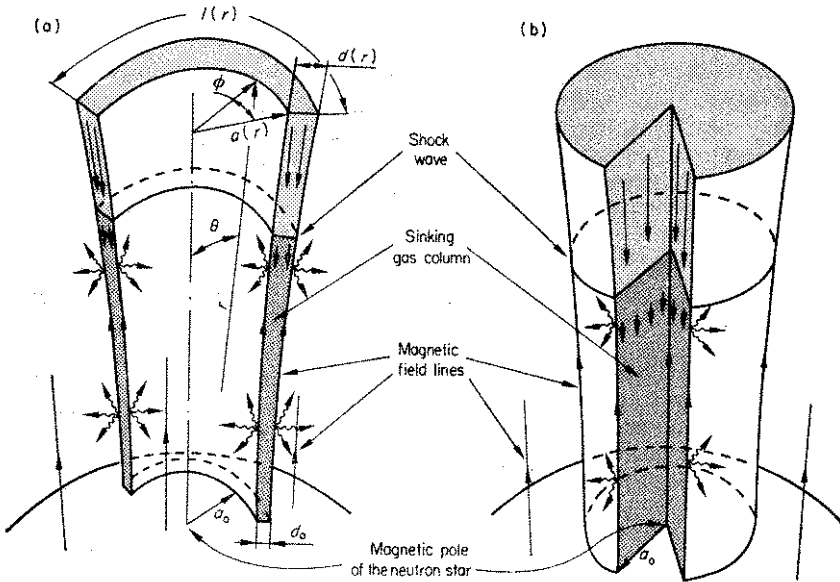


Figure 1.6: A sketch of the accretion column for “hollow” and “solid” geometries as presented by Basko & Sunyaev (1976). The magnetic field confines the optically thick plasma in the accretion structures. X-rays can only escape through the side-walls and therefore the column extends upwards due to the radiation pressure. The radiation pressure dominates in the region below the so-called “radiative shock”, where the plasma sinks with a velocity determined by the emissivity of the column.

Wolff (2005) models only calculate the spectrum which emerges from the accretion column, and rely also on a significant number of simplifying assumptions in order to find analytical solutions. I would like to note that the observed spectrum may be quite different due to: (1) the re-processing of the column emission close to the surface of neutron star or in the accretion stream (Ferrigno et al. 2009), (2) geometrical considerations and gravitational light deflection (Kraus et al. 2003), and (3) to the relativistic beaming generated by the fast motion of the plasma in the accretion stream (Lyubarsky & Sunyaev 1988). While this is not the main topic of the thesis, I will discuss qualitatively how these effects may affect the observed spectrum in greater detail in the next sections.

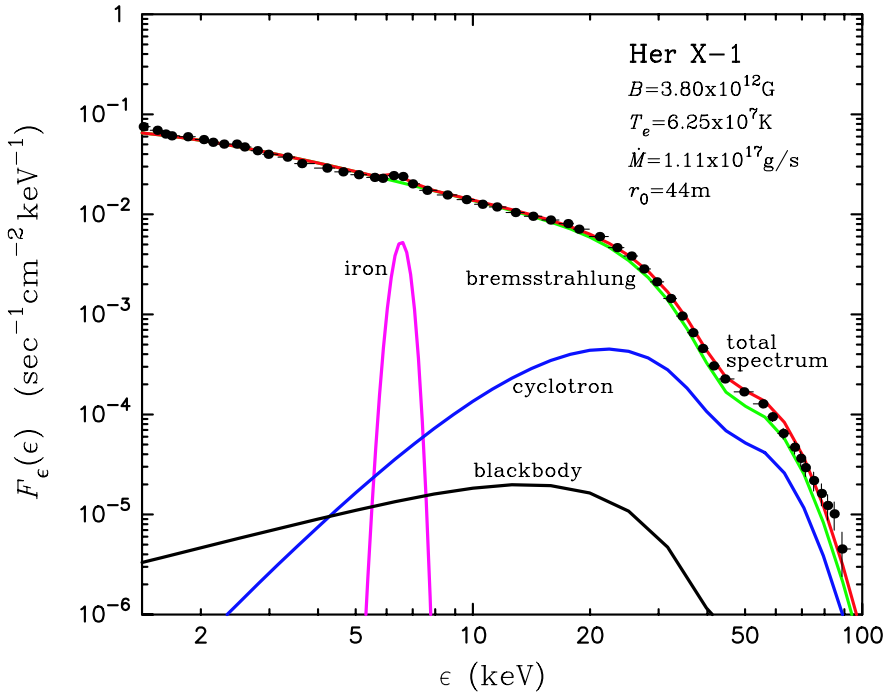


Figure 1.7: Theoretical column-integrated count rate spectrum of an accretion column as calculated by Becker & Wolff (2007) for Her X-1 compared with the observed one (dal Fiume et al. 1998). The plot shows the total spectrum as well as contributions from the comptonized thermal, bremsstrahlung and cyclotron emission.

CHAPTER 2

Magnetic fields of neutron stars

It was anticipated that neutron stars must have rather strong magnetic fields (Ginzburg 1964). Indeed, the neutron star is basically a collapsed core of a normal star and most of the optical stars are believed to be magnetized (Clayton 1968). During the collapse the magnetic flux is conserved and the magnetic field of the neutron star will therefore increase:

$$B \propto R^{-2} \tag{2.1}$$

Main sequence stars have $B \sim 100$ G which implies $B \sim 10^{12} - 10^{14}$ G for neutron stars collapsed to a radius of 10 km (Lipunov 1987).

X-ray and radio pulsars (Giacconi et al. 1962; Hewish & Okoye 1965; Hewish et al. 1968; Shklovsky 1967) were discovered and soon after interpreted as neutron stars with magnetic fields of the expected magnitude. In both cases a lower limit on the magnetic field strength can be obtained from very basic physical considerations even if the exact details of the emission mechanisms remain unclear.

In fact, all radio-pulsar models, starting with the originally proposed interpretation by Gold (1968), require a magnetic field strength of $\sim 10^{12}$ G to produce the observed radio emission since the electrons producing the synchrotron emission must be accelerated to ultra-relativistic energies (via the Lorentz force).

In the case of X-ray pulsars the energy density of the magnetic field $B^2/8\pi$ shall exceed the energy density of the in-falling plasma in order to be able to funnel the plasma onto the polar cap. This yields a lower limit on the magnetic field strength of $B \sim 10^9$ G (Lipunov 1987).

2.1 *Rotation powered neutron stars*

2.1.1 *Radio pulsars*

The bolometric luminosity of radio pulsars (including the kinetic energy of the out-flowing relativistic plasma) is estimated to be very close to losses of the rotational

kinetic energy of the neutron star. The latter is well constrained from pulse frequency measurements. The observed frequency evolution is similar to what can be expected assuming magneto-dipole energy losses (Rose 1998):

$$\dot{E} = -I\Omega\dot{\Omega} \propto B^2\Omega^4 \quad (2.2)$$

Here I is the moment of inertia, B is the magnetic field, and $\Omega, \dot{\Omega}$ are the angular pulse frequency of the pulsar and its derivative. More detailed studies also seem to agree with the magneto-dipole approximation (Cordes & Chernoff 1997). The magnetic field of the pulsar may be estimated in this case as

$$B = \sqrt{\frac{3Ic^3}{8\pi^2R^6} P \frac{dP}{dt}} \quad (2.3)$$

Note that this estimate relies on the assumption that the rotational energy losses are due to magneto-dipole emission.

The magnetic fields of radio pulsars determined in this way span the complete allowed range. The lower limit is imposed by the requirement that the electric field induced by the rotating magnetosphere is sufficient to produce a e^+/e^- plasma (Chen & Ruderman 1993). The radio pulsar is expected to switch off when its pulse period drops below a certain value in the course of gradual spin-down, simply because the relativistic electrons responsible for the emission cannot be produced anymore (the so-called “charge-straved” magnetosphere). This is in fact supported by the observations. The “death-line” is clearly observed on the “period–magnetic field” diagram, as predicted by the models of Chen & Ruderman (1993). This is illustrated in Fig. 2.1. The exact position of the “death-line” depends on how exactly the pair-production mechanism operates in pulsars. In Fig. 2.1 the most conservative (i.e. lowest B) estimate by Chen & Ruderman (1993) is shown.

The upper limit is imposed by the so-called “quantum critical” or Schwinger limit

$$B_{\text{crit}} = m_e^2 c^3 / e\hbar \sim 4.4 \times 10^{13} \text{ G} \quad (2.4)$$

where the cyclotron energy equals the electrons rest mass. Most of the emission models for radio pulsars predict the suppression of the emission above this critical field. There are, however several objects with a field exceeding this value but still visible in radio, the so-called high magnetic field radio pulsars (HBRP). For instance PSR J1847–0130 (McLaughlin et al. 2003) exceeds the critical value by factor of 2. There are several hypotheses why this may happen (see McLaughlin et al. (2003) and references therein for details). This discussion is however beyond the scope of the thesis. It is sufficient to say here that the radio pulsars do seem to populate the complete allowed region where the radio emission is expected to be produced ($B_{\text{RP}} \propto 10^6 - 10^{13}$ G), with some pulsars having even stronger fields.

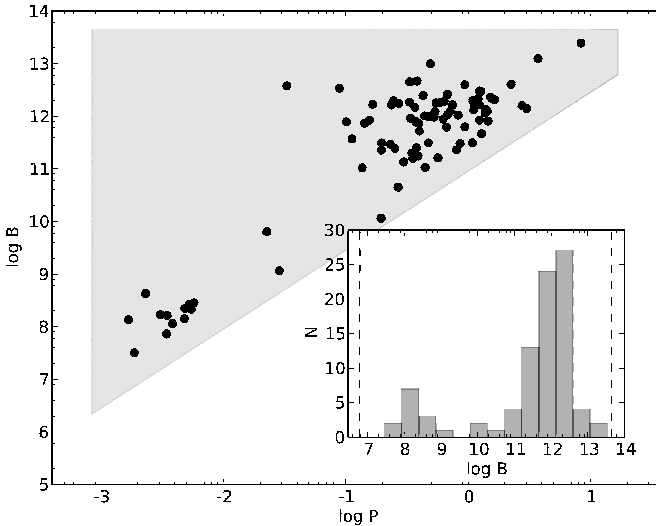


Figure 2.1: The “period–magnetic field” diagram for rotation-powered pulsars using data from the ATNF pulsar catalogue (Manchester et al. 2005). The radio-emission from a pulsar is expected to switch-off outside of the shaded area, limited by the “critical quantum field” from the top and by low limit on induced electric field from below (Chen & Ruderman 1993). The inset shows the distribution of the magnetic fields with the limits mentioned above indicated by vertical lines. Note the gap between millisecond or “recycled” and normal pulsars. The former are believed to be old neutron stars which were once accreting and thus spun up to the short periods (Rose 1998). This figure illustrates a broad range of magnetic field values measured for rotation-powered pulsars.

2.1.2 Magnetars

A magnetar is defined as a neutron star with ultra-strong ($B \geq B_{\text{crit}} \sim 4.4 \times 10^{14}$ G) magnetic field which powers its extremely strong X-ray and γ -ray emission. It is common, however to use the term magnetar for any highly magnetized neutron stars, including those not powered by the decay of the magnetic field (i.e. the HBRPs mentioned above).

Historically the magnetar hypothesis was introduced to explain the short GRBs, particularly the March 5, 1979 SGR 1806–20 event (Mazets et al. 1979). The 150 ms flare, observed by the Venera spacecrafts and several other missions, saturated the X-ray and γ -ray detectors on all satellites with a peak flux by two orders of magnitude higher than ever detected before from any source. However the shocking

discovery came later when the position of the burster was determined by comparing the flare timing observed by different satellites. The burster turned out to coincide with a young supernova remnant (SNR) in the *Large Magellanic Cloud* (LMC, see Fig. 2.4), which yielded a fluence of 1.3×10^{46} erg or luminosity of 9×10^{46} erg s⁻¹.

The burst location in a young SNR (with an age of $\sim 10^4$ yr) and the observed pulsations with a period of ~ 8 s strongly suggested that a neutron star was responsible for the burst. The problem is, however, that the observed luminosity by far exceeded the Eddington limit and the flare could not be accretion powered. On the other hand, the flare was too short to originate deep in the neutron star since it would take much longer for the emission to get out (Hurley et al. 2005; Mereghetti 2008). Also, the neutron star was not destroyed and continued to pulsate. Moreover, on the next day another somewhat weaker flare was observed. The source remained active with several hundreds of recurrent flares detected to date. Obviously most of these flares were less intense. The fluence distribution is in fact very broad and varies by four orders of magnitude (see Fig. 2.2)

Other similar sources were detected later making up a new class of sources, the Soft Gamma Ray Repeaters (SGRs). As of 2010, 9 SGRs (7 confirmed and 2 candidates) are known¹.

Roughly half of the known SGRs have been detected in X-rays and other energy bands in quiescence (Mereghetti 2008). The X-ray emission is typically pulsed with a hard, non-thermal spectrum (Trümper et al. 2010). In most cases a spin-down of the neutron star has been measured in quiescence or via comparison of the pulse period values in consequent outbursts. The observed spin-down rate implies huge magnetic fields, assuming the same spin-down mechanism as for radio pulsars (see (2.3) and Fig. 2.3). In fact, the first such measurement by Kouveliotou et al. (1998) has triggered the strong corroboration to the magnetar model.

The magnetar model was proposed by Duncan & Thompson (1992). In this model the giant flares of SGRs are explained as a result of large scale changes in the magnetosphere of a highly magnetized neutron star (or magnetar). As the tremendous magnetic field drifts through the solid crust of the magnetar, it stresses the crust with magnetic forces which get stronger than the solid can bear. This causes shifts in the crust structure, leading to bright outbursts.² The short duration and energetics of outbursts as well as spin-down timescales are considered the main arguments in favor of magnetar scenario (Mereghetti 2008).

Aside from SGRs, there is another class of sources considered as magnetars, namely the anomalous X-ray pulsars. These are soft X-ray pulsating sources with

¹<http://www.physics.mcgill.ca/pulsar/magnetar/main.html>

²In fact, historically Duncan & Thompson (1992) were interested in estimating the magnetic field of a neutron star and only when they found that the field could be ultra-strong, they realized that magnetars may be a plausible interpretation for the SGRs.

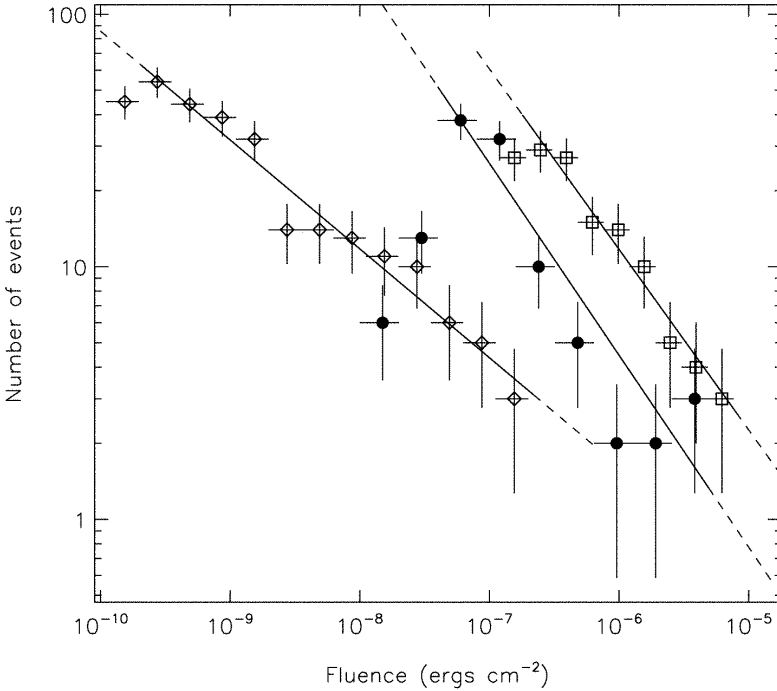


Figure 2.2: The differential fluence distribution of the SGR 1806-20 bursts as seen by RXTE (diamonds), BATSE (circles) and ICE (squares) as reported by Göğüş et al. (2000). The lines are obtained fitting a power-law model with the maximum likelihood technique. Image credit Göğüş et al. (2000).

no companion identified. No orbital modulation has been reported in pulse frequency history of any AXP so they are considered isolated stars (Mereghetti 2008). The pulse frequency steadily decreases at a rate which suggests a magnetar-like magnetic fields. The X-ray emission is thought to be powered by the same mechanism as the quiescent emission of the SGRs, namely by shear friction of the diffusing magnetic field. It is important to note, however, that while the giant flares from SGRs lack other explanation besides a “trapped fireball” model, the properties and the magnetar nature of the AXPs are still debated (Trümper et al. 2010).

Duncan & Thompson (1992) discussed also a possible origin of the strong magnetic field. Aside from the magnetic flux conservation considerations already mentioned above, the magnetic field of the neutron star may be amplified via an efficient helical dynamo mechanism. If the neutron star is formed with a significant fraction

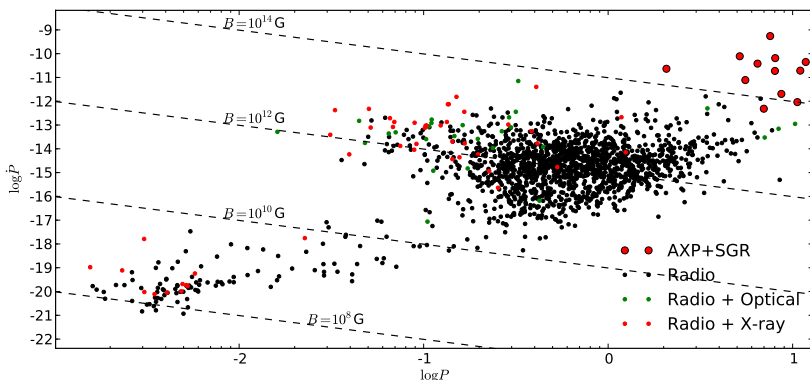


Figure 2.3: $\dot{P} - P$ diagram for rotationally powered pulsars using ATNF catalogue data (Manchester et al. 2005). Lines indicate the magnetic field calculated with (2.3): note huge spin-down magnetic fields of magnetars (AXPs and SGRs).

of differential rotation, the wrapping of the field lines around the star due to shear motion allows the small-scale magnetic field structures associated with the convection to grow, producing the amplification of the magnetic field. The free energy associated with the differential rotation $E_{\Omega} \sim 10^{52} (P/1 \text{ ms})^{-2} \text{ erg}$ is enormous and may lead to the generation of fields as strong as $B \sim 10^{17} (P/1 \text{ ms})^{-1}$ (i.e. factor of 100 stronger than from magnetic flux conservation considerations) as the rotation is smoothed by growing magnetic stresses (Duncan & Thompson 1992).

2.2 Accretion powered pulsars

In the case of radio pulsars and magnetars, the estimates of the magnetic fields are based on measurements of the spin-down rate. All radio pulsars spin-down losing rotational energy and this spin-down is typically very stable (aside from the small glitches observed in some cases). Magnetars (i.e. SGRs and AXPs) are no different in this regard. In both cases the neutron star is isolated and the measured spin-down rate provides a straightforward estimate of the rotational energy losses, and assuming some model (namely the magneto-dipole emission for the radio pulsars, or the heating of the neutron star by the magnetic shear forces for magnetars) also of the magnetic field.

The situation with the accreting pulsars is more complicated. The neutron star accretes matter and so it is not isolated. Taking into account the small intrinsic mo-

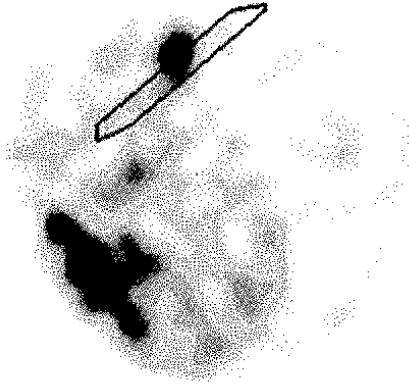


Figure 2.4: A ROSAT X-ray map of the supernova remnant N49 in the Large Magellanic Cloud overlaid with error-box (combined data of multiple satellites) for the March 5, 1979 event. Image credit: NASA

ment of inertia of the neutron star, the spin-frequency evolution is completely governed by the angular momentum exchange with the accreting matter. In most cases the accretion is non-stationary, as is the pulse frequency behavior. Most accreting pulsars exhibit erratic changes in the pulse frequency, often on-top of general spin-up or spin-down trends (Bildsten et al. 1997). However it is still possible to estimate the magnetic moment of the neutron star by studying the pulse frequency evolution.

2.2.1 Accretion torques

The spin frequency evolution of the neutron star gives insight into the interaction of the accretion flow with the neutron star. The rotational dynamics are determined by the equation

$$I \frac{d\omega}{dt} = K_+ + K_- \quad (2.5)$$

where K_+ and K_- are the acceleration and deceleration torques, ω is the pulse frequency, and I the momentum of inertia of the neutron star. The accelerating torque is associated with the angular momentum of the accreting matter. Braking torque must also be present as suggested by the long spin-down episodes observed in many accreting pulsars. The origin and magnitude of both torques depends on the properties of the binary system, particularly on the presence of an accretion disk. In this section I focus on quasi-spherical accretion from the stellar winds in detached binaries. This is indeed the relevant scenario for the sources I study in the thesis.

More details on angular momentum transfer in the case of accretion from disks may be found in Ghosh & Lamb (1978) and Lovelace et al. (1995).

As discussed by Illarionov & Sunyaev (1975), the accreting matter possesses a certain angular momentum due to the orbital motion of the neutron star. This implies an accelerating torque

$$K_+ = k_w \Omega R_G^2. \quad (2.6)$$

Here Ω is orbital frequency,

$$R_G = \frac{GM}{v_{\text{rel}}^2} \quad (2.7)$$

is the capture radius, v_{rel} is a relative velocity of the wind and the neutron star, and k_w a dimensionless coefficient defined by the accretion geometry.

The braking torque is associated with the magnetosphere-plasma interaction and is dependent on the magnetosphere radius, the rotational frequency and the plasma density (i.e. on the accretion rate). The interaction must proceed close to a so-called magnetosphere radius

$$R_M = \left(\frac{\mu^2}{2\dot{M} \sqrt{2GM}} \right)^{2/7}. \quad (2.8)$$

This equation is derived from the assumption that the ram pressure of the free-falling matter ($\rho(R_M)v_{\text{ff}}^2(R_M)$) is balanced by the pressure of the magnetic field ($B^2(R_M)/8\pi$). Here $\mu \simeq BR_{\text{ns}}^3$ is the magnetic moment of the neutron star, where B is the magnetic field strength at the surface. The density of the plasma at a given radius r , ($\rho(r) = \dot{M}/4\pi r^2 v_{\text{ff}}$) may be found for the observed accretion rate assuming that the matter away from the magnetosphere boundary is free falling with velocity

$$v_{\text{ff}} = \sqrt{\frac{2GM}{r}} \quad (2.9)$$

and using the continuity equation $\dot{M} = 4\pi r^2 v_{\text{ff}}$.

The braking torque can be thought as some tangent drag force applied to the magnetosphere boundary

$$K_- = F \times R_M. \quad (2.10)$$

The drag force may be for instance estimated under the assumption that the rotation of the magnetosphere in plasma is similar to the rotation of a sphere submerged in a viscous liquid (Lipunov 1987). The torque in this case is expressed as

$$K_- = 8\pi\nu_T \rho(R_M) R_M^3 \omega \quad (2.11)$$

where

$$\nu_T \sim \frac{1}{3} v_T l_T \quad (2.12)$$

is a turbulent viscosity coefficient and v_T and l_T are the characteristic velocity and size of the turbulent cells respectively. The size of the turbulent cells is assumed to be proportional to the magnetosphere size and v_T to the linear velocity of magnetic field lines at the magnetosphere boundary. The turbulent viscosity can then be expressed as:

$$\nu_T = k_T \omega R_A^2 \quad (2.13)$$

where $k_T \sim 1/3$ is a dimensionless turbulent viscosity coefficient. The resulting relation for the braking torque is then:

$$K_- = 8\pi k_T R_A^5 \omega^2 \frac{\dot{M}}{4\pi R_A^{3/2} \sqrt{2GM}} = \frac{k_T \omega^2 \mu^2}{2GM} = \frac{k_T}{2} \frac{\mu^2}{R_C^3} \quad (2.14)$$

where the co-rotation radius (the radius where the local Keplerian velocity of the accreting matter matches the angular velocity of the neutron star, Lipunov 1987) is defined as

$$R_C = \left(\frac{GM}{\omega^2} \right)^{1/3}. \quad (2.15)$$

A similar result may be obtained under the assumption that the supersonic rotation of an asymmetric magnetosphere in the plasma generates shock waves which dissipate the rotational energy (Davies et al. 1979; Bisnovatyi-Kogan 1991). The drag force is proportional to the magnetosphere area (or more precisely, to the area of the shock) and ram pressure of the matter moved by the shock with characteristic velocity v_m :

$$F \sim 4\pi R_A^2 \rho(R_M) v_m^2 \quad (2.16)$$

As a velocity estimate the linear velocity $v = \omega R_M$ at the magnetosphere radius is usually taken. The braking torque will be in this case:

$$K_- = \frac{\dot{M}}{\sqrt{2GM}} \omega^2 R_M^{7/2} = \frac{\omega^2 \mu^2}{4GM} = \frac{1}{4} \frac{\mu^2}{R_C^3}. \quad (2.17)$$

Alternatively, one may assume that some kind of outflow is present in the system and carries part of the accreted angular momentum away. For instance Illarionov & Kompaneets (1990) assumed that such an outflow may be driven by buoyancy force due to the non uniform Compton heating of the plasma by the anisotropic X-ray emission of the pulsar. The braking torque may be in this case estimated as (refer to the original paper for more details)

$$K_- = k_{IK} \dot{M} \omega R_M^2 \quad (2.18)$$

where k_{TK} depends on the outflow geometry.

The spin frequency remains constant if the braking and the accelerating torques are balanced ($K_+ = K_-$) and is usually called the “equilibrium frequency”. Taking into account the torque models described above, and assuming that the observed pulse frequency is close to the equilibrium value, it is possible to estimate the magnetic field if the accretion rate is known. As I will discuss, the information on the frequency derivative dependence on the flux provides additional constraints on some of the model parameters such as k_w .

A similar approach may be used in the case of disk accretion (Ghosh & Lamb 1978; Lovelace et al. 1995). In the Ghosh & Lamb (1978) model and follow-up works (Wang 1995), it is assumed that the accretion disk is threaded by the field lines, which couple with the disk at certain radius. Since the disk is locally rotating with the Keplerian velocity (that is according to third Kepler law, $P^2 \propto R^3$), the radius of interaction determines whether the magnetosphere rotates at this radius faster (in this case the neutron star brakes down) or slower (spin-up of the neutron star) than the disk. The radius of the magnetosphere is determined by the magnetic field and thus, measuring the pulse frequency changes allows us to estimate it.

In the model of Lovelace et al. (1995), the disk is not threaded by the field lines which being unable to penetrate the disk, become open. The matter leaves the system along the open field lines carrying angular momentum away. The mass and the angular momentum outflow rates depend again on the field strength.

2.2.2 Cyclotron Resonance Scattering Feature (CRSF)

The energy of electrons in a strong magnetic field shall be quantized in the so-called “Landau levels”. Indeed, the electrons moving in the magnetic field follow a helicoidal trajectory because of the Lorentz force. The gyration frequency (or Larmor frequency) is given by:

$$\omega_L = \frac{v_{\perp}}{r} = \frac{eB}{m_e} \quad (2.19)$$

where m and e are the electron mass and charge respectively, and B is the magnetic field strength. The gyration radius can therefore be derived as

$$r_L = \frac{m_e v_{\perp}}{eB} \quad (2.20)$$

which decreases as the magnetic field grows. As the field strength approaches the values typically seen in neutron stars, the gyration radius gets comparable with the so-called *de Broglie* wavelength

$$\lambda_{\text{de Broglie}} = \frac{\hbar}{mv} \quad (2.21)$$

so quantum effects become important (Araya & Harding 1996). The kinetic energy of the electron becomes quantized in the direction perpendicular to the field lines. This quantum-mechanical problem was first considered by Lev Landau, so the possible kinetic energy values are usually referred to as “Landau levels”, given by:

$$E_n = m_e c^2 \sqrt{1 + \left(\frac{p_{\parallel}}{m_e c}\right)^2} + 2n \frac{B}{B_c}. \quad (2.22)$$

Here n is level number, $p_{\parallel} = m_e v_{\parallel}$ is the momentum of the electron parallel to the magnetic field and $B_c \sim 4.4 \times 10^{13}$ G is the quantum critical field at which the cyclotron energy of the electron becomes comparable with its rest mass. For $B \geq B_c$ a relativistic treatment of the problem is required. In this case both components of the electron momentum become important and energies of the Landau levels become angular-dependent. In the non-relativistic approximation the levels are equidistant (Lipunov 1987) and

$$E_{\text{cyc}} = \hbar\omega = \frac{\hbar e B}{m_e} \sim 11.57 \frac{B}{10^{12} \text{ G}} \quad (2.23)$$

Gnedin & Sunyaev (1974); Basko & Sunyaev (1976) suggested that this leads to important implications for the X-ray spectra of accreting pulsars. Indeed, the fact that the electron’s kinetic energy is quantized, implies it may change only discretely. The Compton scattering cross-section for the scattering of photons at the electrons will be therefore enhanced for photons with energies $h\nu = E_n$, where E_n is defined by (2.22). The decay rate from the excited to lower levels is however extremely large (Latal 1986):

$$\nu_r = \left(\frac{\alpha m_e c^2}{\hbar}\right) \left(\frac{B}{B_c}\right)^{1/2} \sim 10^{15} \frac{B}{10^{12} \text{ G}} \text{ s}^{-1} \quad (2.24)$$

The lifetime of the electrons in the excited levels is, therefore, extremely short and the photons are almost instantly re-emitted with energy of $h\nu = E_n$. The energy of the photon is basically not changed and the process is called “resonant scattering”. The mean free path of the photons with energies close to E_n is much smaller, due to increased probability of interaction. Photons with energies close to the resonant one become effectively trapped in plasma. This leads to the formation of line-like absorption features in the emerging X-ray spectrum as the photons with energies $n \times E_0$ basically cannot leave the plasma due to the short mean free path (Herold & Ruder 1979). The theoretical dependence of the effective cross-section on energy is plotted in Fig. 2.5 (Araya-Góchez & Harding 2000). The absorption features are called “Cyclotron Resonance Scattering Features” (CRSF). For $n=0$ we have a “fundamental” cyclotron line, while for $n \geq 0$ we have harmonic lines. The energy

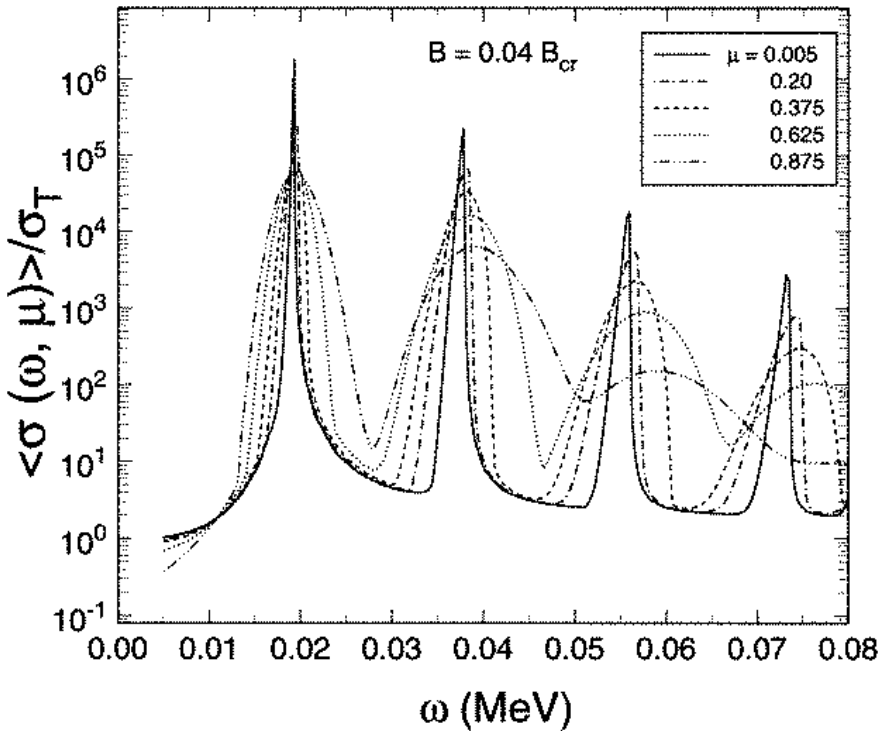


Figure 2.5: The cross-section for Compton-scattering in a strong magnetic field. Figure credit: Araya & Harding (1999)

of a CRSF is a function of the magnetic field in the line forming region (2.23) and therefore measuring it allows us to estimate the magnetic field of a neutron star directly.

The picture outlined above is of course very simplified and the connection of what can really be observed in the spectrum of an X-ray pulsar with underlying physical processes is not trivial. Even though line-like features in the spectra of X-ray pulsars were anticipated, it was unclear whether they do really exist and if they appear in emission or absorption. In fact, the line formation is still not understood completely. Numerical simulations show that the shape of the lines strongly depends on plasma properties in the emission region, its geometry and also a number of other factors. For more details please see Araya & Harding (1999); Schönherr et al. (2007) and Fig. 2.6.

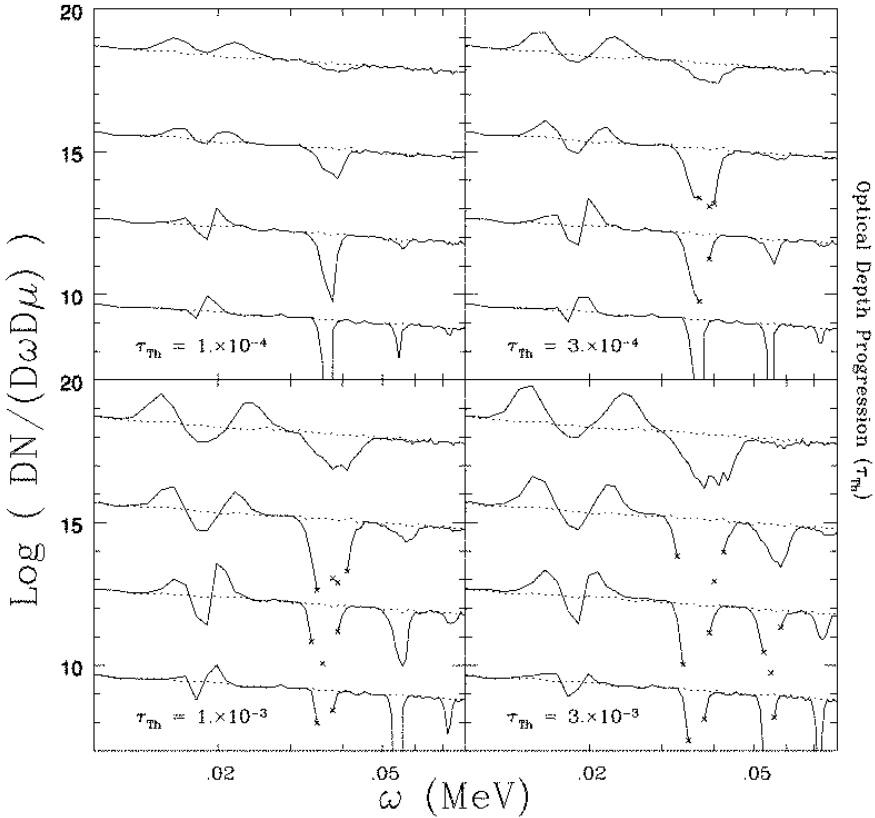


Figure 2.6: Example of CRSF profiles calculated by Araya & Harding (1999) for a “slab” geometry of the emission region, magnetic field of 1.7×10^{12} G, input power-law spectrum (indicated with dotted line), and several optical depths (increasing from upper left to lower right). Note the complicated shape of the lines. Figure credit: Araya & Harding (1999).

On May 3, 1976 Trümper et al. (1977) using a balloon detector (“Ballon-HEXE”) observed a very strong emission line-like feature at ~ 58 keV in the spectrum of X-ray pulsar Hercules X-1 (see Fig. 2.7). This discovery sparked a broad discussion about the interpretation of this *emission* feature (Herold & Ruder (1979); Yahel (1979); Nagel (1980) and others). In the following years, as space-based detectors appeared and more data was accumulated, it became clear that the line was not in emission at ~ 58 keV but rather in absorption at ~ 42 keV (Voges et al. 1982; Mihara et al. 1990). Also a number of similar features in the spectra of other pulsars were

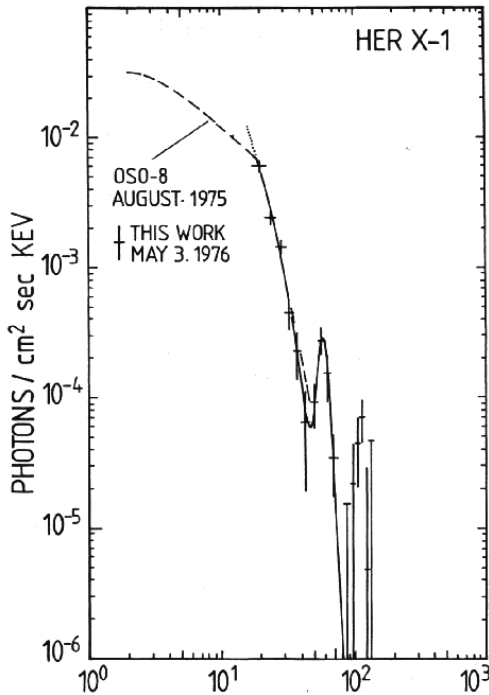


Figure 2.7: First evidence of a CRSF in spectrum of Her X-1 as reported by Truemper et al. (1978). The feature was originally interpreted as an emission line at ~ 58 keV, while subsequent observations showed that it was in fact an absorption feature at ~ 42 keV.

discovered as summarized in Table 2.1. In some cases more than one harmonic could be detected, which is a strong argument that the observed features are indeed due to the resonant scattering in a strong magnetic field. A particularly striking example is 4U 0115+63, which is not only the first source with a CRSF harmonic detected (White et al. 1983), but also exhibits four equally spaced harmonics aside from the fundamental (Santangelo et al. 1999).

As the number of pulsars exhibiting CRSF in their spectra increased, the number of open questions regarding the physics of the CRSF increased as well. A number of attempts were made to account for more details and solve the problem analytically employing various simplifications (Yahel 1979; Nagel 1980; Wang & Frank 1981; Meszaros & Nagel 1985a). With the availability of fast computers the fo-

Source	E_{cyc} (keV)	Mission	Reference
Her X-1	41	Balloon	Trümper et al. (1977)
4U 0115+63	14,24,36, 48,62	<i>HEAO-1</i>	Wheaton et al. (1979)
V 0332+53	26,49,74	<i>Ginga</i>	Makishima et al. (1990)
Cen X-3	28.5	<i>RXTE</i>	Heindl & Chakrabarty (1999)
		<i>BeppoSAX</i>	Santangelo et al. (1998)
4U 1626-67	37	<i>RXTE</i>	Heindl & Chakrabarty (1999)
		<i>BeppoSAX</i>	Orlandini et al. (1998)
XTE J1946+274	36	<i>RXTE</i>	Heindl et al. (2001)
Cep X-4	28	<i>Ginga</i>	Mihara et al. (1991)
A 0535+26	46,100	<i>HEXE</i>	Kendziorra et al. (1992)
MXB 0656-072	36	<i>RXTE</i>	Heindl et al. (2003)
Vela X-1	24,52	<i>HEXE</i>	Kendziorra et al. (1992)
4U 1907+09	18,38	<i>Ginga</i>	Makishima & Mihara (1992)
4U 1538-52	20	<i>Ginga</i>	Clark et al. (1990)
GX 301-2	37	<i>Ginga</i>	Makishima & Mihara (1992)
X Per	29	<i>RXTE</i>	Coburn et al. (2001)
1A 1118-61	55	<i>RXTE</i>	Doroshenko et al. (2010b)
EXO 2030+375	1118	<i>RXTE</i>	Wilson et al. (2008)
	63?	<i>INTEGRAL</i>	Klochkov et al. (2008)
OA0 1657-415	36?	<i>BeppoSAX</i>	Orlandini et al. (1999)
LMC X-4	100?	<i>BeppoSAX</i>	La Barbera et al. (2001)
GS 1843+00	20?	<i>Ginga</i>	Mihara (1995)
GX 304-1	51?	<i>Suzaku</i>	Mihara et al. (2010)
Swift J1626.6-5156	10?	<i>RXTE</i>	DeCesar et al. (2009)
CGRO J1008-57	88?	<i>CGRO</i>	Shrader et al. (1999)
XMMU J054134.7-682550	10?,20?	<i>RXTE</i>	Markwardt et al. (2007)

Table 2.1: List of sources with cyclotron line(s) significantly detected in their spectrum (mainly taken from Makishima et al. (1999); Heindl et al. (2004), and updated with catalogue data (Liu et al. 2006) and ADS). The line energy value is followed by a question mark if the feature could not be confirmed, is model dependent or questionable in other way.

cus shifted towards finding a numerical solution to the problem using Monte Carlo simulations (Araya & Harding 1996; Isenberg et al. 1998; Araya & Harding 1999; Araya-Góchez & Harding 2000; Schönherr et al. 2007). More recently it has been realized that the emission region geometry may play an important role. If the cyclotron line is formed in the accretion column, one may expect large gradients of the physical parameters across the scattering region which may significantly affect the emerging spectrum (Nishimura 2008). Even if the presence of the CRSF in the X-ray spectrum is considered as the only “direct” method to estimate of the magnetic field in the line forming region, it is not as clear where the line formation

region is located and how exactly the observed features are formed. The CRSF formation problem appears to be extremely complicated and constant verification of theory with the observations is required to find the solution. I will discuss these questions in more details in the next chapters.

CHAPTER 3

Instrumentation

In this thesis I use the data obtained with several X-ray missions, namely *INTEGRAL*, *RXTE* and *Suzaku*. In the discussion of the physical properties of GX 301–2 and Vela X-1, I also use the pulse frequency histories measured with *CGRO BATSE*. In this chapter I wish to give a brief overview of the scientific capabilities of these missions.

3.1 Rossi X-Ray Timing Explorer

3.1.1 Overview

The Rossi X-ray Timing Explorer (*RXTE*) is one of the most influential missions dedicated to study of galactic X-ray sources. Launched on December 30, 1996 (with a target lifetime of 2 years), the *RXTE* is still operating now although not all instruments are fully functioning. The mission is tailored to explore the variability of X-ray sources on time scales from microseconds to months with moderate spectral resolution in the range from 3 to 250 keV. *RXTE* carries two collimated copointed instruments to cover low and high energy range with a good overlap. The Proportional Counter Array (or PCA, Jahoda et al. 1996) covers the energy range from 3 to 60 keV (although the sensitivity and the reliability of the calibration drop above 25 keV). The High Energy X-ray Timing Experiment (HEXE, Rothschild et al. 1998) covers the upper energy range (18–250 keV). The field of view is limited to around one degree for both instruments due to the collimators that provides a low background level of ~ 0.2 mCrab, so even dim sources can be detected. In addition to the pointed instruments *RXTE* carries a small 1D coded mask All Sky Monitor (*ASM*, Levine et al. 1996) telescope. The *ASM* scans about 70% of the sky in every spacecraft revolution. The main purpose of this instrument is to regularly monitor the complete sky in order to detect numerous transient sources and to trigger the follow-up pointed observations with the main instruments on board *RXTE* along with other X-ray missions. Long mission life-time and regular time

sampling of most sources in the sky and the relatively high sensitivity of the *ASM* also make it a very valuable addition to *RXTE* assets for monitoring the activity of known persistent sources.

The spacecraft operates in a low-earth circular orbit at a height of about 580 km which corresponds to a 90 minute orbital period. This restricts the length of uninterrupted observations to about half an hour due to earth occultation. On the other hand this time is not wasted but rather used to observe other visible sources.

The data from the detectors are pre-processed onboard by the Experiment Data System (EDS), which allows a flexible selection of data modes for data compression to ease telemetry constraints. In fact *RXTE* is not telemetry limited (in most cases) despite the huge effective area and inability to use ground stations to transmit the data due to the low orbit. The tracking and data relay (TDRSS) system is used to stay in contact with the satellite and provides a steady downlink of about 20 kbps only, and 256 kbps once a day for about half an hour. A schematic view of the spacecraft and of the instruments is presented in Fig. 3.1.

3.1.2 *PCA: proportional counter array*

The *PCA* on board Rossi XTE consists of five identical Xenon proportional counter units (PCUs) with a geometrical collecting area of 1600 cm² each. The PCUs are nearly co-aligned with the collimators slightly displaced to allow a better estimate of the positions of the point sources in the field of view via the comparison of the count-rates from different PCUs. Each of the PCUs consists of several layers. The propane layer at the top acts as a veto Layer. An additional veto layer is situated at the bottom of the detector. The three Xenon detector layers in between are surrounded by additional veto counters, which makes it possible to select only photons from the top and to discriminate photons coming from the sides, thus reducing the background. The presence of the collimator at the top further reduces the background. The field of view of one degree was selected to ensure, that the sensitivity of the instrument is not limited by the background but rather by source confusion.

The total effective area of all layers in all PCUs is about 6000 cm² in the nominal energy range from 2 to 60 keV, with an energy resolution of about 18% at 6 keV. Not all PCUs are operating simultaneously. The PCU 1 for instance lost its top propane layer in 2000 and since then it has significantly increased the background rate, which makes it less useful for many applications. All PCUs are switched off from time to time to reduce the frequency of the so-called breakdown events, when the high voltage applied to the anodes breaks through the Xenon layer. Often only one PCU is operating, but still the effective area of just one PCU is unprecedented in this energy range.

The subtraction of the background is crucial for non-imaging instruments like the

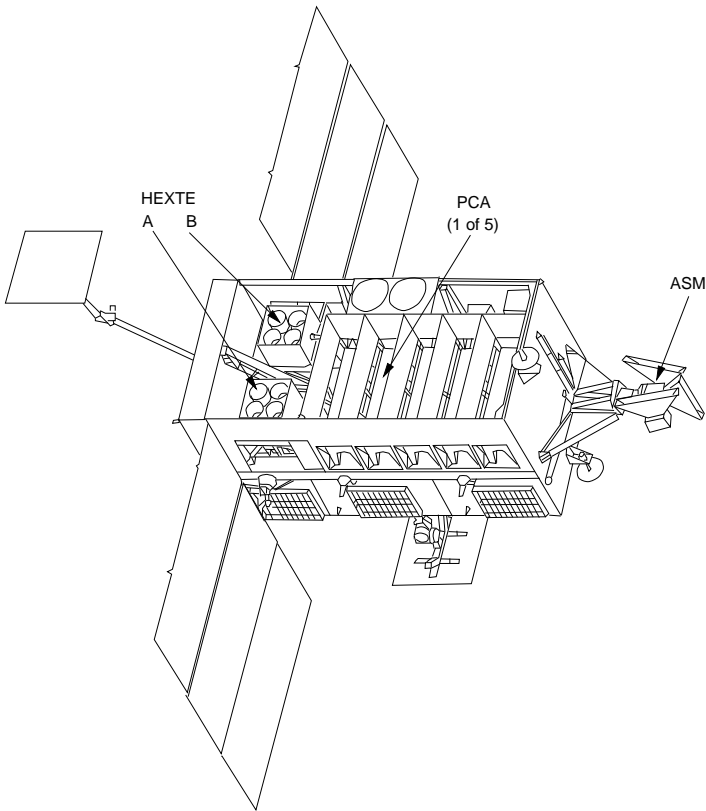


Figure 3.1: Schematic view of the *RXTE* spacecraft. Most of the satellite is occupied by five *PCA* PCUs. The *HEXTE* clusters can be seen in the left part of the figure. The *ASM* is on the right. Image credit: J. Wilms

PCA. In the case of the *PCA*, the background is modeled using the data from the veto layers and is a major source of uncertainty (up to 1%) in the measured source spectrum. For calibration purposes the *PCA* uses an ^{241}Am source, which emits 59.6 keV photons and α -particles which are detected by a dedicated α -detector located alongside the Americium source. This allows for an automatic on-board gain correction since any photon received simultaneously with an α -particle is known to have an energy of 59.6 keV. Although the *PCA* is sensitive up to 100 keV, the effective area drops sharply above 30 keV, which implies that a second instrument is required for the broad-band observations.

3.1.3 *HEXTE: High Energy X-ray Timing Experiment*

The High Energy X-ray Timing Experiment is an improved version of the A4 detector onboard the High Energy Astrophysics Observatory (HEAO). It was developed at the Center for Astrophysics and Space Sciences of the University of California in San Diego (UCSD). HEXTE consists of two clusters (A and B) of four NAI(Tl)/CsI(Na)-Phoswich scintillation detectors each (Rothschild et al. 1998) with a total effective area of about 1600 cm^2 at 50 keV. Each detector has a magnetic and anti-coincidence shielding to minimize the instrumental background and stabilize the response. An automatic gain correction is also implemented using a calibration ^{241}Am source.

The field of view of each detector is limited by a collimator to about one degree. This only partially reduces the sky background which above 30 keV contributes a significant fraction of the total count-rate even for the brightest sources. Moreover, the background variations are not smooth, so it is crucial to measure it directly. This is accomplished by rocking the two clusters in perpendicular directions so that each swaps source and off-source positions every 32 seconds. This provides a direct background measurement in four areas around the source at cost of considerably reduced on-source time. Unfortunately the rocking mechanisms of *HEXTE* clusters ceased to work on January 6, 2006 (cluster A) and December 20, 2010 (cluster B). Now, cluster A is fixed on source and cluster B off-source. This makes the spectral analysis with *HEXTE* possible, though problematic since the clusters are not exactly identical and the background of cluster A must now be estimated using the data from cluster B. Both clusters will most likely remain locked in the current positions till the end of the mission, though software developments may ease the issue.

3.2 *International Gamma-Ray Astrophysics Laboratory*

3.2.1 *Overview*

The *International Gamma-Ray Astrophysics Laboratory (INTEGRAL)*, is a medium-sized ESA observatory. It was launched on October 17, 2002, with an originally planned lifetime of 5 years, which was extended in October 2009 till at least the end of 2012. The main scientific goals of the mission are to perform broadband imaging and spectroscopy within a very wide field of view using the coded-mask imaging technique. The wide field of view and relatively high sensitivity make *INTEGRAL* a very good tool to discover new hard X-ray sources. For instance *INTEGRAL* has doubled the number of known SgXRBs (Negueruela 2004). The two main instruments on-board *INTEGRAL* are the imager *IBIS* (20 keV–1 MeV) and the imaging spectrometer *SPI* (20 keV–8 MeV). There are also two monitor-

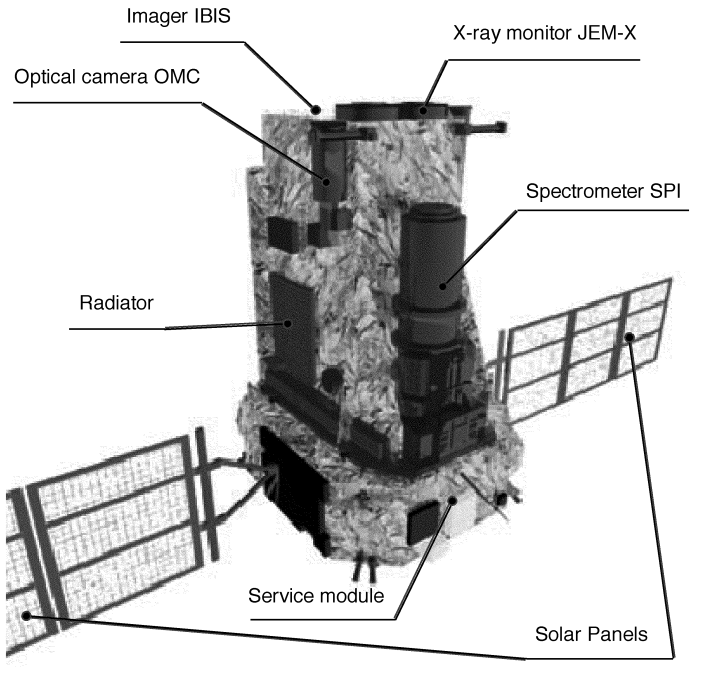


Figure 3.2: Schematic view of the *INTEGRAL* spacecraft. Main instruments are marked in figure. Image credit: ESA

ing instruments: *JEM-X* for soft X-rays (3-30 keV) and the optical monitor OMC (V-band). All instruments are co-aligned. A schematic view of the spacecraft is presented in Fig. 3.2. The satellite has a highly eccentric orbit with an orbital period of ~ 72 hours and a perigee altitude of about 10000 km. The inclination of the orbit with respect to the equatorial plane was 51.6 degrees at launch. This angle has increased slowly with time towards the almost polar current orbit. This highly eccentric orbit was chosen to minimize the periods with highly unstable instrument background due to the electrons and protons trapped in the radiation belts and to allow for long periods of uninterrupted observations.

3.2.2 *IBIS*

The Imager on Board the *INTEGRAL* Satellite (*IBIS*) has been optimized for the imaging and precise detection of point sources. All instruments on-board *INTE-*

GRAL, including *IBIS*, employ a coded-mask technique for the imaging. Coded mask imaging is the extension of a pin-hole camera concept to have more “holes” and hence a larger aperture. In this approach the opening of the telescope is partially masked and the shadow from the mask is measured in the detector plane. The location of the source can then be determined from the shadow position. The reconstruction is trivial if only one source is present in the field of view but gets extremely complicated as their number grows, since one needs to deconvolve the intensity measured in the detector plane into a set of shadow patterns corresponding to each source. The illustration of the problem is presented in Fig. 3.3 for two sources. Technically only the positions of point sources can be reconstructed. This is done either iteratively or via global optimization techniques, which minimize the regular residuals found after the subtraction of all sources in the field of view. It is important to note that the coded-mask instruments are background-dominated since the mask does not focus X-rays, so a point spread function effectively covers the whole detector and there are only few counts from each source in each pixel. On the other hand, the background flux is measured simultaneously with the source flux, similarly to truly imaging instruments. For coded-mask instruments the source and background fluxes are, however, model-dependent and it is crucial to ensure that the imaging reconstruction is done properly.

The mask pattern is optimized to have a delta-like autocorrelation function and at the same time, not to obscure too much light. A mask technically consists of a supporting structure and a set of opaque elements arranged in a pattern. The resolution of a coded-mask telescope is limited by the angular size of a detecting element as viewed from the mask and reaches $12'$ for *IBIS*. Two different fields of view are defined in coded-masks telescopes: the Fully Coded Field of View (FCFOV), for which all the source flux is modulated by the mask, and the Partially Coded Field of View (PCFOV), for which only a fraction of the source flux is coded by the mask.

The detector of the *IBIS* telescope is veto shielded and has two layers: PICsIT and *ISGRI* for hard and soft Gamma-rays respectively. The *ISGRI* layer consists of 128×128 pixels composed of *CdTe* semiconductor crystals. With their small area, the *CdTe* detectors are ideally suited to build an image with good spatial resolution. The lower PICsIT layer consists of 64×64 pixels made of *CsI* (Caesium Iodide) scintillation crystals.

IBIS contains a ^{22}Na calibration source, which allows regular calibration using the 511 keV line. The summary of the *IBIS* scientific performance parameters is presented in Table 3.1.

	IBIS	JEM-X
Operating energy range	15 keV – 10 MeV	3–35 keV
Energy resolution (FWHM)	7% @ 100 keV 9% @ 1 MeV	40/ \sqrt{E} %
Effective Area	ISGRI: 960 cm ² at 50 keV PICsIT: 870 cm ² at 300 keV	125 cm ² at 6 keV
Field of view	8.3° × 8° (FCFOV) 19° × 19° (PCFOV @50%)	4.8° (FCFOV) 7.5° (PCFOV @50%)
Angular resolution (FWHM)	12'	3'
Location accuracy (90% confidence)	30'' @100 keV ≤ 5' @1 MeV	30''
Continuum sensitivity, ph cm ⁻² s ⁻¹ keV ⁻¹ (3 σ detection, $\Delta E=E/2$, 100 s integration)	3.8 × 10 ⁻⁷ @100 keV 2 × 10 ⁻⁷ @1 MeV	1.4 × 10 ⁻⁵ @6 keV 8 × 10 ⁻⁶ @30 keV

Table 3.1: A summary of *INTEGRAL* scientific performances (Ubertini et al. 2003; Lund et al. 2003)

3.2.3 *SPI*

The Spectrometer on board Integral (*SPI*) operates in the 20 keV–8 MeV energy range. It also uses a coded-mask for imaging but has significantly lower angular resolution ($\sim 3^\circ$). The detector plane of the instrument consists of 19 cooled, hexagonal shaped, high purity *Ge* (Germanium) detectors, providing a total area of about 500 cm². The main feature of the instrument is a very good energy resolution, 2.35 keV at 1.33 MeV. The whole telescope is veto shielded and has a fully coded field of view (FCFOV) of $16^\circ \times 16^\circ$.

Unfortunately the low angular resolution limits the usage of this instrument in crowded fields of view, especially for time-dependent spectral studies. I used *SPI* only for the verification of the *IBIS/ISGRI* results.

3.2.4 *JEM-X*

The Joint European Monitor for X-rays (*JEM-X*) on-board *INTEGRAL* complements *IBIS* at energies below 35 keV. It consists of two identical coded-mask telescopes (referred as *JEM-X1* and *JEM-X2*), but most of the time only one of the two operates because the detectors degrade faster than anticipated.

Each *JEM-X* detector is a microstrip gas chamber with a sensitive geometric area of 500 cm² per unit. The gas inside the steel pan-shaped detector vessel is a mixture of xenon (90%) and methane (10%) at 1.5 bar pressure. The incoming photons are absorbed in the xenon gas by photo-electric absorption and the resulting ionization cloud is then amplified near the microstrip anodes. Significant electric charge is picked up on the strip as an electric impulse. The detectors are veto shielded with an efficiency of particle background rejection $\geq 99.9\%$.

The mask is $\sim 25\%$ transparent and is placed 3.4 m above the detector, which yields about 3' angular resolution. The mask transparency was chosen to optimize

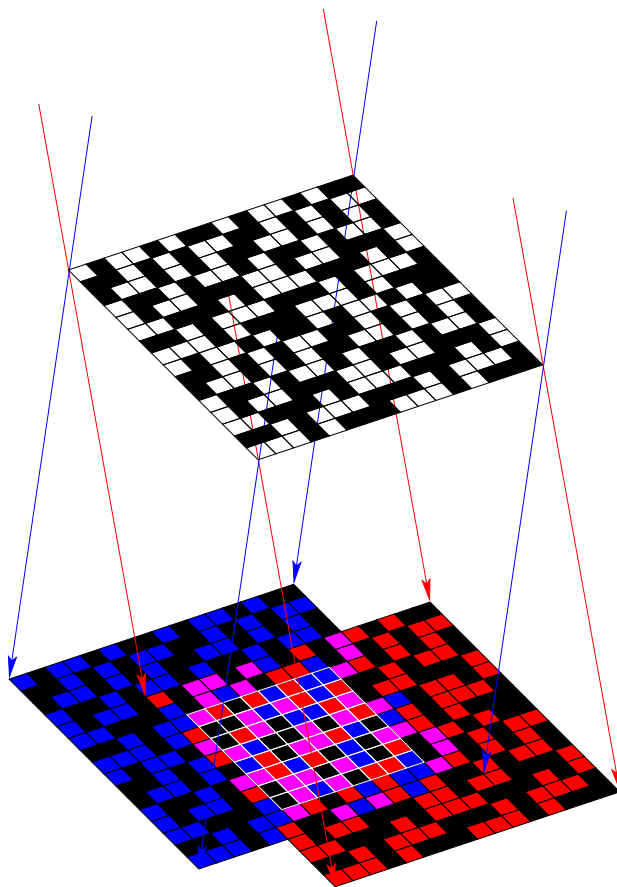


Figure 3.3: Schematic illustration of the coded mask imaging technique with two sources in the sky (a red and blue one), each projecting the mask pattern on the detector plane. The sky image is reconstructed by decomposing the image in the detector plane in a set of shadows cast by the point sources in the sky. Image credit: ISDC

performance in crowded fields and to satisfy the telemetry constraints. This however reduces the effective area of each *JEM-X* unit to $\sim 100\text{ cm}^2$ at 10 keV. It drops sharply above 25 keV, meaning the telescope is usable in energy range 3–35 keV. The energy resolution of the instrument is moderate: $\sim 12\%$ at 10 keV. The summary of the scientific performance is presented in Table 3.1.

3.3 Compton Gamma-Ray Observatory

The Compton Gamma Ray Observatory was the second of the NASA's Great Observatories. Compton, at 17 tons, was the heaviest astrophysical payload ever flown at the time of its launch on April 5, 1991 aboard the space shuttle Atlantis. Compton was safely deorbited and re-entered the Earth's atmosphere on June 4, 2000. In my thesis I only use high level pulsar data products provided by NASA (Bildsten et al. 1997) for The Burst and Transient Spectrometer Experiment (*BATSE*) instrument of the observatory. So here I wish to give a brief description of the instrument and of the data analysis involved in obtaining these data products.

BATSE was an all sky monitor sensitive in the 20-600 keV energy range. Each detector module contains two NaI(Tl) scintillation detectors: a Large Area Detector (LAD), optimized for sensitivity and directional response, and a Spectroscopy Detector (SD), optimized for energy coverage and energy resolution. The eight planes of the LADS are facing outwards from the corners of the *CGRO* spacecraft. A spacecraft sketch, with the indicated position of the *BATSE* detectors is presented in Fig. 3.4.

The LADs are non-imaging NaI(Tl) scintillators with a 2π sr field of view. The high level data products used in my thesis primarily utilize the background data from these detectors. These are folded on board or available continuously at 1.024 s time resolution with four energy channels (DISCLA telemetry data type) and at 2.048 s time resolution with 16 energy channels (CONT data type). The pulsed emission from the X-ray pulsars is typically detected by *BATSE* in the first DISCLA channel (20-50 keV) or channels 1-4 of CONT data (20-70 keV).

The high-level pulsar data products provided by NASA contain, for a particular pulsar, a set of pulse-profiles obtained in a series of fixed time intervals (typically ~ 5 d), the pulsed flux in each interval, the folding frequency (found for each interval individually) and, sometimes, the frequency derivative. The pulse profiles are either folded on-board (when the telemetry constraints do not allow to transmit the complete background light-curve) or on the ground. In both cases the light-curve is folded with the best-estimate period for a particular time-interval, which is obviously more robust for the ground-folded data. I use the *BATSE* data for three pulsars and, in all three cases, the on-ground folded data are used. For the on-ground folded data, the pulse frequency and its derivative are estimated either using a blind search for frequency (for 1A 1118-61) or with coherent pulse timing (GX 301-2 and Vela X-1). More details on the data analysis performed are available in Bildsten et al. (1997).

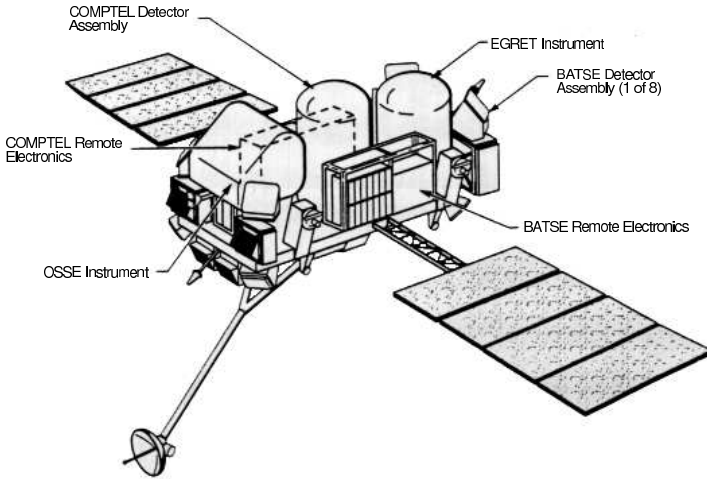


Figure 3.4: Sketch of the *CGRO* spacecraft. Data from the *BATSE* detectors (in the corners of the spacecraft) are used in the thesis. Image credit: NASA

3.4 *Suzaku* (*ASTRO-EII*)

3.4.1 Overview

The X-ray observatory *Suzaku* (formerly *ASTRO-EII*) is a joint Japanese-US mission, developed by the Institute of Space and Astronautical Science of JAXA in collaboration with the National Aeronautics and Space Administration's Goddard Space Flight Center (NASA/GSFC). The *ASTRO-EII*, the fifth Japanese X-ray mission, was launched on July 10, 2005 and was renamed to *Suzaku* (a red bird protecting the south skies in asian mythology) after launch. It is a replacement mission for *ASTRO-E* which was lost for the failure of launch vehicle in February 2000.

The scientific payload of *Suzaku* initially consisted of three co-aligned scientific instruments (see Fig. 3.5). The X-ray imaging spectrometer (XIS) consists of four X-ray telescopes (XRTs) equipped with X-ray sensitive imaging CCD cameras with moderate energy resolution (Koyama et al. 2007) three front-illuminated (FI, energy range 0.4-12 keV) and one back-illuminated (BI, energy range 0.2-12 keV). The Hard X-ray detector (Takahashi et al. 2007) is a broadband (10-600 keV) collimated

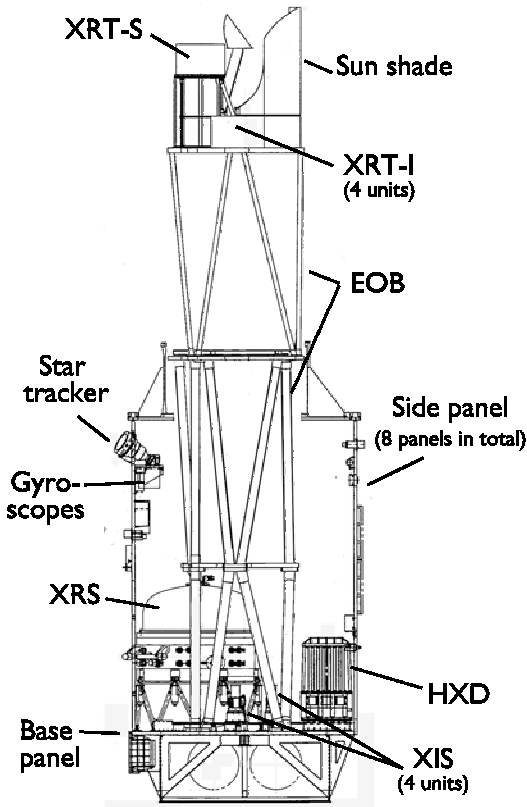


Figure 3.5: A side view of *Suzaku* spacecraft and instrumentation, figure credit JAXA.

instrument with two detector layers (PIN and GSO) with very low background level for a collimated instrument. The last instrument, the X-ray spectrometer (XRS), was a new-generation micro-calorimeter detector for the fifth XRT, designed to substitute the gratings used in *XMM-Newton* and *Chandra*. It was supposed to provide, for the first time, an unprecedented energy resolution of ~ 6 eV (which is factor of 20 better than for typical solid-state detectors) and good sensitivity in one instrument. Unfortunately the detector was only operational for 2 weeks when it was lost due to a failure in the cooling system. No useful science could be done with it. The performance of the instrument could, however, be verified and most likely another incarnation of the instrument will fly on one of the next-generation missions. Below I will focus on properties of XIS and HXD.

3.4.2 X-ray Imaging spectrometer (XIS)

The XIS consists of four X-ray telescopes (XRT-I0 to XRT-I3) equipped with CCDs operating in photon counting mode, similar to that used in the ASCA SIS (Burke et al. 1994), the *Chandra* ACIS (Weisskopf et al. 2002), and the *XMM-Newton* EPIC (Strüder et al. 2001). The XRTs are grazing-incidence reflective optics consisting of tightly nested, thin-foil conical mirror shells with high density nesting and thus large aperture efficiency in the operational energy range of 0.2-12 keV. The angular resolution is moderate (around $2'$), which makes the XIS less vulnerable to pile-up problems and at the same time, still sensitive enough due to the large effective area and the very low background.

The incident X-ray photons are converted in the CCD to charge-clouds with magnitude of charge proportional to photon energy. This charge is then shifted to the readout-area applying a time-varying electrical potential. The resulting voltage increase is amplified by the CCD electronics. The height of the voltage pulse allows to reconstruct the photons energy. In the XIS there are four CCDs, 1024×1024 pixels each, which corresponds to $17.8' \times 17.8'$ area on the sky (each pixel has $24 \mu\text{m}^2$, so the physical size of the CCD is $\sim 25 \times 25$ mm). One of the XIS (XIS1) uses a back-illuminated CCD for improved low-energy (below 1 keV) sensitivity, while the others use front-illuminated CCDs. Note that even for front-illuminated CCDs, the pulse-height distribution to monochromatic X-rays has a much smaller low-pulse-height tail compared to the CCDs on previous missions. This makes it possible to clearly recognize low-energy lines, e.g. *K*-shell emission lines of *C, N, O*.

3.4.3 Hard X-ray detector (HXD)

The Hard X-ray Detector (HXD) is a non-imaging, collimated instrument sensitive in the 10-600 keV energy range. The instrument consists of 16 identical veto shielded detector modules arranged in 4×4 array. Each “well”-unit is composed of two detector layers at the bottom of a passive collimator (i.e. “well”): a GSO/BGO phoswich counter (scintillator), sensitive above ~ 30 keV; and, on top of it, a 2-mm thick PIN silicon diode, sensitive below ~ 60 keV. The scintillator signals from GSO/BGO are read out by photomultiplier tubes located below the crystals.

The array of 16 “well”-units is surrounded by 20 crystal scintillators for active shielding, which are also used as a wide-field hard X-ray detector, referred to as the Wide-band All-sky Monitor (WAM). This can be used to detect and locate (as part of Interplanetary Gamma-Ray Burst Timing Network, or IPN) bright X-ray transients, GRB and solar flares.

The field of view of the HXD changes significantly with energy. Below ~ 100 keV the passive collimators define a $34' \times 34'$ square opening, which is significantly less

than in the *RXTE* HEXTE or in the *BeppoSAX* PDS and together with the active shielding ensures a very low background level, a key distinction of the HXD from the previous missions. The background rate of *Suzaku* is the lowest among the existing missions for most X-ray energies. The background is also very stable for *Suzaku*, so it can be modeled with better precision than for other collimating instruments (currently the uncertainty in background approaches a target value of 1%). Above 100 keV the fine collimators become transparent and the active shielding defines a $4.5^\circ \times 4.5^\circ$ field of view.

The HXD features an effective area of $\sim 160\text{cm}^2$ at 20 keV, and $\sim 260\text{cm}^2$ at 100 keV. The energy resolution is $\sim 3\text{keV}$ (FWHM) for the PIN diodes, and $7.6/\sqrt{E_{\text{MeV}}}\%$ (FWHM) for the scintillators, where E_{MeV} is energy in MeV. The HXD time resolution is $61\ \mu\text{s}$.

Part II

Observational study of a sample of galactic HMXBs

CHAPTER 4

1A 1118–61

4.1 Introduction

In this chapter I summarize my work on the accreting pulsar 1A 1118–61 for which for the first time since 1982 a major outburst was observed in January 2009. The main content of this chapter has been published in Doroshenko et al. (2010b); Staubert et al. (2011).

The hard X-ray transient 1A 1118–61 was first discovered during an outburst in 1974 by the *Ariel-5* satellite (Eyles et al. 1975). The outburst lasted for ~ 10 days and no significant flux could be observed afterwards. Pulsations with a period of 405.6 s were observed by Ives et al. (1975) and were initially interpreted as the orbital period of a system containing two compact objects. It was suggested by Fabian et al. (1975) that the observed period was due to a slow rotation of the neutron star. The optical counterpart was identified as the Be-star He 3–640/Wray 793 by Chevalier & Ilovaisky (1975) and classified as an O9.5IV-Ve star with strong Balmer emission lines and an extended envelope by Janot-Pacheco et al. (1981). The distance was estimated to be 5 ± 2 kpc (Janot-Pacheco et al. 1981). The classification and distance were confirmed by Coe & Payne (1985) by UV observations of the source. The X-ray spectrum of the pulsar was fitted with a power law with a photon index of $\Gamma \sim 1$, with a marginal spectral softening (to $\Gamma \sim 0.9$) during the peak of the outburst (significant at 1σ confidence level).

A second outburst occurred in 1992 and was observed by *CGRO/BATSE* (Coe et al. 1994). The measured peak pulsed flux was ~ 150 mCrab for the 20–100 keV energy range, similar to the 1974 outburst (Coe et al. 1994; Maraschi et al. 1976). It was followed by a period of elevated emission ~ 25 days after the main outburst. This lasted for ~ 30 days (see Coe et al. 1994, Fig.1). Pulsations with a period of 406.5 s were detected up to 100 keV and the pulse profile showed a single, broad peak, asymmetric at lower (20–40 keV) energies. A spin-up of 0.016 s/day was observed during the decay of the outburst. The pulsed spectrum was described with

a single-temperature optically-thin, thermal bremsstrahlung model with a temperature of (15.1 ± 0.5) keV for the main outburst and (18.5 ± 0.9) keV during the later phase of elevated emission. Multi-wavelength observations revealed a strong correlation between the H_α equivalent width and the X-ray flux, which allowed Coe et al. (1994) to conclude that expansion of the circumstellar disk of the optical companion was mainly responsible for the increased X-ray activity. The periastron passage would then trigger an outburst if enough matter had accumulated in the system. This conclusion was supported by the pulsations with a period of ~ 409 s, which were also detected in quiescence (Rutledge et al. 2007).

The source remained in quiescence until 2009 January 4, when a third outburst was detected by *Swift* (Mangano et al. 2009). Pointed observations with *Swift*/XRT allowed the detection of pulsations with a period of 407.68 ± 0.02 s reported later by Mangano (2009). The complete outburst was regularly monitored with *RXTE*. *INTEGRAL* observed a flaring activity ~ 30 days after the main burst (Leyder et al. 2009). *Suzaku* observed 1A 1118–61 twice, once during the peak of the outburst and also ~ 20 days later when the flux returned to its previous level (S. Suchy, in preparation).

We report here on the monitoring observations by *RXTE*. A timing analysis to determine the pulse period of the source and the rate of the observed strong spin-up was carried out. Pulse phase averaged spectral analysis revealed an absorption feature at ~ 55 keV, confirmed independently with *Suzaku* (S. Suchy, in preparation). We interpret this feature as a cyclotron resonance scattering feature (CRSF), which is observed for the first time in this source.

4.2 Observations

The outburst was observed by several X-ray missions. The source light-curve as observed by *Swift*/BAT with marked observation times by various satellites is presented in Fig. 4.1. The source flux peaked on 2009 January 14, (*Swift*/BAT count-rate 0.12 counts/s corresponding to ~ 500 mCrab in the 15–50 keV energy range) and slowly decreased afterwards. The source was regularly monitored with *RXTE* between January 10 2009, and February 4 2009, with a total exposure of 86 ks (PCA) and a dead-time-corrected live time of 29 ks (HEXTE-B). The data from the HEXTE-A detector were not used as it was not rocking during the entire observation and the background could not be properly estimated. The data were reduced with the HEASOFT version 6.8 and a set of calibration files version 20091202. The spectral modeling was performed with the XSPEC package version 12.5.1n. The energy range 3.5–25 keV was used for the PCA and 18–120 keV for the HEXTE spectra. Based on an analysis of recent Crab observations performed during the

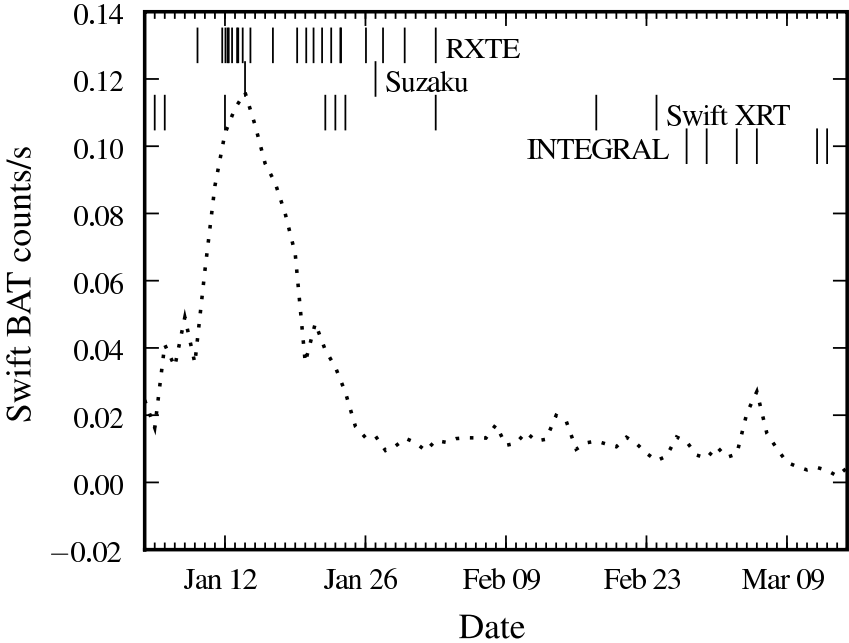


Figure 4.1: *Swift*/BAT daily light-curve of the outburst in 2009 January (dotted line). Observation times by various missions are indicated with vertical lines.

same time frame (2008 December 16, – 2009 March 11, proposal ID P94802), a systematic error of 0.5% was determined for the *PCA* data. No systematic error was required for the *HEXTE* data.

4.3 Results

4.3.1 Timing analysis

To determine the pulse period of 1A 1118–61 the *PCA* light-curve covering the complete observation in the 3–50 keV energy range was used. We searched for the pulse period and pulse period derivative using the phase connection technique (Staubert et al. 2009). Our best-fit results give $P_{\text{spin}}=407.719(9)$ s, $\dot{P}_{\text{spin}} = -4.6(2) \times 10^{-7} \text{ s s}^{-1}$, at a folding epoch of MJD 54841.62 (the uncertainties given in parenthesis are at 1σ confidence level and refer to the last digit given). The best-fit residuals for pulse arrival times are presented in Fig. 4.2. Note that the obtained parameters

characterize the pulse period evolution during the *RXTE* observations only and are not consistent with the pulse period value provided by Mangano (2009). This inconsistency is not surprising, because the luminosity and hence the accretion rate were significantly higher during the *RXTE* observations. The spin-up rate of the neutron star depends on the accretion rate, and therefore extrapolating the timing solution obtained close to the peak of the outburst (with a stronger spin-up) to the beginning of the outburst (where the spin-up rate is expected to be significantly lower) gives a longer pulse period than indeed was directly measured at the time. Note also that our solution does not account for the Doppler delays caused by orbital motion, because the parameters of the orbit are unknown and our data do not allow us to find an unambiguous solution for the orbit. The estimated value for an orbital period from “pulse period”–“orbital period” diagram Corbet (1986) lies in the 400–800 d range, which is much longer than the span of our data. The intrinsic spin-period evolution is expected to be complicated, so it is difficult to separate it from the effects of the orbital motion. Moreover, Coe et al. (1994) suggested that the orbit may be almost circular, and the outbursts may occur at any orbital phase, so a possible orbital period value derived from the comparison of outburst times is also potentially ambiguous.

Both the spin-up rate $\sim 0.04 \text{ s d}^{-1}$ and flux are somewhat higher (by a factor of ~ 2 – 3) than reported by Coe et al. (1994) for the previous outburst observed with *CGRO/BATSE*. The stronger spin-up measured for the current outburst is likely caused by the higher flux and consequently higher accretion rate (although it is difficult to directly compare BAT and BATSE fluxes, because BATSE measured only pulsed flux and the energy ranges are slightly different). A potential difference in the orbital phase during the two observations may also be responsible for the difference in the observed spin-up rate.

A set of pulse profiles in several energy ranges was constructed with the determined period. The pulse profile significantly changes with energy as shown in Fig. 4.3. At energies below 10 keV the pulse profile has two peaks. The secondary peak amplitude decreases towards higher energies, disappearing above 10 keV. A shoulder appears on the other side of the main peak at about the same energy. The pulse profile becomes single peaked and gradually more symmetric and narrow at higher energies. A similar behavior was observed previously with *CGRO/BATSE* (Coe et al. 1994). The pulse fraction, defined as $(A_{max} - A_{min}) / (A_{max} + A_{min})$ increases with energy in a similar way to other accreting pulsars, except for a drop at around 8 keV, where the second peak disappears (see Fig. 4.3).

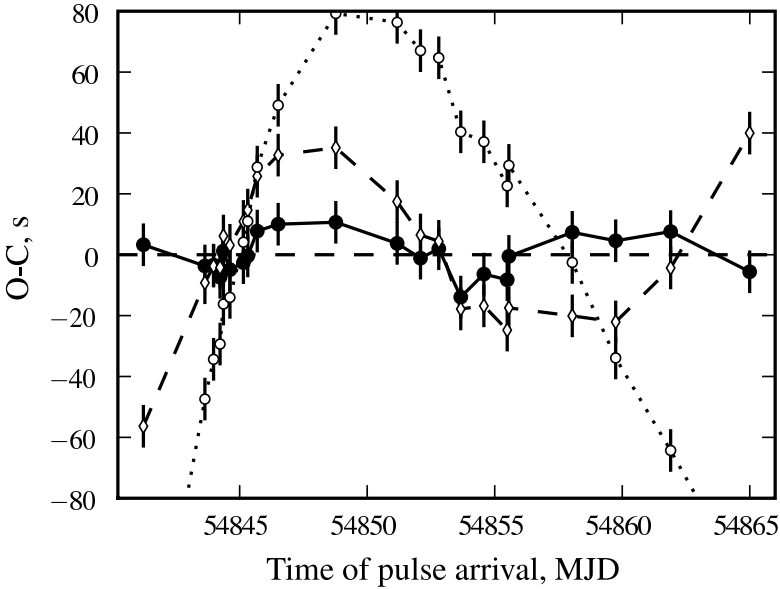


Figure 4.2: Best-fit residuals for the pulse arrival times determined using *RXTE* *PCA* light-curve (i.e. difference between pulse arrival times as observed (O) and as calculated (C) with an assumed pulse period and derivative). Solid, dashed and dotted lines correspond to fits including the pulse period derivatives up to second, first and none (constant period) respectively.

4.3.2 A hint on orbital period from timing

As I mentioned above, the potentially complicated spin-period evolution together with a limited span of the *RXTE* data makes it difficult to unambiguously identify the Doppler delays associated with the orbital motion, hence the orbital parameters. This is particularly the case if the system has a long orbital period and the outbursts are triggered only by the activity of the primary, which has been suggested previously and can not be excluded. On the other hand, an orbital solution can be found if we restrict ourselves to relatively short orbital periods (less than data-span, i.e. ~ 26 days) and assume that the outbursts are tied to some orbital phase.

Such a search was carried out by Staubert, Pottschmidt, Doroshenko, Wilms, Suchy, Rothschild, & Santangelo (2011) using the same *RXTE* pulse-arrival times

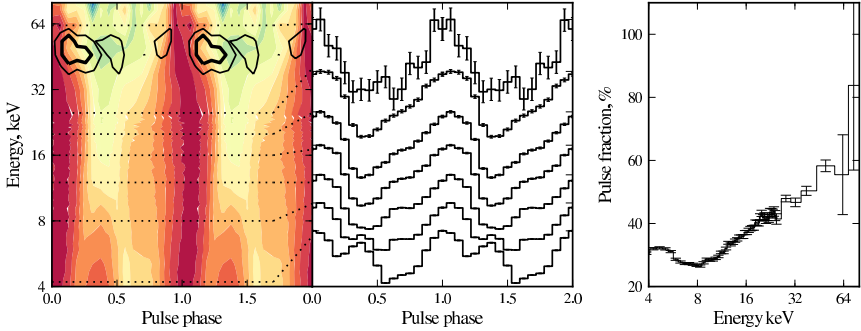


Figure 4.3: Normalized “pulse phase”-“energy” matrix using *PCA* (below 22 keV) and *HEXTE* (above 22 keV) data and pulse profile evolution with energy. A slice at a constant energy gives a background-subtracted pulse-profile normalized to unity at the pulse maximum (shown in the middle pane, the pulse profiles are shifted with respect to each other to avoid confusion). Contours represent 2σ and 3σ significance levels for the absorption feature in the residuals to the fit with *CompTT* model modified by photoelectric absorption and emission line at 6.4 keV. The pulse fraction, defined as $(A_{max} - A_{min}) / (A_{max} + A_{min})$ is shown as a function of energy in the right panel.

as above, and additionally the ones measured using the *CGRO BATSE* data obtained in the previous outburst (Coe et al. 1994).

First we attempted to fit the *RXTE* pulse arrival times assuming no 2nd pulse period derivative and a circular orbit which yielded $a \sin i \sim 55 \text{ lt s}$, $P_{\text{orb}} \sim 24 \text{ d}$, $T_{90} \text{ MJD} \sim 54845$, $P_{\text{spin}} \sim 407.7 \text{ s}$ and $\dot{P}_{\text{spin}} \sim -1.8 \times 10^{-7} \text{ s s}^{-1}$. Here I wish to stress once again, that the orbital period estimate can be only feasible if at least one full orbital cycle is covered by the data, so only periods shorter than 27 days were inspected. Switching to an eccentric orbit (best-fit eccentricity and longitude of periastron passage are $e = 0.10(2)$, $\Omega = 310(30)^\circ$) yielded a marginal statistical improvement (χ decreased from 21/15 dof to 16.4/15 dof) with chance probability of improvement of $\sim 22\%$, so we assumed the circular orbit from here on. Note, however that if we assume that the orbital period is short and the X-ray activity is associated with orbital motion, one does expect the orbit to be at least slightly eccentric. The final best-fit parameters are summarized in Table 4.1.

To determine the pulse-arrival times for the *BATSE* data I used the daily phase-

T_{90} , MJD	54845.4(1)
P_{orb} , d	24.0(4)
$a \sin i$, lt. s	55(1)
Ω^* , deg	310(30)
e^*	0.10(2)
P_{spin} s	407.655(1)
\dot{P}_{spin} s s ⁻¹	$1.8(2) \times 10^{-7}$

Table 4.1: Orbital elements, $P_{\text{spin}}, \dot{P}_{\text{spin}}$ at $T_{\text{ref}} = 54841.259391$. Parameters marked by * are not formally required by the fit (see text).

energy channel matrices for all eight detectors available in the HEASARC archive¹. I averaged the data from eight *BATSE* detectors and also from channels in the 20–40 keV energy range (with energy-channel conversion according to the provided calibration) to obtain a set of 12 pulse profiles (~ 1 d integration interval for each). For each resulting pulse-profile I then determined the arrival time in the same way as for the *RXTE* data via template matching (a high quality *RXTE* pulse profile in the same energy range was used as a template). The *BATSE* data only covers ~ 12 d, so we fixed all orbital parameters except for T_{90} to the ones estimated from the *RXTE* fit. This resulted in the best-fit solution with $P_{\text{spin}} = 406.53(2)$, $\dot{P}_{\text{spin}} = -3.1(9) \times 10^{-7}$ s s⁻¹, and T_{90} MJD = 48633.5 ± 2.5 .

Note, that the difference between the T_{90} values determined for *RXTE* and *BATSE* datasets corresponds to 258.83 orbital cycles assuming the orbital period of 24.0 d.

¹ftp://heasarc.gsfc.nasa.gov/compton/data/batse/pulsar/ground_folded/A1118-61

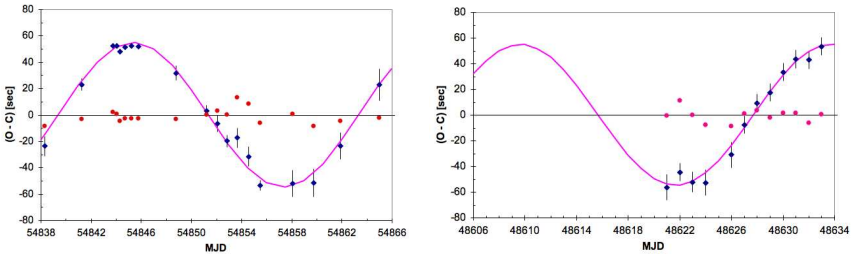


Figure 4.4: Best-fit residuals for the pulse arrival times determined using *RXTE* PCA (outburst January 2009, left) and *CGRO* *BATSE* data (outburst January 1992, right), assuming uniform spin-up and a circular orbit. Figure credit: Staubert et al. (2011).

If, on the other hand, we divide the separation by 259 cycles (closest integer multiple), we can determine a cycle length of 23.98(1) d when taking into account the uncertainties for T_{90} values. We can therefore potentially improve the accuracy for P_{orb} . The problem is, however, that the accuracy of P_{orb} from the *RXTE* timing measurements does not allow us to state that the separation is indeed 259 cycles. In fact, the uncertainty of 0.4 d implies the separation of 255 to 263 orbital cycles between the T_{90} measurements, so the inclusion of *BATSE* data does not allow to improve the P_{orb} at this point. On the other hand, the estimate of T_{90} from *BATSE* data agrees well with the *RXTE* result (yielding also a similar pulse period and spin-up rate), and will allow to refine the orbital solution as more observations of the source will become available.

Additional evidence for the ~ 24 d orbital period comes from the timing of the observed X-ray activity. Indeed, the three large outbursts observed from the source so far occurred on MJD 42407.0 (Eyles et al. 1975; Ives et al. 1975), MJD 48626.0 (Coe et al. 1994) and MJD 54845.4 (Mangano et al. 2009; Doroshenko et al. 2010b; Leyder et al. 2009) with an uncertainty of about 1 day in each case. Assuming that 24.0 d is indeed the orbital period, all three outbursts occurred close to the periastron and are separated by 259 orbits. Again, the uncertainty in P_{orb} allows the separations of 255 to 263 orbital cycles, so the timing of major outbursts also does not really allow to pin the exact value of the orbital period.

On the other hand, the outbursts in 1992 and 2009 were followed by periods of enhanced activity with peaks separated from the main outburst by ~ 24 d. Particularly Fig. 1 in Coe et al. (1994) shows that the main outburst was followed by several peaks, the largest of which are around ~ 26 d and ~ 49 d (the intensity of these peaks is by factor of 2 lower than that of the main outburst). In Fig. 4.5 we show the *RXTE ASM* daily light-curve in vicinity of the third big burst (of January 2009). Three peaks may be identified within ~ 70 d after the main outburst, none of which is exactly at periastron. The second and the third peaks are however close to it. The mean of the three separations starting with the main outburst is ~ 23 d.

A search for periodicities in a mission-long daily *RXTE ASM* light-curves reveals no significant periodicities, however the bins with count-rate above the average background level tend to cluster around phase 0, assuming the period of ~ 24 d (see Fig. 4.6). Note, that the rate of coincidences of small flares with phase zero is significantly higher if we assume that the separation between the large outbursts is 259 cycles (i.e. $P_{\text{orb}} = 24.012(3)$ d) than for other values in range from 255 to 263. This is definitively not a proof (otherwise it would be also evident from the periodogram), but is probably an indication that the separation may be indeed 259 cycles.

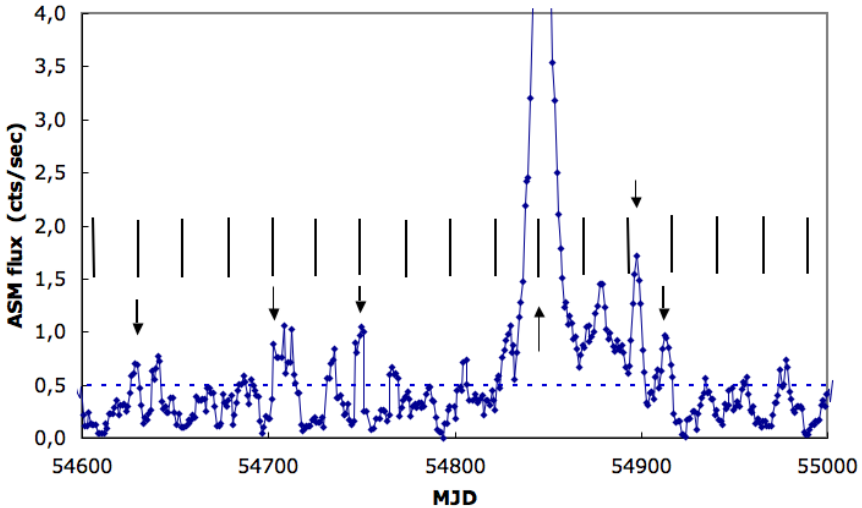


Figure 4.5: *RXTE* ASM light-curve in the vicinity of January 2009 outburst. Three minor flares separated by ~ 24 d can be identified after the main outburst. Figure credit: Staubert et al. (2011).

4.3.3 Spectral analysis

The longest observations of the January 2009 outburst were obtained during the maximum. I focused on these data for the spectral analysis (observations 94032-04-02-03 to 94032-04-02-10). The spectra of 1A 1118–61 in different energy ranges were previously described by power law and bremsstrahlung models (Maraschi et al. 1976; Coe et al. 1994). These models, however, do not describe our data adequately. Our results show that the broadband continuum of 1A 1118–61 can be well described by the FDCUT, NPEX, and CompTT models (Coburn et al. 2002; Mihara 1995; Titarchuk & Lyubarskij 1995), modified by photoelectric absorption and an iron emission line at ~ 6.4 keV.

All tested continuum models in their best-fit residuals show a prominent absorption feature at ~ 55 keV. The inclusion of an absorption line with a Gaussian optical depth profile leads to a significant improvement of fit quality in all cases (see Table 4.2). We interpret this absorption feature as a CRSF. This feature was detected in the spectrum of 1A 1118–61 for the first time. The observed energy of the feature is one of the highest known and corresponds to a magnetic field $B \sim 4.8 \times 10^{12}$ G (Harding & Lai 2006) in the scattering region. Preliminary phase-resolved analysis

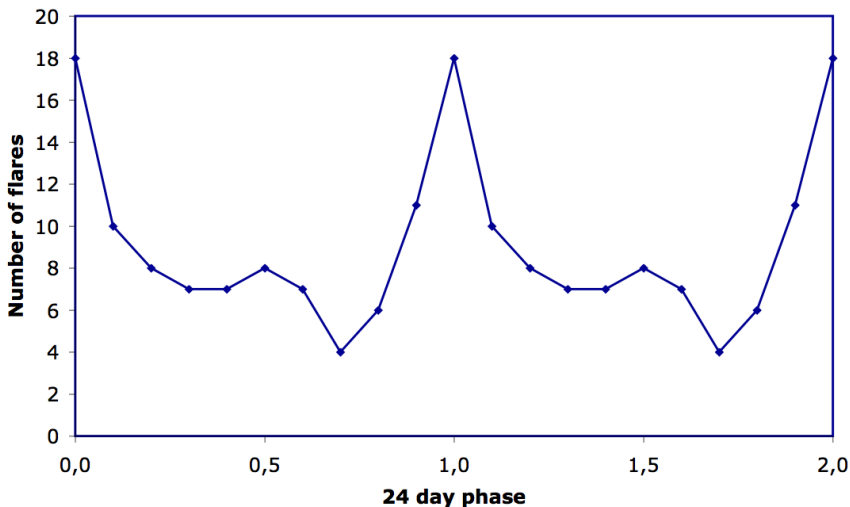


Figure 4.6: Frequency histogram of small flares with peak flux ≥ 0.5 cts/s (from smoothed daily *RXTE* ASM light-curve) as function of 24.012 d phase. Figure credit: Staubert et al. (2011).

has shown that the energy of the CRSF does not change significantly with the pulse phase (see Fig. 4.3).

The best-fit residuals of FDCUT and NPEX models show also a prominent emission line-like feature at ~ 8 keV. Similar features at different energies were reported for a number of sources (Coburn et al. 2002; Rodes-Roca et al. 2009 and references therein). Coburn et al. (2002) suggested that the employed phenomenological models for the continuum may be oversimplified for the real sources and hence may be responsible for this effect. On the other hand, Rothschild et al. (2006) suggested that the feature may be associated with the fluorescence copper line from the *Be/Cu* collimator of the *PCA* instrument. To clarify the situation a more detailed analysis of the *Suzaku* data is currently made and will be presented in a separate paper (S. Suchy et al, in preparation).

We found that the inclusion of an emission line with Gaussian profile may help to account for this feature and does not significantly affect other model parameters. The χ^2 substantially improves for fits with FDCUT and NPEX models, accordingly we included the line in all fits with those models. The energy and the width of the line were fixed at 8.04 keV and 0.01 keV, corresponding to the copper K_α line, as proposed by Rothschild et al. (2006).

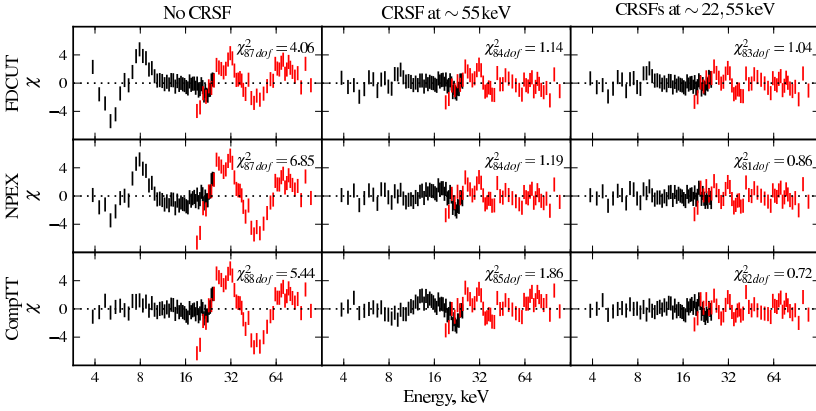


Figure 4.7: Best-fit residuals for various continuum models of 1A 1118–61. A line-like emission feature at ~ 8 keV was modeled with a narrow line with Gaussian profile as described in text. The absorption feature at ~ 23 keV was included for *PCA* only, to account for the similar residuals in the Crab spectrum (see text).

The fit may be slightly improved by the inclusion of an additional absorption feature at ~ 23 keV for the *PCA* data only. The investigation of the Crab residuals shows that a similar feature is also present in the *PCA* Crab spectrum (more than 99% significance with maximum likelihood ratio (MLR) and F tests (Protassov et al. 2002, p-value ~ 0.006). This is consistent with our 1A 1118–61 data, because the line is not required by the *HEXTE* data. On the other hand, a shallow fundamental line at 22 keV (with a first harmonic at 55 keV) could be more difficult to detect due to this instrumental feature using *PCA* data. A comparison of our *RXTE* results with the *Suzaku* observations will help to clarify the picture (S. Suchy et al, in preparation).

4.4 Conclusions

For the first time since 1992 a major outburst of the Be/X-ray binary 1A 1118–61 was observed in 2009 January with *RXTE*, following a trigger from *Swift/BAT*. Strong pulsations with a period of 407.72 s and a spin up of $-4.6 \times 10^{-7} \text{ s s}^{-1}$ were detected. A similar temporal behavior was observed with *CGRO/BATSE* during the previous outburst. The *RXTE* timing data also provides a hint on 24 d orbital periodicity.

Parameter	FDCUT	NPEX	CompTT _{fix23}	CompTT
$N_{\text{H}}^{(e)}$	$4.9^{+0.6}_{-0.6}$	$3.5^{+0.4}_{-0.4}$	$0.0^{+0.4}_{-0.0}$	$0.2^{+0.5}_{-0.2}$
$E_{22}^{(b)}$	$22.76^{(a)}$	$22.76^{(a)}$	$22.76^{(a)}$	$23.5^{+1.5}_{-0.8}$
$\sigma_{22}^{(b)}$	$1.8^{(a)}$	$1.8^{(a)}$	$1.8^{(a)}$	$4.6^{+1.9}_{-1.1}$
τ_{22}	$0.02^{+0.01}_{-0.01}$	$0.032^{+0.01}_{-0.01}$	$0.05^{+0.01}_{-0.01}$	$0.09^{+0.04}_{-0.02}$
$E_{\text{cyc}}^{(b)}$	$55.1^{+1.6}_{-1.5}$	$55.2^{+1.6}_{-1.5}$	$52.9^{+1.7}_{-1.4}$	$55.5^{+2.5}_{-2.1}$
$\sigma_{\text{cyc}}^{(b)}$	$10.4^{+1.1}_{-1.0}$	$11.8^{+1.2}_{-1.1}$	$10.2^{+1.5}_{-1.2}$	$13.3^{+2.2}_{-2.0}$
τ_{cyc}	$0.8^{+0.1}_{-0.1}$	$0.9^{+0.2}_{-0.1}$	$0.6^{+0.1}_{-0.1}$	$0.9^{+0.3}_{-0.2}$
Γ	$0.73^{+0.05}_{-0.06}$	Γ_1 $0.16^{+0.03}_{-0.03}$		
$E_{\text{cut}}^{(b)}$	$16.5^{+2.5}_{-2.9}$	Γ_2 -2.0	τ $6.0^{+0.1}_{-0.1}$	$6.0^{+0.2}_{-0.2}$
$E_{\text{fold}}^{(b)}$	$12.0^{+0.5}_{-0.5}$	$A_2^{(c)}$ $kT^{(b)}$ $0.16^{+0.02}_{-0.02}$ $7.9^{+0.3}_{-0.3}$	$T_0^{(b)}$ $1.47^{+0.02}_{-0.03}$ $7.2^{+0.2}_{-0.2}$	$1.44^{+0.04}_{-0.05}$ $7.7^{+0.4}_{-0.3}$
$E_{\text{Fe}}^{(b)}$	$6.5^{+0.1}_{-0.1}$	$6.45^{+0.07}_{-0.08}$	$6.4^{+0.02}_{-0.09}$	$6.4^{+0.02}_{-0.09}$
$\sigma_{\text{Fe}}^{(b)}$	≤ 0.4	≤ 0.3	≤ 0.3	≤ 0.3
$A_{\text{Fe}}^{(d)}$	3^{+3}_{-1}	$3.2^{+0.7}_{-0.7}$	$2.7^{+0.3}_{-0.3}$	$2.7^{+0.3}_{-0.3}$
$A_{\text{Cu}}^{(d)}$	2^{+2}_{-2}	$1^{+0.3}_{-0.3}$		
$A_{\Gamma,1,\text{CompTT}}^{(e)}$	22^{+2}_{-1}	$10.7^{+0.7}_{-0.7}$	$10.1^{+0.2}_{-0.2}$	$9.8^{+0.3}_{-0.3}$
$\chi_{\text{red/dof}}$	1.04/83	0.85/83	1.08/84	0.72/82

Table 4.2: Best-fit results for different models. An emission line (Cu) with energy and width fixed at 8.04 keV and 0.01 keV was added to FDCUT and NPEX models. All models include also an absorption like feature at ~ 23 keV for PCA to account for similar residuals seen in Crab spectra (with the line energy and width fixed to those obtained from Crab fits). For CompTT model the χ^2 may be improved by allowing the line parameters to vary (last column).

Notes. ^(a) Parameter frozen during the fit. ^(b) [keV] ^(c) [10^{-2} ph keV $^{-1}$ cm $^{-2}$ s $^{-1}$] ^(d) [10^{-3} ph cm $^{-2}$ s $^{-1}$] ^(e) [atoms cm $^{-2}$]

A broadband spectrum of the source was obtained for a first time, and an absorption feature at ~ 55 keV, interpreted as a CRSF was detected. The inclusion of the feature significantly improves fit results with all applied continuum models and its energy does not depend significantly on the model used.

CHAPTER 5

GX 301–2

This part of the thesis is dedicated to the observational study of three galactic accreting pulsars, namely GX 301–2, Vela X–1 and 1A 1118–61. I also discuss how the interpretation of the observed properties may help to constrain the magnetic field of a neutron star in those sources. The content of this part is mostly based on several papers published and submitted during the work on the thesis, i.e. Doroshenko et al. (2010a,b); Staubert et al. (2011); Doroshenko et al. (2011b,a).

5.1 Introduction

GX 301–2 (also known as 4U 1223–62) is a high-mass X-ray binary system, consisting of a neutron star orbiting the early B-type optical companion Wray 977. The neutron star is a ~ 680 s X-ray pulsar (White et al. 1976), accreting from the dense wind of the optical companion. The wind’s mass-loss rate of the optical component is one of the highest known in the galaxy: $\dot{M}_{\text{loss}} \sim 10^{-5} M_{\odot} \text{yr}^{-1}$ (Kaper et al. 2006). Because the terminal velocity of the wind is very low ($w_0 \sim 300 - 400 \text{ km s}^{-1}$, Kaper et al. 2006), the accretion rate is high enough to explain the observed luminosity of $L_X \sim 10^{37} \text{ erg s}^{-1}$. The distance to the source is estimated to be between 1.8 ± 0.4 kpc (Parkes et al. 1980) and 5.3 kpc (Kaper et al. 1995), depending on the spectral classification of Wray 977. The latest estimate is 3 kpc (Kaper et al. 2006). The orbit is highly eccentric with an eccentricity of ~ 0.5 and an orbital period of ~ 41.5 d (Koh et al. 1997). The absence of X-ray eclipses, despite the large radius ($R \sim 43 R_{\odot}$) of Wray 977 (Parkes et al. 1980), constrains the inclination angle in the range $44 - 78^{\circ}$ with a best-fit value of $i \sim 66^{\circ}$ (Kaper et al. 2006; Leahy & Kostka 2008). The source exhibits regular X-ray flares about 1–2 d before the periastron passage (orbital phase ~ 0.95). There is also an indication of a second flare at orbital phase ~ 0.5 (Koh et al. 1997). Several hypotheses have been proposed to explain the observed orbital lightcurve, including a circumstellar disk (Koh et al. 1997) and a quasi-stable accretion stream (Leahy & Kostka 2008). Similar to other wind accreting systems, the pulse period behavior of GX 301–2 on short time scales is

described well by a random walk model (de Kool & Anzer 1993). GX 301–2 exhibits a long-term pulse period evolution as well. The observed pulse period remained ~ 700 s until 1984 when it began to decrease during a rapid spin-up episode observed by *BATSE* (Koh et al. 1997; Bildsten et al. 1997). The spin-up trend reversed in 1993 (Pravdo & Ghosh 2001) and ever since the pulse period has been increasing (La Barbera et al. 2005; Kreykenbohm et al. 2004).

The X-ray spectrum of the GX 301–2 is rich in features. The lower energy range is subject to heavy and variable photoelectric absorption (White et al. 1976). As shown by Kreykenbohm et al. (2004) and La Barbera et al. (2005), a partial covering model with two absorption columns is required to describe the spectrum. There is a complex of iron lines at 6.4 to 7.1 keV (Watanabe et al. 2003). A high-energy cutoff at ~ 20 keV, together with a deep and broad cyclotron resonance scattering feature (CRSF) at 30–45 keV, is present at higher energies (Makishima & Mihara 1992; Orlandini et al. 2000; Kreykenbohm et al. 2004; La Barbera et al. 2005). The CRSF is highly variable with pulse phase, and it exhibits interesting correlations with the continuum parameters (Kreykenbohm et al. 2004).

The nature of accreting pulsars with long pulse periods is still poorly understood. Because of the low moment of inertia of the neutron star, the accelerating torque of the accreted matter can spin up a neutron star very efficiently. Braking torques are then required to explain the observed long pulse periods. It is commonly assumed that the observed pulse period is determined by the equality of torques affecting the neutron star or relaxes to the value determined by this equality. Braking torques are generally associated with the coupling of the neutron star’s magnetic field with the surrounding plasma. The drag force depends on the relative linear speed of the field lines at a certain effective radius, which in turn depends on the magnetic field strength. The efficiency of braking decreases for slowly rotating and weakly magnetized neutron stars so a strong field (up to 10^{15} G, Shakura 1975) is required to spin down a slowly rotating accreting X-ray pulsar even further. This results in an apparent contradiction with field estimates obtained from the CRSF centroid energy, which is $B \sim (E_{\text{cyc}} \text{keV} / 11.57) \times 10^{12} \text{G} \sim 4 \times 10^{12} \text{G}$ in the case of GX 301–2 and in the same order of magnitude as for other sources.

We suggest that this contradiction may be resolved if the line-forming region resides in an accretion column of significant height (Basko & Sunyaev 1976), comparable to the neutron star radius. We investigate this hypothesis using *INTEGRAL* and *BATSE* observations to study the spectral and timing properties of GX 301–2.

5.2 Observations and data selection

We rely on data from *IBIS* (the *ISGRI* layer) and *JEM-X*, because of limited *SPI* sensitivity for variable sources. Among the *INTEGRAL* instruments, *IBIS* has the largest field of view and, therefore, the highest probability of observing the source. We used a total of 554 available public pointings with GX 301–2 within the *IBIS* half-coded field of view for the pulse period determination (i.e. for Table 5.3.1). These data include a long observation that covers $\sim 60\%$ of the orbital cycle and is long enough to allow binary ephemeris estimation (283 pointings in *INTEGRAL* revolutions 322–330). Three dedicated observations (see Table 5.3.2) were also performed during the pre-periastron flare and were used to study the spectrum of the source.

We also used results provided by the *ASM/RXTE* teams at *MIT* and at the *RXTE SOF* (Science Operation Facility) and *GOF* (Guest Observer Facility) at *NASA's GSFC* (Goddard Space Flight Center) and *CGRO BATSE* pulsar *DISCLA* histories data by Bildsten et al. (1997) to study the long-term evolution of the spin period.

5.3 Results

5.3.1 Timing analysis

To derive the intrinsic pulse period of the source, the lightcurve must be corrected for Doppler delays due to the orbital motion of the source and the satellite. Phase connection or pulse time arrival analysis is a precise timing technique, based on measuring arrival times of individual pulses or groups of pulses (Staubert et al. 2009). It allows to determine the Doppler delays and therefore the orbital parameters of the system. A fixed phase of the pulsating flux from a pulsar is observed at times (Nagase et al. 1982):

$$T_n = T_0 + P_0 n + \frac{1}{2} \dot{P} P_0 n^2 + \frac{1}{6} \ddot{P} P_0^2 n^3 + \dots \quad (5.1)$$

$$\dots + a \sin(i) F_n(e, \omega, T_{\text{PA}}, \theta)$$

referred to as Time Of Arrival (TOA), where P_0 , \dot{P} , and \ddot{P} are the intrinsic pulse period and its time derivatives at the initial epoch T_0 . The last term represents the Doppler delays due to the orbital motion as a function of the Kepler parameters for an eccentric orbit. These are the projected semi-major axis $a \sin i$ in light seconds (i is the orbit inclination), the eccentricity e , the longitude of the periastron ω , time of periastron passage T_{PA} , and the mean anomaly $\theta = 2\pi(T - T_{\text{PA}})/P_{\text{orb}}$. To obtain a solution for the unknown pulse and orbital parameters, a number of measurements of T_n (for known n) must be obtained. Usually only $T_{n,\text{obs}}$ is measured, while n

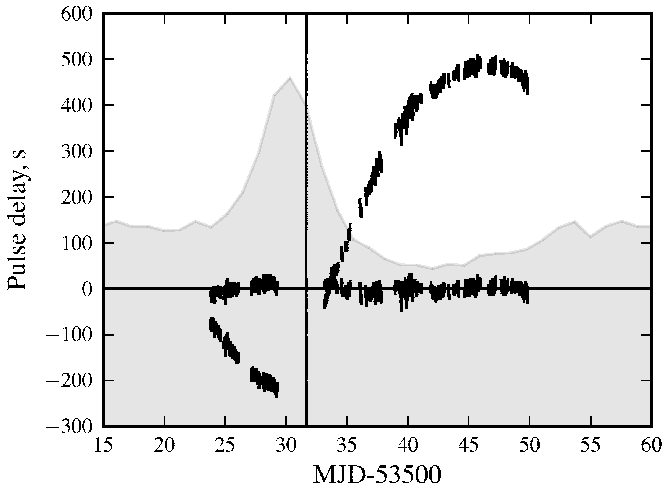


Figure 5.1: Time delays of pulse arrival times induced by the orbital motion. Changes due to the intrinsic variation of the spin period are subtracted. Best-fit residuals are also shown. The best-fit periastron passage time is marked with a vertical line. The folded *RXTE ASM* orbital profile with the pre-periastron flare is plotted in gray.

must be found during the fitting procedure to obtain a self-consistent solution. The orbital period may be estimated either directly as one of the free parameters or by comparing periastron passage times of subsequent cycles (i.e. similarly to the pulse period). The latter method is more precise (see e.g. Staubert et al. 2009).

Using archival *ISGR1* observations and the standard *OSA 6.1* software provided by *ISDC*¹, we constructed lightcurves with 20 s time bins in the energy range 20–40 keV and determined the pulse arrival times (each pulse profile obtained by folding ~ 20 individual pulses) for data from revolutions 322–330 using a technique similar to the one by Koh et al. (1997). This is the only *INTEGRAL* observation to cover a significant fraction of the orbital cycle, and it allows the estimation of binary parameters. We then used Eq. 5.1 to determine P , \dot{P} and T_{PA} . The other orbital parameters were fixed to values reported by Koh et al. (1997). Our best-fit values are $P_{\text{pulse}} = 684.1618(3)$ s, $\dot{P}_{\text{pulse}} = 4.25(22) \times 10^{-8}$ s s⁻¹ at the epoch 53523.8, and $T_{\text{PA}} = 53531.63(1)$ MJD. All uncertainties are at 1σ confidence level unless otherwise stated. Pulse delays from the orbital motion and residuals of the best-fit are plotted in Fig. 5.1. Comparing our T_{PA} value with the historical values reported by White & Swank (1984), Sato et al. (1986) and Koh et al. (1997)

¹<http://isdc.unige.ch>

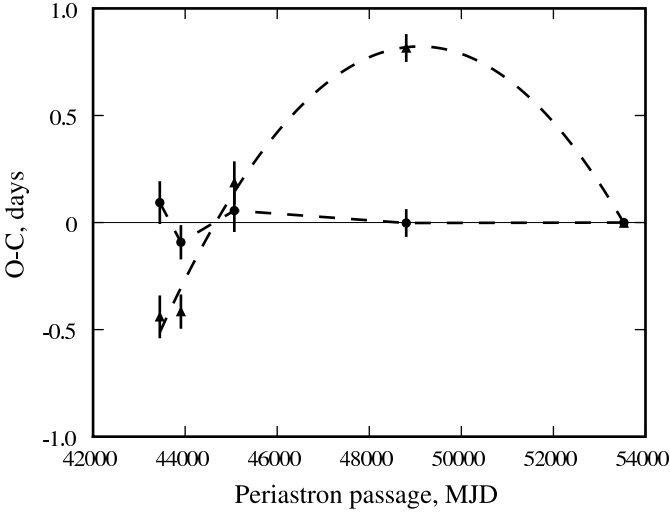


Figure 5.2: Residuals to fit over periastron passage times for orbital period with (circles) and without (triangles) inclusion of the orbital period derivative.

allows estimation of the orbital period. Inclusion of our measurement requires introducing of a secular change to the orbital period. The quality of the fit improves significantly². The residuals to fit both with and without inclusion of a secular change are plotted in Fig. 5.2. Our best fit values are $P_{\text{orb}} = 41.506 \pm 0.003$ d and $\dot{P}_{\text{orb}} = (-3.7 \pm 0.5) \times 10^{-6} \text{ s s}^{-1}$ at the reference time reported by Sato et al. (1986): $T_{\text{PA},0} = 43906.06 \pm 0.11$. This estimate is consistent with the direct measurements of the orbital period both by Sato et al. (1986) and by Koh et al. (1997).

It should be emphasized that the commonly used value of $P_{\text{orb}}=41.498$ d by Koh et al. (1997) was obtained by comparison of the T_{PA} values as well (the authors compared their value to that by Sato et al. (1986) under the assumption of a constant orbital period). On the other hand, all published measurements including ours are consistently described when an orbital period derivative is included. For the time of the *INTEGRAL* observation, the predicted orbital period is ~ 41.472 d. The periastron passage time measured with the orbital period value fixed to this prediction does not change significantly: $T_{\text{PA}} = 53531.65 \pm 0.01$ MJD.

Because the pre-periastron flare in the orbital lightcurve of the source is associated with the periastron passage time, an additional check can be made using the

²The χ^2 drops from 52 to 0.52 with an F-test significance of $\sim 98\%$

MJD _{obs}	Period, s.	MJD _{obs}	Period, s.
52833.5	681.33 ± 0.04	53538.0	684.59 ± 0.12
53088.0	683.42 ± 0.07	53541.6	684.4 ± 0.04
53525.9	683.9 ± 0.1	53545.6	684.27 ± 0.04
53528.5	684.19 ± 0.16	53549.4	684.15 ± 0.05
53529.7	684.15 ± 0.44	54111.9	684.62 ± 0.06
53535.0	684.73 ± 0.05	54277.6	685.15 ± 0.07

Table 5.1: Pulse period values obtained with archival *INTEGRAL* data. An updated ephemeris was used to correct the lightcurve for binary motion. The error is estimated as 10% of the width of the peak in the periodogram.

long-term lightcurve of the source. We split a 10-year long *RXTE ASM* barycentered daily lightcurve of GX 301–2 (all bands combined) into parts of ~ 5 orbital cycles in length and folded each part with the orbital period $P_{\text{orb}}=41.498$ d to obtain a series of orbital profiles. The relative phase shifts and the associated orbital periods were then determined in the same way as for the pulse period. The best-fit value for a constant period is $P_{\text{orb}} = 41.482 \pm 0.001$ d. The mean value of the orbital period, calculated using P_{orb} and \dot{P}_{orb} obtained above, is consistent with the observed value at the time of the *ASM* observations, although an orbital period derivative is not formally required by the *ASM* data alone.

A set of pulse period measurements with epoch folding was performed with the updated ephemeris. We grouped all available *INTEGRAL* data by the observation time by the “k-means” clustering algorithm (MacQueen 1967). The number of groups was chosen such that the mean number of X-ray pulses within one group was ~ 50 . We searched for pulsations in each of the groups with epoch folding (Larsen 1996). A few groups where no pulsations were found because of insufficient statistics were rejected afterwards. The results are listed in Table 5.3.1 and plotted in Fig. 5.3 together with historical values for clarity. On average, GX 301–2 continues to spindown after the first *INTEGRAL* observation of the source.

5.3.2 Spectral analysis

The observations listed in Table 5.3.2 were used to obtain the broadband spectrum of the source. Since all three observations were made at almost the same orbital phase, we combined all data to have better statistics. We used the standard OSA 6.1 pipeline³ for spectral extraction. A systematic error of 1% for all *ISGRI* and of 2% for all *JEM-X* spectra was assigned as suggested in the OSA documentation.

³available at <http://isdc.unige.ch>

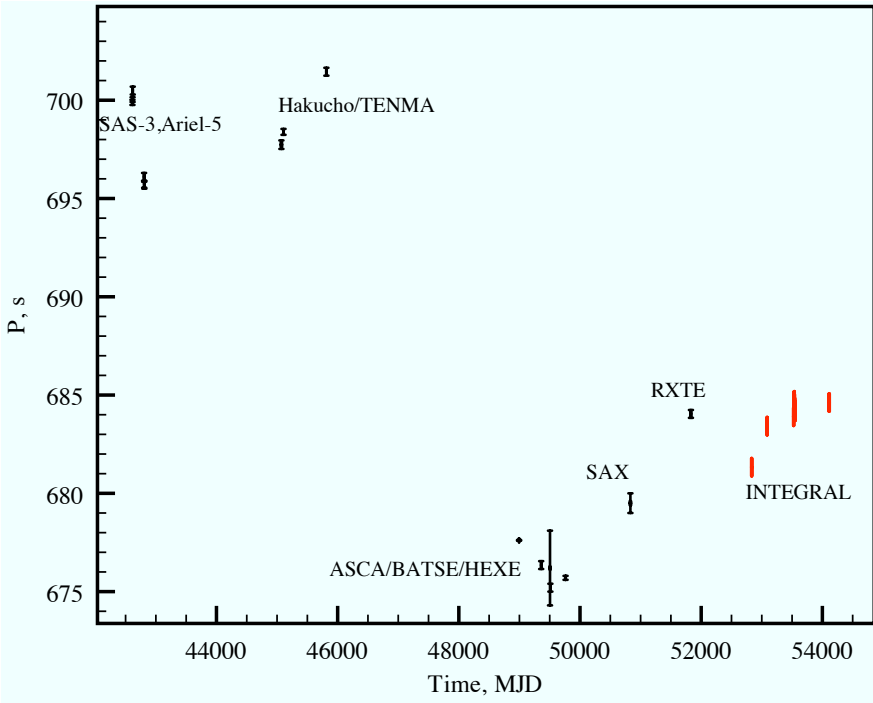


Figure 5.3: Long-term pulse period evolution of GX 301-2.

Spectra of X-ray pulsars are usually described with phenomenological multi-component models. The continuum of GX 301-2 has been modeled with a cut-off power law modified at low energy by photoelectric absorption. An iron emission K_{α} line has been also observed. In fact, there is a complex of iron lines between 6.4

<i>INTEGRAL</i> science window	MJD of observation	Orbital phase	Exposure, ksec	Rate cts s ⁻¹
05180027-66	54110.5-12.2	0.96-1.02	91.66	98
05730048-60	54276.3-76.9	0.95-0.97	31.98	163
05740012-40	54277.6-78.9	0.99-1.02	69.38	76

Table 5.2: Pointed observations of GX 301-2 by *INTEGRAL*, with an updated ephemeris to calculate the orbital phase (rate is in 20-60 keV energy range using the *ISGRI* light-curve).

and 7.1 keV (Watanabe et al. 2003; La Barbera et al. 2005). These are not resolved with *JEM-X*. We therefore used a simple Gaussian-shaped profile with larger width to formally describe this feature.

The photoelectric absorption of the source’s spectrum is strongly variable, and at least two absorption columns are identified. Part of the X-ray emission is thought to be strongly absorbed close to the neutron star, while all emission from this region is also subject to absorption in the overall stellar wind of the optical companion. A model describing this physical situation is the absorbed partial covering model (Kreykenbohm et al. 2004; La Barbera et al. 2005).

From a more physical point of view, the spectrum of an accreting pulsar is believed to be mainly the result of a Comptonization processes of thermal photons in the accretion column and in the neutron star atmosphere. The emerging spectrum depends on the optical depth and generally has a power-law shape, with a cut-off at an energy corresponding to the temperature of the Comptonizing medium ($\sim 3kT_e$, Sunyaev & Titarchuk 1980). Phenomenological models aim at describing this shape regardless of the optical depth. For GX 301–2 two models have been used in literature. La Barbera et al. (2005) adopted a modified “high energy” cut-off, while Kreykenbohm et al. (2004) used a so-called Fermi-Dirac cut-off. As discussed in Doroshenko et al. (2008), both models describe the *INTEGRAL* data well with parameters close to the published ones. It is somewhat difficult, however, to interpret these results from a physical point of view. We therefore focus here on a different description.

One of the first physical models to describe Comptonization spectra was proposed by Sunyaev & Titarchuk (1980). Compton scattering in strong magnetic field is a more complicated problem (Lyubarsky 1986; Meszaros & Nagel 1985b), but for the saturated case ($\tau_e \gg 1$) a blackbody-like spectrum is formed in both cases (Lyubarsky 1986). The Sunyaev & Titarchuk (1980) model is included in the standard *XSPEC* distribution as *COMPST*. Free parameters include the electron temperature of the medium T_e , optical depth τ_e , and normalization A_{st} . We used this model because it contains the least number of free parameters and produces identical results to more complex models for GX 301–2. The pulse-phase averaged spectrum was extracted and fitted with the partially absorbed *COMPST* model. The fit results are listed in Table 5.3.2. Since the optical depth of the Comptonizing medium is very high, we verified that a simple black body model provides an equally good description of the data. The unabsorbed source flux in the same energy range is $\sim 1.8 \times 10^{-8}$ erg cm $^{-2}$ s $^{-1}$ in both models.

A CRSF was necessary in the fit. This was included assuming a Gaussian-shaped profile. With the inclusion of the line the χ^2_{red} dropped from ~ 3.8 (depending on the model) to values around 1.2 (see Table 5.3.2).

Parameter	Absorbed blackbody	Absorbed <i>COMPST</i>
$N_{H,1}$ [10^{22} atoms/cm ²]	≤ 4	≤ 4
$N_{H,2}$ [10^{22} atoms/cm ²]	$178.3^{+6.9}_{-6.7}$	$175.6^{+10.4}_{-9.9}$
c_F	$0.798^{+0.008}_{-0.008}$	$0.78^{+0.01}_{-0.01}$
E_{gabs} [keV]	$45.8^{+1.7}_{-1.6}$	$45.9^{+1.8}_{-1.6}$
σ_{gabs} [keV]	$15.0^{+1.8}_{-1.7}$	$15.1^{+2.0}_{-1.8}$
d_{gabs}	$57.45^{+23.66}_{-17.89}$	$57.93^{+25.93}_{-18.19}$
$A_{bb/st}$	$0.31^{+0.06}_{-0.04}$	$0.35^{+0.09}_{-0.05}$
T_e [keV]	$5.1^{+0.2}_{-0.2}$	$5.1^{+0.3}_{-0.2}$
τ_e	–	$42.3^{+4.8}_{-3.9}$
E_{Fe} [keV]	$6.32^{+0.02}_{-0.02}$	$6.32^{+0.02}_{-0.02}$
σ_{Fe} [keV]	$0.36^{+0.04}_{-0.05}$	$0.38^{+0.04}_{-0.04}$
χ^2/dof	1.18/149	1.17/148

Table 5.3: Fit results for phase averaged spectra. Uncertainties are expressed at 90% confidence level.

5.4 Discussion

5.4.1 Orbital period evolution

Our estimate of the rate of orbital period decay $\dot{P}_{\text{orb}}/P_{\text{orb}} \simeq -3.25 \times 10^{-5} \text{ yr}^{-1}$ exceeds that of other known sources at least by one order of magnitude. Previous detections include Cen X–3 with $\dot{P}_{\text{orb}}/P_{\text{orb}} = -1.738 \times 10^{-6} \text{ yr}^{-1}$ (Bagot 1996, and references therein), SMC X–1 with $\dot{P}_{\text{orb}}/P_{\text{orb}} = -3.36 \times 10^{-6} \text{ yr}^{-1}$ and Her X–1 with $\dot{P}_{\text{orb}}/P_{\text{orb}} = -1.0 \times 10^{-8} \text{ yr}^{-1}$ (Staubert et al. 2009). GX 301–2 is very different from all these systems. It is younger and has a highly eccentric orbit, while other systems have almost circular orbits. Both real and apparent changes in the orbital period are expected to be greater for an eccentric orbit.

We measured the rate of decay of the orbit by comparing the times of several periastron-passages. Those are determined by fitting the observed pulse delays as a function of the orbital phase, and they may in principle be correlated with other model parameters, particularly with the longitude of periastron due to apsidal motion. The span of our data used for the pulse time arrival analysis does not allow both T_{PA} and ω to be reliably constrained simultaneously. All published estimates of ω are also consistent with each other within uncertainties, but still we cannot rule out that apsidal motion contributes to the observed apparent change in the orbital period.

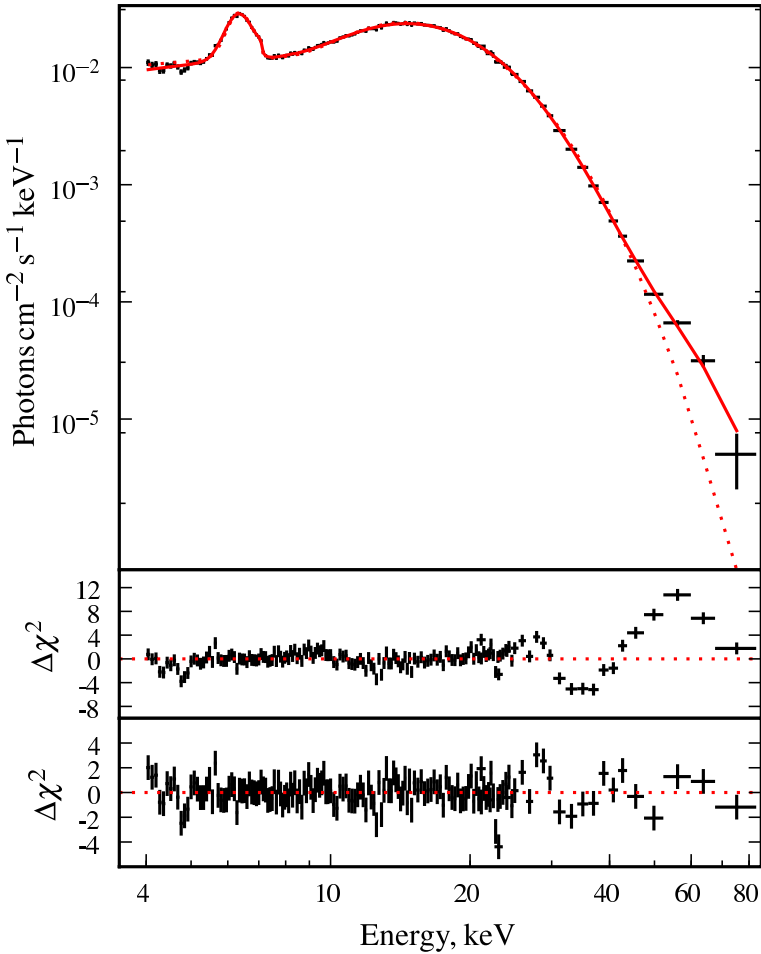


Figure 5.4: Unfolded spectrum and residuals for the *COMPST* model without (dotted line and second panel) and with the inclusion (solid line and bottom panel) of a CRSF at ~ 46 keV, using *ISGRI* (20-80 keV) and *JEM-X* (4-20 keV) data.

The eccentric orbit and very strong mass transfer in the system (the mass loss by the optical component is $\dot{M}_{\text{loss}} \sim 10^{-5} M_{\odot} \text{ yr}^{-1}$, Kaper et al. 2006) suggest that some intrinsic changes in the orbital period are also expected.

The optical companion is much heavier than the neutron star and contributes almost nothing to the orbital angular momentum of the system. Direct mass loss via the stellar wind by the optical companion therefore does not lead to significant loss of the angular momentum. The optical star becomes less massive, leading to a longer orbital period (Hilditch 2001), which is the opposite of what is observed, although the rate of such change is very low.

To explain the decrease in the orbital period, one has to assume that the material carrying the angular momentum away must come from the vicinity of the neutron star, since it is the neutron star's orbital motion that is responsible for the bulk of the angular momentum in the system. Two mechanisms could be responsible for the loss of angular momentum. First, the material of the stellar wind that is streaming by the neutron star can feel the gravitational pull of the moving neutron star. Only a fraction of this material is eventually accreted onto the neutron star, and the larger part is leaving the binary system and carrying some angular momentum away, since the interaction with the neutron star changed its trajectory. Second, before the matter is accreted onto the neutron star, it interacts with the neutron star's magnetosphere (leading to spin-up and spin-down of the neutron star, as will be discussed below). However, the interaction with the magnetosphere may also lead to a magnetically driven outflow of material (Illarionov & Kompaneets 1990; Lovelace et al. 1999; Klochkov et al. 2009), again carrying angular momentum away. In addition, tidal coupling of the rotational frequency of the optical star with the orbital frequency could play some role, although estimates by Leahy & Kostka (2008) and Hilditch (2001) suggest that, despite the high eccentricity, this is probably not very efficient. The details of the mass transfer and angular momentum loss in this system are not understood well, and more observations are required to secure the rate of change in the orbital period.

5.4.2 *Torque balance and magnetic moment of the neutron star*

Two rapid spin-up episodes observed by Koh et al. (1997) indicate that a long lived accretion disk may sometimes form in GX 301–2. Both episodes are characterized by an increased source flux, which implies an increased accretion rate. The infrequent occurrence of such episodes argues against the hypothesis that they are triggered by tidal overflows at periastron (see Layton et al. 1998) and suggests that mass loss episodes of Wray 977 may be responsible for them (Koh et al. 1997). As concluded by Koh et al. (1997), the pulse period decrease in 1984–1992 can be attributed entirely to similar spin-up episodes, while most of the time the neutron star accretes from the wind, and no net change of the pulse period is observed. It is therefore important to understand the torque balance in this case. This is why we focus on wind-accretion models.

The torque balance, hence the rotational frequency derivative, depends on \dot{M} (see below), so one has to investigate this dependence to study the rotational dynamics. Since the longest continuous pulse frequency monitoring campaign (~ 10 yr) for this source was carried out with *BATSE* (Bildsten et al. 1997), we used the data products available at the *CGRO* mission web-page.⁴ The pulse frequency and pulse frequency derivative histories are provided for the entire *BATSE* lifetime. Both were determined for a set of ~ 4 d intervals using the phase connection technique assuming the ephemeris by Koh et al. (1997) for binary-motion corrections (see Bildsten et al. 1997; Koh et al. 1997 for details). The corresponding *BATSE* pulsed flux in the 20–50 keV energy range, averaged over the interval is also provided.

Contrary to the report by İnam & Baykal (2000), a correlation between the angular frequency derivative ($\dot{\omega} = 2\pi\dot{\nu}$) and the flux (see Fig. 5.5) was found (Pearson correlation coefficient 0.96, null hypotheses probability 8×10^{-6}).

The discrepancy between our findings and the ones reported in İnam & Baykal (2000) lie in their method of estimating frequency derivatives. With the *BATSE* data set that we used, İnam & Baykal (2000) estimate pulse frequency derivatives by grouping the provided frequency values in intervals of ~ 30 d and averaging between the left and right frequency derivatives calculated using these values for each interval. This approach is incorrect because it assumes that the frequency values provided by Koh et al. (1997) alone characterize the average pulse frequency during the corresponding observation time, while the average pulse frequency also depends on the frequency derivative included in the fit and on the observation length. For this approach to work it is required to remove the frequency derivative in the fit for the pulse arrival times in the raw *BATSE* data, which was not done by İnam & Baykal (2000). There is also a second point to question in their analysis. To obtain values of the first derivative, İnam & Baykal (2000) use frequency values on intervals of ~ 30 d, comparable to the orbital period of the system. Both the pulse frequency and the flux are known to change on much shorter time scales in GX 301–2. Averaging on such a long interval smoothes out most of the flux and pulse frequency variations, making it difficult to find the correlation between the two quantities.

On the other hand, we used $\dot{\omega}$ and flux values directly measured for each observation with phase connection. The points in Fig. 5.5 were obtained by averaging the provided frequency derivative values of points with flux in a given range. The standard error was used as an uncertainty estimate. We excluded both spin-up episodes observed by Koh et al. (1997) (i.e. MJD 48440–48463 and MJD 49230–49245) and

⁴ftp://heasarc.gsfc.nasa.gov/compton/data/batse/pulsar/histories/DISCLA_histories-gx301m2_psr_hist.fits

intervals where pulsations were not detected reliably (see Koh et al. 1997) from the further analysis.

To investigate the accretion models and compare them to the data, we need to express the accretion rate as a function of the count rate, not a trivial task. The conversion depends on the distance, the radiative efficiency of accretion, and the beaming factor. We assumed that the mean source flux derived from the spectra obtained with the *INTEGRAL* pointed observations corresponds to the mean *BATSE* count-rate at the same orbital phase. Then we assumed a conversion factor of $10^{37} \text{ erg s}^{-1} \simeq 10^{17} \text{ g s}^{-1}$ which corresponds to a radiative accretion efficiency of $\sim 10\%$, $L_x \sim 0.1 \dot{M} c^2$ to estimate the accretion rate. The distance to the source is uncertain so the derived value should account for the spread of the estimates (1.4–5.3 kpc). The accelerating torque K_+ , hence the torque balance, depends significantly on the efficiency of angular momentum transfer k_w and on the relative velocity of the neutron star and the wind.

The orbit of GX 301–2 is eccentric, so the orbital speed of the neutron star changes significantly along the orbit. The wind, on the other hand, is also accelerated from the sound speed at the surface of Wray 977 ($\sim 10 \text{ km s}^{-1}$) to a terminal velocity of 300–400 km s^{-1} at infinity (Castor et al. 1975):

$$v_w(r) = v_0 + (v_\infty - v_0)(1 - R_*/r)^\beta \quad (5.2)$$

where v_0 is the velocity at the surface of the star close to the sound speed, v_∞ the terminal wind speed, and $\beta \sim 1$ for O-type stars. Radial and tangential velocity components of the neutron star as function of orbital phase θ are

$$v_r = \sqrt{\frac{\mu}{p}} e \sin \theta, \quad v_t = \sqrt{\frac{\mu}{p}} (1 + e \cos \theta) \quad (5.3)$$

where $\mu = G(M_{\text{opt}} + M_{\text{NS}})$, $p = a(1 - e^2)$, e is the eccentricity, and $a \sim 1.2 \times 10^{13} \text{ cm}$ is the semi-major axis for $i = 66^\circ$. It turns out that, while both the orbital speed of the neutron star and the wind speed are strong functions of the orbital phase, the relative velocity varies only by a factor of 2 (see Fig. 5.6). Each flux bin in Fig. 5.5 contains measurements performed at different orbital phases. We then calculated an average relative speed for each flux bin to properly estimate R_A . It turns out, however, that the relative speed varies only within 5% and consequently R_A does not change significantly (see Fig. 5.5).

The absolute value of k_w cannot be arbitrarily small, otherwise the source will not be able to spin up, while this is clearly the case when the flux exceeds a certain value. The value of k_w can, therefore, be estimated using the observed frequency derivative over accretion rate dependence. We only measure flux, so the accretion rate and k_w are parametrized by the assumed distance. For each distance in the

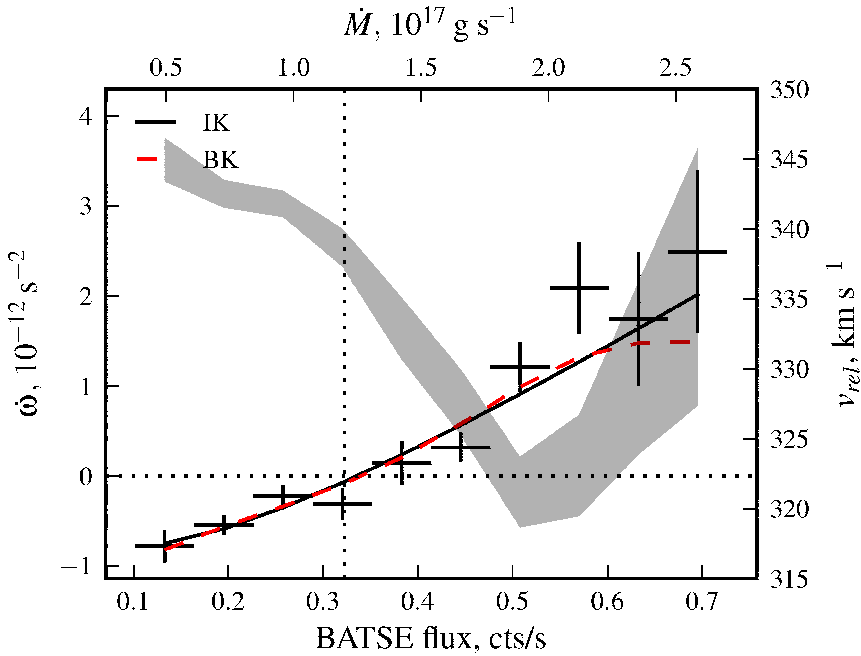


Figure 5.5: Angular frequency derivative correlation with flux. Flux is *BATSE*-pulsed flux in the 20–40 keV energy range. *BATSE DISCLA* data provided by Bildsten et al. (1997) on the *CGRO* mission page are used to obtain the plot. Example of fitting Illarionov & Kompaneets (1990) (solid black) and Davidson & Ostriker (1973); Davies et al. (1979); Bisnovatyi-Kogan (1991) (dashed red) models for an assumed distance of 3 kpc is plotted. Top axis shows the estimated accretion rate for this distance. The vertical line indicates the mean flux during the observation. Shaded area represents average relative velocity of the neutron star and wind for a given flux bin (right scale).

range of published estimates from 1.4 to 5.3 kpc, we calculated the accretion rate and estimated k_w and B as free parameters of models defined by equations 2.17–2.6 where we assumed $M=1.4M_\odot$, $R=10^6$ cm, $I=1.4\times 10^{45}$ g cm², $v_\infty=300$ km s⁻¹, $k=2/3$, and $\xi=0.87$. The estimated values are presented in Fig. 5.7. The k_w range is in line with estimates obtained by Ho (1989) and with later claims that the average amount of angular momentum transferred from the wind to the neutron star is relatively small (Ruffert et al. 1992; Ruffert 1997). It is likely that the mechanisms to generate the braking torques assumed in the models may act simultaneously, so we attempted to find the magnetic field required in this case by including both torques.

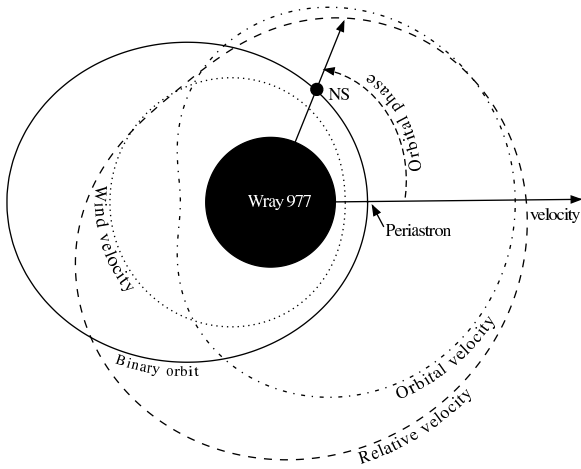


Figure 5.6: Sketch of the GX 301–2 system. The relative speed of the neutron star and wind, the orbital velocity of the neutron star, and the intrinsic velocity of the wind close to the neutron star are plotted as a function of the orbital phase. Velocities are normalized to maximal relative velocity $\sim 380 \text{ km s}^{-1}$, and distances to the periastron distance $\sim 1.75 \times 10^{13} \text{ cm}$.

The required field strength, however, is not significantly reduced and still exceeds 10^{14} G (see Fig. 5.7).

It is important to emphasize that the frequency derivative and therefore the torque affecting the neutron star are consistent with zero for the average source flux. This means that, for the average conditions during the observations, the period is close to a so-called equilibrium period (i.e. when the torques are balanced). This is also in line with the long-term pulse period evolution (see Fig. 5.3). The knowledge of the equilibrium period allows to estimate the magnetic field for the average luminosity even without knowing the exact dependency of torque with luminosity. For example, for the Davidson & Ostriker (1973), Davies et al. (1979), Bisnovaty-Kogan (1991) model in the case of torque equivalence, the field strength may be expressed as

$$\begin{aligned}
 B \approx 3 \times 10^{14} \text{ G} & \left(\frac{k_w}{0.25} \right)^{1/2} \left(\frac{\dot{M}_{\text{eq}}}{10^{17} \text{ g/s}} \right)^{1/2} \left(\frac{v_{\text{rel}}}{400 \text{ km/s}} \right)^{-2} \\
 & \times \left(\frac{P}{680 \text{ s}} \right) \left(\frac{P_{\text{orb}}}{41.5 \text{ d}} \right)^{-1/2} \left(\frac{M}{1.4 M_{\odot}} \right)^{3/2} \left(\frac{R}{10^6 \text{ cm}} \right)^{-3}.
 \end{aligned} \tag{5.4}$$

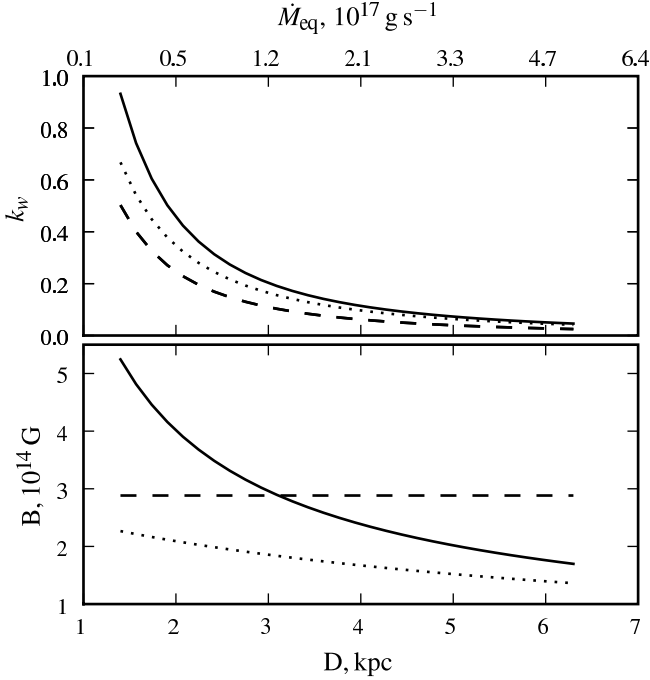


Figure 5.7: Results of fitting frequency derivative – flux correlation (see Fig. 5.5) with Illarionov & Kompaneets (1990) (solid), Davidson & Ostriker (1973), Davies et al. (1979), Bisnovatyi-Kogan (1991) (dashed) and a model with both braking torques in place (dotted) depending on assumed distance, hence mean accretion rate. The required magnetic field strength B (bottom panel) depends on the efficiency of angular momentum transfer k_w (top panel), which is constrained by the fit.

The equivalent equation for the Illarionov & Kompaneets (1990) model is

$$\begin{aligned}
 B \approx 2 \times 10^{14} \text{ G} & \left(\frac{k_w}{0.25} \right)^{7/8} \left(\frac{k}{2/3} \right)^{-7/8} \left(\frac{\xi}{0.87} \right)^{-7/8} \left(\frac{\dot{M}_{\text{eq}}}{10^{17} \text{ g/s}} \right)^{1/2} \\
 & \left(\frac{v_{\text{rel}}}{400 \text{ km/s}} \right)^{-7/2} \left(\frac{P}{680 \text{ s}} \right)^{7/8} \left(\frac{P_{\text{orb}}}{41.5 \text{ d}} \right)^{-7/8} \left(\frac{M}{1.4 M_{\odot}} \right)^2 \left(\frac{R}{10^6 \text{ cm}} \right)^{-3}.
 \end{aligned} \tag{5.5}$$

Both values are in the same order of magnitude as first estimated by Lipunov (1982). The strength of the magnetic field calculated under the assumption of

an equilibrium period using the models for systems accreting from the persistent disk (Lovelace et al. 1999; Ghosh & Lamb 1979) is even stronger ($\sim 10^{15}$ G).

5.5 Conclusions

In this work we studied the timing and spectral properties of GX 301–2 using the archival data of *INTEGRAL* and data products of *CGRO BATSE* and *RXTE ASM*. An orbital-period's secular change was detected and the pulse period history since May 2005 determined. This shows a steady spin-down trend. The apparent rate of decay of the orbital period is about an order of magnitude higher than for other known sources. We argue that this is probably caused by angular momentum loss by material expelled from the vicinity of the neutron star to the outside world. However, we cannot at this time exclude some contribution from a possible apsidal motion to the observational appearance.

Results of the spectral analysis are consistent with previous works, although we find that the spectrum is described well not only with phenomenological models, but also with a saturated comptonization model.

We discussed a possible scenario to explain the long pulse period and long spin-down trends observed despite steady accretion of matter and angular momentum onto the neutron star. We studied the balance of the torques affecting the neutron star using *BATSE/DISCLA* data by Bildsten et al. (1997) and find that the rotational frequency derivative is correlated with the flux. We also find that the frequency derivative is zero for the average count rate, which is a signature that the observed pulse period reflects torque equilibrium during the observations time span. We investigated several published torque models to constrain the magnetic field strength and found that all of them require the field to be $\sim 10^{14}$ G. The magnetic field strength derived from the observed CRSF energy turns out to be $\sim 4 \times 10^{12}$ G, i.e. at least an order of magnitude less than from the timing. Possible scenarios to reconcile the two estimates are discussed in Chapter 7.

CHAPTER 6

Vela X-1

6.1 Introduction

Vela X-1 is a persistently active close high mass X-ray binary system consisting of a massive neutron star ($1.88M_{\odot}$, Quaintrell et al. 2003) and a B0.5Ib supergiant (HD 77581), which eclipses the neutron star every orbital cycle of $P_{\text{orb}} \sim 8.964$ d (van Kerkwijk et al. 1995). The optical companion has a mass of $M \sim 23M_{\odot}$ and radius of $R \sim 30R_{\odot}$ (van Kerkwijk et al. 1995). The mass-loss rate is $\dot{M}_{\text{opt}} \sim 10^{-6}M_{\odot}\text{yr}^{-1}$ (Nagase et al. 1986) via a fast wind with terminal velocity of $v \sim 1100$ km s $^{-1}$ (Watanabe et al. 2006), typical for this class. The neutron star was discovered as an X-ray pulsar with a spin period of $P_{\text{spin}} \sim 283$ s (Rappaport 1975).

The X-ray spectrum of Vela X-1 is similar to the one of other accreting pulsars, and is usually described with a cutoff power law. A cyclotron resonance scattering feature (CRSF) at $E_1 \sim 25$ keV (Makishima & Mihara 1992) and the first harmonic at $E_2 \sim 55$ keV (Kendziorra et al. 1992) were reported for the source, although there are also non-detection reports for the low-energy feature (Orlandini 2006).

The source is highly variable with an average X-ray luminosity (assuming a distance of 2 kpc, as reported by Nagase 1989) of $\sim 4 \times 10^{36}$ ergs s $^{-1}$. Aside from the usual flaring activity, similar to that seen in other wind-accreting pulsars, abrupt “off-states” (when the source becomes undetectable for several pulse periods), giant flares (with flux up to 20 times brighter than typical flares), and quasi-periodical oscillations are observed in the source (Kreykenbohm et al. 2008a).

6.2 The torque models and the data

The rotational dynamics of a neutron star is governed by the accelerating and braking torques affecting it (2.5). The accelerating torque K_+ is due to the transfer of angular momentum from the accreting matter in orbital motion to the neutron star.

In case of wind accretion it can be estimated (Illarionov & Sunyaev 1975) as shown in (2.6). Note, that (2.6) simply shows that the orbital angular momentum captured at R_G is transferred to the magnetosphere, and while the coefficient k_w does depend on wind structure, the functional dependence does not (Illarionov & Sunyaev 1975). This fact is also confirmed by hydrodynamical simulations (Ho 1989; Ruffert et al. 1992; Ruffert 1997) with $k_w \in [-1.2, +0.4]$. It is also worth to mention that the magnetosphere adjusts to changes in wind structure on the *Alfven* timescale $\sim R_M/c$ which is short comparing to the timescale of typically observed accretion rate fluctuations, so hysteresis effects may be neglected and one may rely on average values of frequency and accretion rate to study rotational dynamics on longer intervals.

A number of factors discussed in Chapter 2 can be responsible for the braking torque K_- .

If the braking and the accelerating torques are balanced (i.e. $K_+ = K_-$), the spin frequency remains constant and it is usually called the “equilibrium frequency”. Assuming that the observed pulse frequency is close to the equilibrium value, it is possible to estimate the magnetic field if the accretion rate is known. Under this simple assumption, the magnetic field of Vela X-1 results to be $B \sim 10^{13}$ G for both torque models (assuming the average accretion rate of $\dot{M} = 4 \times 10^{16} \text{g s}^{-1}$). Such a strong magnetic field is required because the braking torque must balance the large specific angular momentum of captured matter. Indeed, if the relative velocity of the neutron star and wind is small ($\sim 575 \text{km s}^{-1}$), then the capture radius and the specific angular momentum of the captured matter are large. To estimate the relative velocity of the wind and the neutron star we follow the same approach as in Chapter 5 and assume the binary system parameters reported by Quaintrell et al. (2003). We would like to stress, that although the terminal wind velocity is often used to estimate the capture radius, this is not correct for close binaries like Vela X-1, in which the wind interacts with the neutron star long before it achieves the terminal velocity.

A more robust estimate of the magnetic field can be obtained if the dependence of the frequency derivative on the accretion rate is known. In our analysis of GX 301–2 we obtained this dependence using the frequency derivative history measured by Bildsten et al. (1997) in a long-term *CGRO BATSE* pulsar monitoring campaign. The analysis of these data revealed a correlation of the frequency derivative with the observed flux and allowed us to simultaneously estimate the magnetic field strength $B \sim 10^{14}$ G and $k_w \sim 0.2$.

For Vela X–1, however no frequency derivative information is available in the corresponding *CGRO BATSE* data set.¹

¹ftp://heasarc.gsfc.nasa.gov/compton/data/batse/pulsar/histories/DISCLA_histories-velax1_psr_hist.fits

To estimate the frequency derivative we compared frequency values reported by Bildsten et al. (1997) in pairs of adjacent time intervals. The method was verified with the data of GX 301–2 and the expected correlation was obtained. Applying the same method to Vela X-1 gives the “flux”–“frequency derivative” correlation shown in Fig. 6.1. We wish to observe that İnam & Baykal (2000) used a linear fit over a number of adjacent frequency values (over an interval of ~ 45 d for Vela X-1) to obtain frequency derivative estimates for several sources of the *CGRO BATSE* sample, and found no correlation of the frequency derivative with the flux. As we argued in Chapter 5, this is in fact an expected result, since the timescale of frequency modulation is known to be much shorter than the intervals used by İnam & Baykal (2000), so short term variations were simply smoothed out.

The observed “flux”–“frequency derivative” correlation can be fitted using equations (2.6), and (2.14) or (2.18) to estimate the magnetic field strength and the k_w coefficient. Note that equation (2.18), which describes the braking torque in the Illarionov & Kompaneets (1990) model, contains the additional unknown coefficient $k_i = k\xi/2\pi \leq 1$ that can not be estimated directly from the observed correlation. While Illarionov & Kompaneets (1990) suggest $k_i \approx 0.1$ on the basis of general considerations, it is still worth to verify how the uncertainty in k_i affects the magnetic field.

It is easy to see from the observed “flux”–“frequency derivative” correlation (Fig. 6.1) that $\dot{\omega} = 0$ for the average flux value. This finding is in line with the fact that the secular pulse period of Vela X-1 remained remarkably stable while showing rather ample short-term variations, and strongly suggests that the neutron star spins at nearly-equilibrium frequency. Assuming that $K_+ = K_-$, from (2.6) and (2.17) we have $k_i = f(k_w, B, \dot{M}_{\text{eq}})$:

$$k_i = k_w \frac{P_{\text{eq}}}{P_{\text{orb}}} \left(\frac{R_{\text{G,eq}}}{R_{\text{M,eq}}} \right)^2 \quad (6.1)$$

The dynamical equation (2.5) in the case of the Illarionov & Kompaneets (1990) model, can then be rewritten as

$$I\dot{\omega} = k_w \dot{M} \frac{2\pi}{P_{\text{orb}}} R_{\text{G}}^2 \left(1 - \frac{P_{\text{eq}}}{P} \left(\frac{R_{\text{M}}}{R_{\text{M,eq}}} \right)^2 \right) \quad (6.2)$$

Here $P_{\text{eq}}/P \sim 1$ because the pulse period is almost constant, and the magnetospheric radius is only a function of the accretion rate $R_{\text{M}} = f(\dot{M})$. We therefore obtain for a

given neutron star

$$\dot{\omega} \simeq 6.9 \times 10^{-12} k_w \left(\frac{\dot{M}}{4 \times 10^{16} \text{g/s}} \right) \left(1 - \left(\frac{\dot{M}}{\dot{M}_{\text{eq}}} \right)^{4/7} \right) \times \left(\frac{P_{\text{orb}}}{8.964 \text{d}} \right)^{-1} \left(\frac{v_{\text{rel}}}{575 \text{km/s}} \right)^{-4} \left(\frac{M}{1.4 M_{\odot}} \right)^2 \quad (6.3)$$

showing that $\dot{\omega} = f(k_w, \dot{M})$. It is now possible to constrain k_w from the slope of the observed correlation, which gives $k_w = 0.44(4)$. The magnetic field is then determined from (6.1). For $k_i \leq 1$ we obtain $B \geq 2.1 \times 10^{13}$ G, assuming $R \sim 10$ km for the neutron star, while for $k_i = 0.1$, as proposed by Illarionov & Kompaneets (1990), we have $B = 1.6(3) \times 10^{14}$ G.

For the Bisnovatyi-Kogan (1991) model the situation is simpler as there are only two unknown parameters, for which we obtain $B = 7.2(3) \times 10^{13}$ G, and $k_w = 0.35(3)$ directly fitting the observed correlation.

6.3 Discussion

The observed “flux”-“frequency derivative” correlation is important for two reasons. First, it shows that the pulse period is close to equilibrium during the observations because $\dot{\omega} \sim 0$ corresponds to the average flux. This rules out the scenario outlined by Ikhsanov (2007), who suggests that the currently observed long pulse periods of many accreting pulsars may be retained from the past periods of low accretion rate. Second, the “flux”-“frequency derivative” correlation allows to eliminate ambiguity in magnetic field strength associated with the unknown constants k_w, k_i , which may in principle depend on wind parameters and differ considerably for different sources.

From a physical point of view, the observed spin-up rate of the neutron star at high accretion rates places a lower limit on the specific angular momentum of captured plasma (no matter how complex the wind structure and its interaction with the neutron star are). The observed spin-down rate allows also to put a lower limit on the braking torque. The dependence of the pulse frequency derivative on flux therefore unambiguously shows, that the long equilibrium pulse period in Vela X-1 is attained due to the effective braking, and not because the orbital angular momentum is transferred to the neutron star inefficiently as often assumed.

The neutron star can only spin-down due to the interaction of the magnetosphere with the in-falling plasma (no matter how complex this interaction may be), and current understanding is that the efficiency of braking depends on the magnetosphere

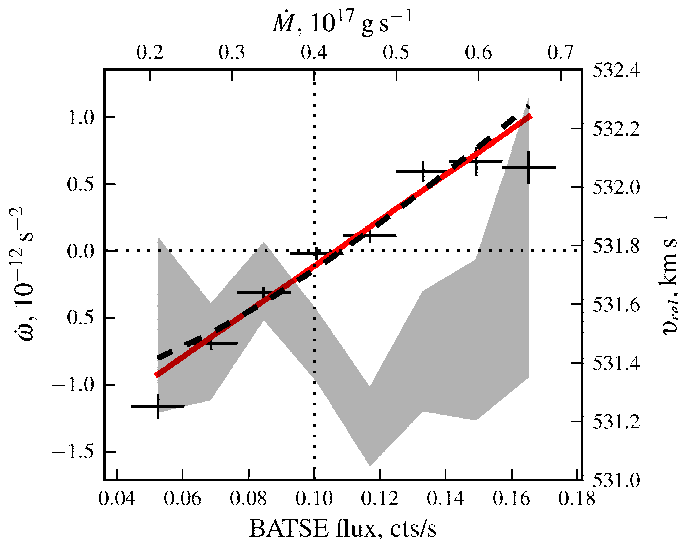


Figure 6.1: Angular frequency derivative correlation with flux for Vela X-1. The flux is *BATSE*-pulsed flux in the 20–40 keV energy range. *BATSE DISCLA* data provided by Bildsten et al. (1997) on the *GGRO* mission page are used to obtain the plot. Best fit predictions for Illarionov & Kompaneets (1990) (dashed black) and Davidson & Ostriker (1973); Davies et al. (1979); Bisnovatyi-Kogan (1991) (solid red) models are plotted. The top axis shows the estimated accretion rate. The vertical line indicates the average flux during the observation.

size, so a strong magnetic field is required as we have demonstrated above.²

We would like to stress, that in the framework of existing torque theory there seems to be no way to explain the observed rotational dynamics of the neutron star without assuming it to be strongly magnetized. Still, it would be extremely interesting to find some indication besides the torque theory, that the magnetosphere of the neutron star in Vela X-1 is indeed large.

²Here we wish to note, that the observations constrain the magnetosphere radius, and not the magnetic field itself. The connection between the magnetosphere radius and the magnetic field is strictly speaking non-trivial (for instance it may depend on the magnetosphere shape and wind structure). The standard definition (2.8) yields however a factor of ~ 2 accurate estimate of the magnetic field strength according to Arons & Lea (1980)

6.3.1 Other evidence for a strong magnetic field

a) The “off-states”

Besides the usual flaring activity typical for the wind-accreting pulsars, several so-called “off states” were reported for Vela X-1 (Inoue et al. 1984; Lapshov et al. 1992; Kreykenbohm et al. 1999, 2008b). In all cases the source flux abruptly and dramatically decreased to a level below the instrumental sensitivity for a duration ranging from several pulse periods to several hours. The recovery to the average flux level was also very fast (tens of seconds) in most cases. These off-states were interpreted by Kreykenbohm et al. (2008b) as the onset of the so-called “propeller regime” (Illarionov & Sunyaev 1975), when the accretion is inhibited by the rotating magnetosphere. This happens when the magnetosphere radius becomes larger than the so-called co-rotation radius: a radius where the local angular Keplerian velocity matches that of the neutron star. Kreykenbohm et al. (2008b) suggested, that the transition to the “propeller” stage is triggered by a significant fluctuation in wind density or wind velocity close to the neutron star. The magnetic field required for the onset of the “propeller” regime for a typical observed bolometric flux of several times 10^{-9} ergs s^{-1} is (Cui 1997):

$$B = 7.6 \times 10^{13} \left(\frac{P}{283.5 \text{ s}} \right)^{7/6} \times \sqrt{\frac{F_X}{10^{-9} \text{ erg cm}^{-2} \text{ s}^{-1}}} \left(\frac{d}{1 \text{ kpc}} \right) \left(\frac{M}{1.4 M_\odot} \right)^{1/3} \text{ G} \quad (6.4)$$

The average flux of Vela X-1 is $\sim 10^{-9}$ ergs $\text{cm}^{-2} \text{ s}^{-1}$, so a significant drop of about a factor of $\sim 10^3$ in wind’s density would be required (Kreykenbohm et al. 2008b) for the onset of the “propeller regime” if one assumes a magnetic field of $B \sim 2 \times 10^{12}$ G as estimated from the CRSF energy. The density in a radiation driven wind may fluctuate by up to factor of 10^3 according to calculations by Runacres & Owocki (2005), so this is not excluded. We would like to point out, however, that normally observed flux variations in Vela X-1 are much smaller as mentioned above, the flux varies typically by less than factor of 20. Moreover, smooth variations of the wind density associated with orbital motion (by factor of 2, as it is evident from the observed orbital light-curve) are negligible comparing to the amplitude of chaotic fluctuations, which is predicted to be almost independent on the distance from the optical companion (Runacres & Owocki 2005), so one would expect the “off states” to occur with the same probability at all orbital phases.

The “off states” reported in the literature however cluster close to the apastron as summarized in Fig. 6.2. The coverage of orbital phases is more or less uniform (in fact, there are more observations at periastron), so this is probably not a selection effect. This implies that the chaotic fluctuations in wind density are unable to trigger an “off-state” on their own, and additional contribution from the smooth variations

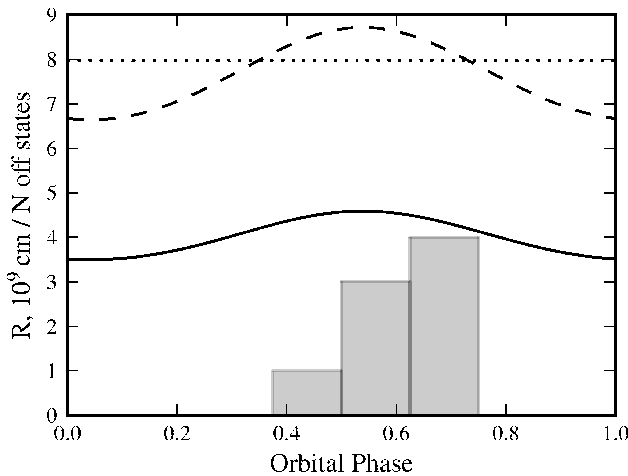


Figure 6.2: Orbital phase distribution of the off states reported in the literature (Inoue et al. 1984; Lapshov et al. 1992; Kreykenbohm et al. 1999, 2008b). The orbital ephemeris by Kreykenbohm et al. (2008b) were used to calculate the orbital phase. Magnetospheric radii for best-fit magnetic field strength with the Davies et al. (1979) model (solid), Illarionov & Kompaneets (1990) model (dashed) and the co-rotation radius (dotted horizontal line) are plotted for reference. The centrifugal barrier inhibits the accretion once the magnetospheric radius matches the co-rotation radius.

due to the orbital motion is required. This can only be the case if the “off-states” are triggered by relatively small wind density fluctuations comparable with the smooth variations due to the orbital motion. The magnetic field must be therefore $B \sim 10^{13}$ G as estimated from Eq. 6.4. Note, that one still does expect to observe the “off-states” at all orbital phases also in this case, but more often in vicinity of apastron.

b) Quasi-periodic oscillations (QPO)

QPOs with a period of ~ 6820 s were reported for Vela X-1 by Staubert et al. (2004); Kreykenbohm et al. (2008b). These oscillations had a transient nature and were seen only in a small part of the light-curve close to apastron. The authors suggested that the orbital motion through a “ray”-like fluctuation (ud-Doula & Owocki 2002) in wind density may be responsible for such a phenomenon. While this may indeed be the case, we would like to point out, that the “beat frequency” model is a viable alternative.

The accretion from the wind is quasi-spherical, but the accreting matter still possesses some angular momentum and, since it is conserved, the matter spirals to the neutron star with a certain frequency even if no accretion disk is formed. The accretion flow is not homogeneous intrinsically and is further disturbed by the gravitational field of the neutron star and turbulent processes close to it (Blondin et al. 1990). The magnetospheric radius is determined by the wind density, and may therefore exceed the co-rotation radius if the density drops below a certain value. In this case the accretion will be temporarily inhibited. The rotation of the magnetosphere may therefore mediate the accretion rate and in this case one expects to see oscillations at beat frequency $\omega_{\text{beat}} \sim \omega_{\text{ns}} - \omega_{\text{co}}$ where ω_{co} is the Keplerian frequency at the magnetospheric radius. This scenario is supported by the fact that the QPOs observed by Staubert et al. (2004) and Kreykenbohm et al. (2008b) occurred close to the apastron and at least one minimum in the oscillating light-curve coincided with the “off-state”. One can therefore estimate the magnetospheric radius

$$R_M = R_C = \left(\frac{GM}{\omega_{\text{co}}^2} \right)^{1/3} = \left(\frac{GM}{(\omega_{\text{ns}} - \omega_{\text{beat}})^2} \right)^{1/3} \sim 8 \times 10^9 \text{ cm} \quad (6.5)$$

This corresponds to the magnetic moment of

$$\mu \sim \sqrt{2\dot{M}(GM)^{1/2}R_M^{7/2}} \sim 3 \times 10^{32} \text{ erg G}^{-1} \quad (6.6)$$

or a surface magnetic field of $\sim 10^{14}$ G, i.e. comparable to the estimates obtained from the accretion torque theory.

c) Noise power spectrum

Another hint on the magnetic field strength comes from the observed power spectrum of the X-ray emission. It has been noted, that the power spectrum of the accreting pulsars has a power law shape with a slope changing at the so-called break frequency close to the spin-period of the neutron star (Hoshino & Takeshima 1993). Among other pulsars this behavior was reported by Revnivtsev et al. (2009) for Vela X-1. A “perturbation propagation” model (Lyubarskii 1997) was proposed to explain the power spectrum in terms of inward-propagating mass-flow perturbations in the accretion disk produced at a broad range of radii. The slope of the power spectrum is determined by the dependence of the perturbation timescale τ on the radius, and the break frequency corresponds to a certain radius where this dependence changes, i.e. the inner accretion disk radius, where the disk is disrupted by the rotating magnetosphere.

Qualitatively, the picture shall be similar in the case of wind accretion because from angular momentum considerations the perturbations timescale $\tau = 1/\omega$ shall

also have a power law dependence on radius $\omega_w(r) \sim \Omega_{\text{orb}}(R_G/r)^2$, while $\omega_k(r) \sim \sqrt{GM/r^3}$ for disk accretion where it is limited by the Keplerian value. In reality, the perturbation frequency is probably $\omega_w \lesssim \omega \lesssim \omega_k$, since otherwise an accretion disk will be formed. The break frequency ω_B and the magnetosphere radius R_M may therefore be estimated as

$$\Omega_{\text{orb}}(R_G/R_M)^2 \lesssim \omega_B \lesssim (GM)^{1/2} R_M^{-3/2} \quad (6.7)$$

$$R_G(\Omega_{\text{orb}} P_{\text{spin}}/2\pi)^{1/2} \lesssim R_M \lesssim (GM)^{1/3} (P_{\text{spin}}/2\pi)^{2/3} \quad (6.8)$$

which for the parameters of Vela X-1 implies a magnetospheric radius of $10^9 \leq R_M \leq 10^{10}$ cm, or a magnetic field strength $10^{13} \leq B \leq 10^{14}$ G, which is compatible with estimates from the accretion torque theory.

d) Flaring activity

We also would like to mention as a side note, that while the giant flares reported by Staubert et al. (2004); Kreykenbohm et al. (2008b) may in principle be explained by means of a flip-flop instability as originally proposed by these authors, this requires rather strong accretion rate fluctuations. On the other hand, Bozzo et al. (2008); Grebenev (2010) proposed that in super fast X-ray transients (SFXTs) similar flares may be explained via transitions between different accretion regimes (i.e. “accretor”-“propeller” and so on) which are triggered by small fluctuations in wind velocity and/or density. Taking into account the phenomenological similarities between Vela X-1 and SFXTs noted by Kreykenbohm et al. (2008b) and the “propeller” interpretation of the “off-states”, the same mechanism may be considered a viable alternative to explain the short giant flares observed in Vela X-1.

6.3.2 Observation of the “off-states” with *Suzaku*

In the previous section we followed the interpretation of the “off-states” proposed by Kreykenbohm et al. (2008b) as onset of centrifugal barrier (Illarionov & Sunyaev 1975), triggered by a drop in wind density/velocity. The quality of the *INTEGRAL* data which Kreykenbohm et al. (2008b) relies on is, however not the best possible, so we decided to check if similar episodes were observed by other missions with better broadband coverage and/or statistics.

Here we report on the analysis of public data obtained during *Suzaku* observation of Vela X-1 in June 2008, with emphasis on three “off-states” found in this observation. To our knowledge it is the first time, when this type of activity was observed with an instrument sensitive enough to reliably constrain the flux from the source during the “off-state”, as well as to perform the spectral analysis, to detect pulsations and to reconstruct pulse profiles.

We will also discuss a possible interpretation of the results in the framework of the “gated accretion” scenario proposed by Bozzo et al. (2008) to explain the flaring activity of SFXTs. In this scenario the observed luminosity swings are associated with the transitions between different accretion regimes, i.e. ways the plasma enters the magnetosphere. The interaction of the rotating magnetosphere with plasma mediates the accretion rate, so matter accumulates in the vicinity of the neutron star during periods when the magnetospheric boundary is strong. Under certain circumstances the magnetospheric instabilities render the barrier transparent and the accumulated matter accretes all at once to produce a bright flare. Some observational evidence for this scenario was reported by Bozzo et al. (2008); Grebenev (2010).

As we will show the accretion still proceeds during the “off-states”, although at much lower rate. The abrupt decrease in accretion rate during the “off-states” may then be explained in the gated accretion scenario as the magnetospheric boundary becomes stable with respect to Rayleigh–Taylor instability, but some matter still leaks as the magnetosphere is still unstable with respect to Kelvin–Helmholtz instability (KHI).

The observation we rely on is a ~ 100 ks long *Suzaku* observation (ID 403045010), performed on June 17–18, 2008, about 1.6 d after the eclipse and close to the periastron passage of the source (orbital phase $\sim 0 - 0.16$). The data reduction was performed using the HEADAS 6.9 with CALDB version 20100812.

e) Timing analysis

To improve the statistics, data from all three XIS units were combined. The light-curve of the observation in the range 0.4–12 keV is presented in Fig. 6.3. Three “off-states” episodes, shown in the upper panels of Fig. 6.3, are observed. As reported in literature (Inoue et al. 1984; Lapshov et al. 1992; Kreykenbohm et al. 1999, 2008b), during the “off-states” the source’s flux drops abruptly and recovers after several pulse periods. Marginal evidence for a residual pulsed emission was reported by Inoue et al. (1984) based on *Tenma* data. With the unprecedented sensitivity of *Suzaku* not only we unambiguously confirm these findings but we can also study the “off-states” in detail.

Using the phase-connection technique (Staubert et al. 2009) and assuming the ephemeris by Kreykenbohm et al. (2008b), we determined the pulse period to be $P_s = 283.473(4)$ (all uncertainties quoted are at 1σ confidence level unless stated otherwise). The marginal evidence for spin-up is not statistically significant and may be explained with the uncertainty on the orbital parameters. No change of the pulse period in “off-states” could be measured. Based on the obtained timing solution, we constructed energy resolved pulse profiles for the entire observation, and

for the “off-states” combining all three episodes. As it can be seen in Fig. 6.4, the pulse profiles significantly vary with both energy and luminosity. Very remarkable appears the change around phase ~ 0.75 at hard energies (20–60 keV) between the normal and the “off-state” profile. We also investigated the flux distribution of the source following the approach of Fürst et al. (2010), who, based on *INTEGRAL* data, showed that the flux distribution is approximately lognormal. Although the lognormal distribution generally describes our data, an excess appears at low count-rates (Fig. 6.5). This excess is due to the “off-states”. The flux distribution of the “off-states” is still approximately lognormal (shaded area of Fig. 6.5) but differs considerably from the distribution of the rest of the light-curve. It is the “off-states” component which mostly contributes to the low-count-rate flank seen in the overall flux histogram. Implications of this finding are discussed below.

f) Spectral analysis

We first analyzed the average spectrum of the entire observation to establish a baseline for the analysis of the “off-state” data. Several phenomenological continua, based on the models reported in literature for *Vela X-1*, were used to fit the average spectrum of the source. None of these models was able to describe the broad-band 0.4–70 keV spectrum. Particularly the spectrum below 5 keV is poorly described by cut-off power law models.

To model the continuum we used two components, combining a comptonization model (Titarchuk et al. 1996) and a power-law. Photoelectric absorption at lower energies, a number of emission lines, an iron absorption edge at ~ 7.26 keV (Nagase et al. 1986) were also necessary to fit our data. Two CRSF harmonics were also required by the fit and were modeled using a multiplicative Gaussian profile. The best-fit parameters are summarized in Table 6.1. The statistics is significantly worse for the “off-state” data, so a simpler model was used in this case: an absorbed comptonization model with the addition of an iron absorption edge. No other spectral features were required by the fit. The results of the best fit are presented in Table 6.1. The best fit spectra and the fit residuals are shown in Fig. 6.6. The average absorption-corrected flux in the 0.4–70 keV energy range was $\sim 3.8 \times 10^{-9}$ erg s $^{-1}$ for the complete observation and $\sim 5 \times 10^{-10}$ erg s $^{-1}$ for the “off-state” spectrum. Results of a more detailed spectral analysis, including phase resolved spectra, will be published elsewhere.

It is interesting to note, that the “off-state” spectrum differs considerably from the spectrum observed during the eclipses. In the latter case the spectrum is dominated by emission-lines (Watanabe et al. 2006) originating in the surrounding plasma illuminated by the X-rays emitted by the eclipsed pulsar.

	$T_{0,e}$	kT_e	τ_e	A_{comp}	$N_{\text{H}} 10^{22} \text{ atoms cm}^{-2}$	Γ	A_{I}	$E_{\text{cyc},25}$	$\sigma_{\text{cyc},25}$	$\tau_{\text{cyc},25}$	$E_{\text{cyc},50}$	$\sigma_{\text{cyc},50}$	$\tau_{\text{cyc},50}$
“On”	0.98(2)	7.97(3)	15(2)	0.07(2)	1.45(8)	3.2(3)	0.07(2)	26.6(9)	7(1)	0.3(1)	55(3)	13(4)	1.7(1)
“Off”	0.83(8)	21.0(1)	$7_{-4.4}^{1.5}$	≤ 0.03	1.4(1)								

Table 6.1: Best fit parameters of the normal and “off-states” spectra. All uncertainties are at 1σ confidence.

6.4 Interpretation and discussion

First, we would like to summarize the observed properties of the source in its “off-state”:

- The flux drops by factor of 10 or more on a timescale comparable to the pulse period. The source remains “off” for several pulse periods, and then the flux is restored to the previous level on the same short timescale.
- Vela X-1 is observed to pulsate in the “off-state”. No pulse frequency change has been detected in the “off-state”.
- A drastic change in the shape of the pulse profile shape appears at high energies. The narrow dip at pulse phase ~ 0.75 , seen in the profiles of the normal state at all energy ranges as well as in the “off-state” profiles at lower energies, is substituted by a prominent peak in the “off-state” profile at hard energies (20-60) keV. This leads to a significant increase in the fraction of the pulsed emission in the hard energy range for the “off-states”.
- The flux distributions of the normal and “off-states” are significantly different. The overall distribution is composed of two approximately lognormal peaks.
- The spectrum, although poorly constrained at high energies, changes significantly during the “off-state”. The temperature of the comptonizing medium increases whereas the optical depth decreases. No CRSF is required by the data, although the statistics at high energies does not allow us to rule out the presence of a CRSF completely, especially if the latter is shifted to higher energies. The absorption corrected flux in the 0.4-70 keV energy range is $\sim 5 \times 10^{-10} \text{ ergs cm}^{-2} \text{ s}^{-1}$, which corresponds to a luminosity of $\sim 2.4 \times 10^{35} \text{ ergs s}^{-1}$ for a distance of 2 kpc.

The observed pulsations, the luminosity and the hard spectrum of the “off-states” can only be explained if the emission is powered by the accretion of plasma onto the magnetized neutron star. The absence of emission lines in the “off-state” spectrum strongly suggests that the source is not eclipsed, but exhibits an intrinsic drop in luminosity hence in the accretion rate. The timescale of the state transition makes

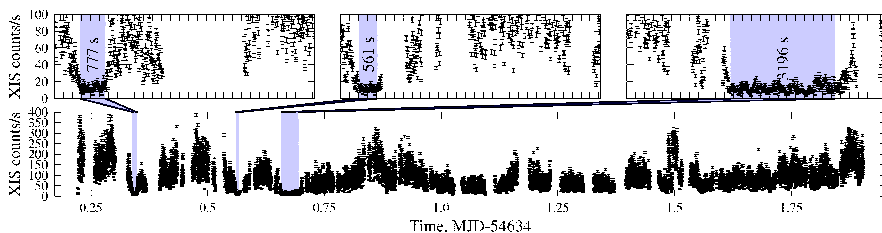


Figure 6.3: The observation-long light-curve in the 0.4–12 keV energy range using data from all XIS units is shown in the bottom panel. The upper panels show close-up views of the three detected off-states. Here, the time axis is ticked every pulse period.

it difficult, as argued by Kreykenbohm et al. (2008b), to explain the onset of the “off-states” with a sudden decrease in wind density and/or velocity, and suggests a magnetospheric origin of the state transition.

This is in agreement with the observed flux distribution. If the “off-states” were due to drops of the wind density, one would expect them to contribute to the lower-flux *tail* of the normal flux distribution. On the contrary, they form a distinct low-flux *peak* as observed in Fig. 6.5. The lognormal flux distribution is most likely due, as discussed by Fürst et al. (2010), to the “grinding” of a clumpy wind by the magnetosphere, while changes of the distribution parameters may be associated with changes in the way the magnetosphere-plasma interaction proceeds.

As discussed by Burnard et al. (1983), plasma generally enters the magnetosphere of accreting pulsars according to various instabilities. These authors also conclude that, for the observed luminosities and spin-periods typical of bright accreting pulsars, the plasma mainly penetrates the magnetospheric boundary via Rayleigh–Taylor instabilities. If the accretion rate decreases, the rotating magnetosphere will inhibit accretion via Rayleigh–Taylor. And therefore for low-luminosity pulsars with intermediate rotation rates the accretion mainly proceeds via KHI (Burnard et al. 1983).

The ways through which the plasma can penetrate the magnetosphere were more recently reviewed by Bozzo et al. (2008), who also provided estimates for the leak rates of various mechanisms. For a system with parameters similar to *Vela X-1* in “off-state”, the largest rate is expected to be provided by KHI (see section 3.2.2 of Bozzo et al. (2008) for the details). The accretion luminosity is estimated in this

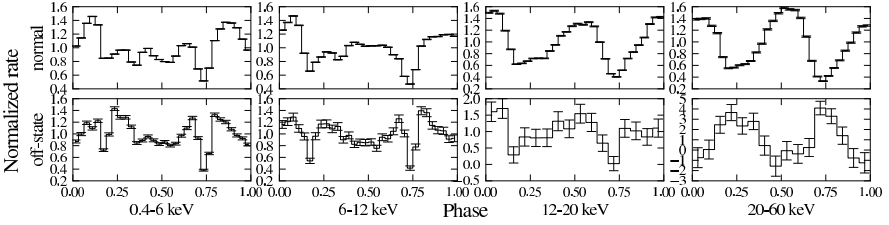


Figure 6.4: The pulse profiles in four different energy ranges are shown for the normal (upper panels) and the “off-state” (bottom panels).

case to be

$$L_{\text{KH}} \approx GM_{\text{NS}}\dot{M}_{\text{KH}}/R_{\text{NS}} = 7.4 \times 10^{35} \eta_{\text{KH}} R_{\text{M10}}^3 (1 + 16R_{\text{G10}}/(5R_{\text{M10}}))^{3/2} \frac{\sqrt{\rho_{\text{i}}/\rho_{\text{e}}}}{1 + \rho_{\text{i}}/\rho_{\text{e}}} \text{ erg s}^{-1}, \quad (6.9)$$

Here $R_{\text{G10}}, R_{\text{M10}}$ are the capture and magnetosphere radius respectively, in units of 10^{10} cm; $\rho_{\text{i,e}}$ are the densities within and outside of the magnetosphere. According to Bozzo et al. (2008), $\eta_{\text{KH}} \sim 0.1$ and the density ratio can be estimated to be between

$$\frac{\sqrt{\rho_{\text{i}}/\rho_{\text{e}}}}{1 + \rho_{\text{i}}/\rho_{\text{e}}} = \begin{cases} \eta_{\text{KH}} h^{-1} R_{\text{M10}}^{3/2} P_{\text{s283.5}}^{-1} \\ 0.1 \eta_{\text{KH}} h^{-1} R_{\text{M10}}^{1/2} \nu^8 \end{cases} \quad (6.10)$$

where h is the fractional height of the area where the plasma and the magnetic field coexist, in units of the total thickness of the KHI unstable layer (Burnard et al. 1983). $P_{\text{s283.5}}$ is the spin-period in units of 283.5 s and we assume a canonical neutron star radius of $R_{\text{NS}} \sim 10$ km. In the case of Vela X-1, for the observed “off-state” luminosity of $\sim 2.4 \times 10^{35} \text{ erg s}^{-1}$, a magnetic field of $B \geq 2 \times 10^{13}$ G is required, if the KHI unstable layer is relatively thin ($h \sim 0.05$), or $B \sim 10^{14}$ G, if $h \sim 1$ as suggested by Burnard et al. (1983).

Evidence for such a high magnetic field in Vela X-1, surprisingly stronger than the one estimated from the CRSF energy, have been already discussed above. Here, we wish to point out, that similarly to GX 301–2, the observed energy of the CRSF may be explained if the line formation region is located several kilometers above the neutron star surface. In fact, for the average observed luminosity of the normal state, $\sim 4 \times 10^{36} \text{ erg s}^{-1}$, one expects that an accretion column with height up to ~ 10 km will arise (Lyubarsky & Sunyaev 1988; Doroshenko et al. 2010a). This implies a factor of 10 decrease in field strength at the top of the column given

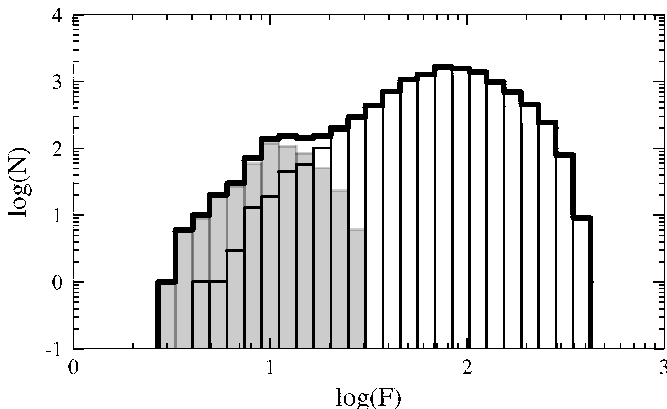


Figure 6.5: Histogram of the measured count-rate of the XIS light-curve (solid line). The same is shown for the off-states (shaded) and for the rest of the light-curve separately.

that $B \sim B_0((R_{\text{NS}} + 10)/R_{\text{NS}})^{-3} \sim 0.1B_0$. It is therefore sufficient to assume that the accretion column exists and that the observed CRSF forms closer to the top of the column to reconcile the strong magnetic field required by the observed “off-states” luminosity and the measured CRSF centroid energy. We will discuss this in more detail in Chapter 7.

The observed change of the high energy pulse profile is well explained under the assumption that an accretion column does indeed exist. The sharp dip, evident at high luminosity and softer energies, would be then due to the eclipse of the polar cap by the accretion column. As the luminosity drops and the column ceases to exist, the hard X-rays can pierce through and the polar cap is observed directly: a pronounced peak is observed instead of a dip. In other words, the high-amplitude peak, which appears in the “off-states” pulse profile at hard energies around pulse phase 0.75, can be explained as due to the direct emission from the polar cap. In this scenario, the accretion stream would still absorb the soft X-rays so the dip is still observed at lower energies. A similar scenario was discussed by Klochov et al. (2008) to explain the pulse profile variations of EXO 2030+375 during outbursts.

6.5 The “off-states” in GX 301–2

Motivated by the fact that it is hard to imagine that Vela X-1 is the only system in which the “off-states” are observed, we performed a search for a similar behavior in the archival PCA *RXTE* light-curves of GX 301–2 and of several other systems.

Unfortunately the *RXTE* observations are rarely uninterrupted, so only one clear example which shows the source to both switch “off” and “on” could be found in GX 301–2 light-curve. It is presented in Fig. 6.7 together with two other examples where only the beginning or end of the “off-state” was observed. A similar behavior may be present also in 4U 1538-52, although the case is not convincing and we will not focus on it here (the results, if any will be published elsewhere).

The discovery of the “off-state” in GX 301–2 (the one covered completely) was reported independently by Göğüş et al. (2011), who presented also the time-resolved spectral analysis results. Here we wish to focus on the comparison of the properties of the “off-states” in GX 301–2 and Vela X-1.

First of all, we wish to make it clear that the similarities in properties of the “off-states” in these sources strongly suggest the same physical origin in both cases (i.e. related to stability of the magnetosphere as discussed above). The duration of the “off-state” in GX 301–2 is ~ 1000 s, about two pulse-periods, also is similar to that observed in Vela X-1. Although it is difficult to discuss the pulse-profile changes during the “off-state” in GX 301–2 (as the “off-state” only lasts less than two pulses), one may also notice some similarity in pulse-profile shape changes. The Fig. 6.8 from Göğüş et al. (2011) shows that, similarly to Vela X-1, in GX 301–2 both pulse peaks disappear during the “off-state” and instead a new one appears in between. The count-rate in all three “off-states” of GX 301–2 is very similar (~ 5 cts/s in the full PCA range), which is in line with what is observed in Vela X-1 and implies similar luminosity (see Table 6.2).

To check if the spectral evolution is also similar we extracted spectra from the “off state” and separately from the complete observation (95354-03-03-00), and fitted both with a *compTT* model. The results are summarized in Table 6.2. Similarly to Vela X-1, with a drop in luminosity the comptonization ceases to be saturated and the temperature rises, which together with the pulse-profile evolution suggests the same interpretation as for Vela X-1.

The unabsorbed flux of $1.8 \times 10^{-10} \text{ erg s}^{-1} \text{ cm}^{-2}$ in “off-state” implies $L_X \simeq 2 \times 10^{35} \text{ erg s}^{-1}$, which is also similar to Vela X-1. Using Eq. 6.9 one may also estimate the magnetic field from the observed X-ray luminosity, which turns out to be $\sim 1 - 6 \times 10^{14}$ G assuming $h \sim 0.05 - 1$, i.e. in line with earlier obtained estimates.

6.6 Conclusion

We have investigated how the timing properties of Vela X-1 can help to constrain its magnetic field. Following the lines of the similar work on GX 301–2, we conclude that, in the framework of existing accretion torques theory, a very strong magnetic field $B \sim 10^{13} - 10^{14}$ G is required to explain the long pulse period of Vela X-1 and

	Normal	“off-state”
$N_{\text{H}}, 10^{22}$ atoms cm^{-2}	12.2(9)	12.2
T_0	0.93(5)	0.93
kT	8.5(4)	223^{+125}_{-180}
τ	9.2(3)	0.06(0.1)
A_{compTT}	0.020(1)	0.0001(5)
E_{Fe}	6.33(4)	6.33
A_{Fe}	0.00079(8)	0.0002(1)
$L_{X,3-50}$	2×10^{36} erg s^{-1}	1.8×10^{35} erg s^{-1}

Table 6.2: Spectral evolution of GX 301–2 in the “off-state” with a *CompTT* model. Linked parameters are shown with script font. The luminosity is calculated assuming a distance of 3 kpc and unabsorbed fluxes derived from spectra in the 3–50 keV energy range.

its evolution. Using the long-term pulse frequency history measured by Bildsten et al. (1997) with *CGRO BATSE*, we show that, consistently with model predictions, the pulse frequency derivative is correlated with the flux, and we use this correlation to estimate the magnetic field in the framework of torque models by Davies et al. (1979) and Illarionov & Kompaneets (1990). In both cases a magnetic field of the order of $10^{13} - 10^{14}$ G is required to explain the observed pulse frequency and pulse frequency dependence on flux.

We argue that similarly to GX 301–2, a rather low relative velocity of the wind and the neutron star is the main reason why a very strong magnetic field is required. While the measurements of terminal wind velocity for GX 301–2 may in principle be questioned as the value of ~ 305 km s^{-1} is rather untypical, the terminal wind velocity in *Vela X-1* has a canonical value of ~ 1100 km s^{-1} and the low relative velocity of the wind and the neutron star is the result of compactness of the system. We find that the strong magnetic field scenario allows also to explain other observed properties of the system, particularly so-called “off-states”, quasi-periodic oscillations, and the noise power spectrum.

We presented first results of the analysis of an 100 ks *Suzaku* observation of the well known X-ray binary *Vela X-1*. With this observation we confirm the CRSF at 25 keV in the normal state. Due to the unprecedented sensitivity of *Suzaku*, for the first time ever it was also possible to study the properties of the source during the “off-states” reported previously as periods when the source is not detected completely. We also detected pulsations, measured the spectrum and the flux distribution in “off state”. We conclude that these observational facts strongly suggest that the emission is still powered by accretion, and that the drop in luminosity has prob-

ably a magnetospheric origin. The observed X-ray luminosity in “off-state” may be explained in the gated accretion scenario developed by Burnard et al. (1983) if the neutron star is strongly magnetized and plasma enters the magnetosphere via KHI instability. To our knowledge this is the first time when theoretical considerations regarding magnetosphere-plasma interactions (Burnard et al. 1983; Bozzo et al. 2008) find an observational support.

In the same context we have reviewed the properties of GX 301–2 during the newly-discovered “off-state”, reported by Göğüş et al. (2011) which we have found independently. We conclude that the “off-states” are also related to the stability of the magnetosphere in GX 301–2. It is important to emphasize, that potentially the “gated accretion” scenario allows to estimate the magnetic field of the accreting pulsar, and the result seems to agree with other estimates for Vela X-1 and GX 301–2. Clearly, other sources may also “switch-off”, so it would be extremely interesting to search for evidence for this and to perform a comparative study of a complete sample of galactic accreting pulsars. We plan to carry out such study using the *INTEGRAL* data, but this is future work.

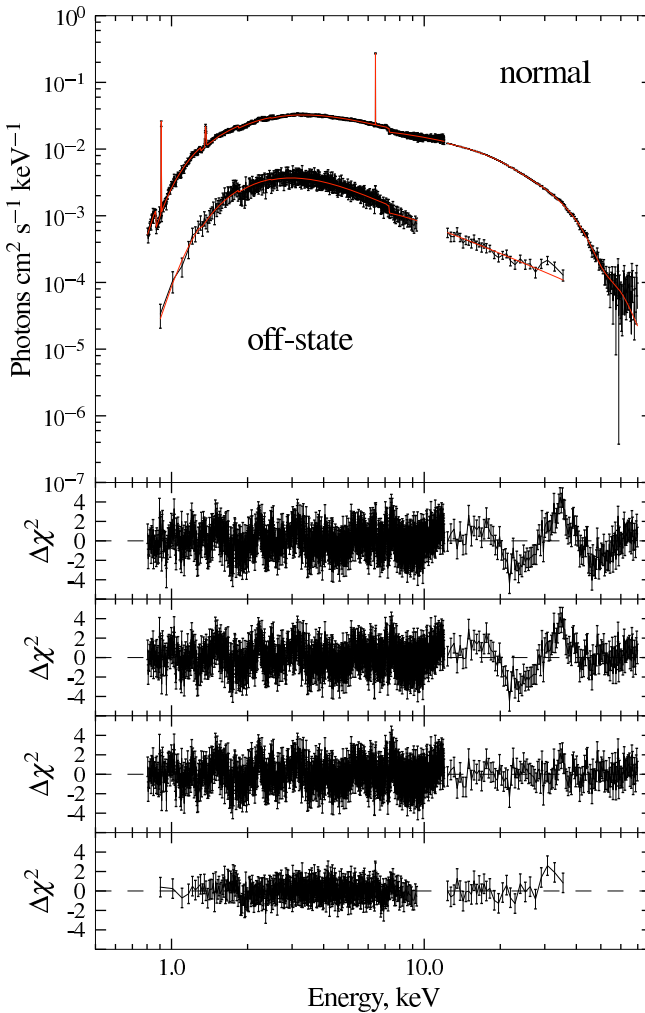


Figure 6.6: Unfolded spectrum of the normal and “off states”. For the normal spectrum the XIS0 and HXD PIN data were used. For the “off” spectrum data from all XIS units were combined to obtain a better statistics. Best-fit residuals are also shown from top to bottom for: the normal state without CRSF; with the inclusion of a CRSF at 55 keV; with the inclusion of two CRSFs, and, eventually, for the “off-state” spectrum.

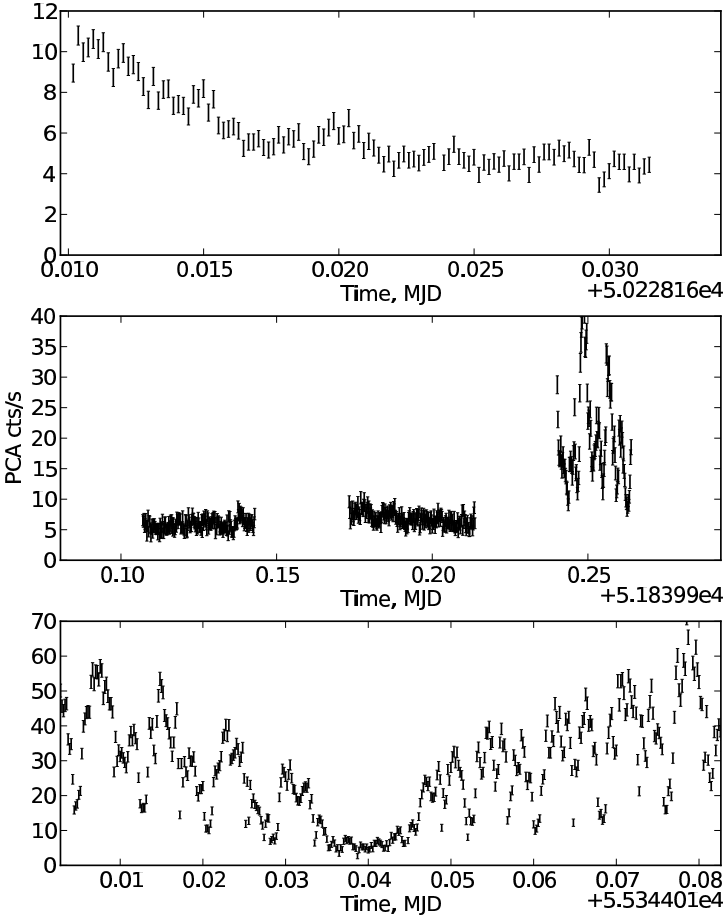


Figure 6.7: The three “off-states” in GX 301–2 observed with PCA *RXTE*, see text for details.

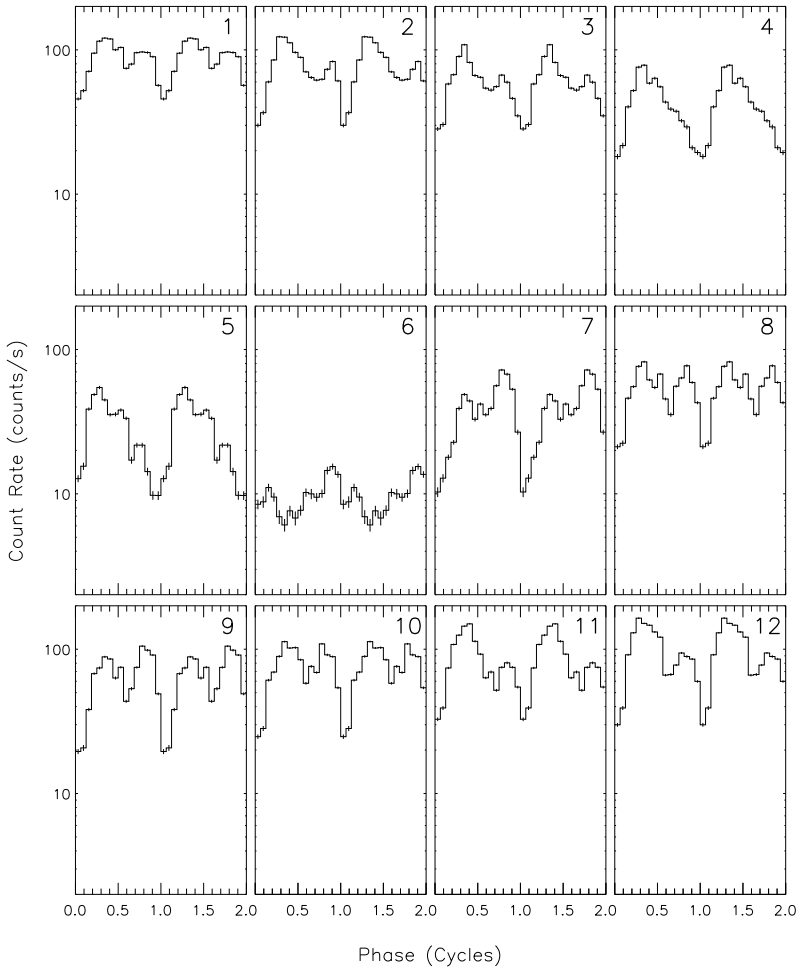


Figure 6.8: Evolution of the pulse-profile in GX 301-2 as reported by Göğüş et al. (2011). Subsequent individual pulses in the vicinity of the “off-state” are plotted with “off-state” occurring at cycle 6. Note the similarity with Vela X-1 (see Fig. 6.4), where two main peaks also disappear in the “off-state” and instead of a minimum a new peak appears.

Part III

Problems and prospects

The magnetic field and the CRSF energy

In the previous chapters the magnetic moment of the neutron stars in Vela X-1 and GX 301-2 has been estimated using the current accretion torque models developed by Illarionov & Kompaneets (1990) and Bisnovaty-Kogan (1991), which, one may argue, is still poorly verified. On the other hand, the result contradicts the estimate from the energy of the CRSF. For instance for Vela X-1 the observed $E_{\text{cyc}} \sim 22 \text{ keV}$ corresponds to a field of $B \sim 10^{12} \times (E_{\text{cyc}}/11.57) \sim 2 \times 10^{12} \text{ G}$. This is an order of magnitude less than the estimate obtained from timing considerations. This inconsistency has to be somehow explained, since both estimates rely on the observational facts.

One needs either to explain why the observed CRSF energy is so low assuming a strong surface field or to adjust the accretion torque theory to avoid the strong field requirement. In the next two chapters we will explore these two possibilities.

First we suggest that the contradiction can be resolved if the CRSF forms high above the surface of the neutron star (i.e. in the accretion column or the accretion flow above the polar caps). Given that the magnetic field weakens with the distance as $B \propto R^{-3}$, a factor of 10 difference between the magnetic field estimates from the accretion torque theory and the CRSF energy may be accounted for if the later forms at a height $H \sim R_{\text{NS}}$ above the surface of the neutron star.

The X-ray pulsars are powered by accretion, so their luminosity is limited by the back-reaction of the X-ray emission onto the accreting matter. Maximum luminosity for the spherically symmetric accretion is $L_{\text{edd}} \sim 1.3 \times 10^{38} \text{ erg s}^{-1}$ and much less for a magnetized neutron star. However there is a number of X-ray pulsars with luminosities exceeding this value. To explain these sources the concept of accretion column was introduced by Basko & Sunyaev (1976).

In the case of a neutron star the accretion geometry is not spherical since the accreting matter is funneled onto the magnetic poles of the neutron star by the strong magnetic field. The ram pressure of in-falling matter in this relatively narrow accretion channel is balanced by the pressure of the X-ray emission. The excess of energy is emitted through the sides of the extended accretion column, with a height

determined by the accretion rate and the accretion channel configuration. The accretion column arises if the luminosity L^{**} exceeds the critical value (Lyubarsky & Sunyaev 1988):

$$L^* = \frac{2cd}{\kappa} \frac{GM}{R} \simeq 6 \times 10^{36} \text{ erg s}^{-1}, \quad (7.1)$$

Both Vela X-1 and GX 301-2 have luminosities comparable with the critical value so the accretion column may in principle arise in both cases.

Besides the observed luminosity, the presence of the column is also supported by several observational facts. For instance, the observed color temperature of 4-5 keV in both cases is in agreement with the value expected for a source with a luminosity close to the Eddington limit. The effective critical temperature is defined from $L_{x,\text{Edd}} = 4\pi R^2 \sigma T_{\text{Edd}}^4$, where $L_{x,\text{Edd}}$ is the standard Eddington luminosity (1.6). This implies $T_{\text{Edd}} \sim 2 \text{ keV}$ for the standard neutron star parameters ($M = 1.4 M_{\odot}$, $R = 10^6 \text{ cm}$) and solar composition of the accreting matter. The observed spectrum is expected to be close to a diluted Planck spectrum $B_E: F_E \approx B_E(T_c)/f_c^4$, with a color temperature $T_c = f_c T_{\text{eff}}$ and a hardness factor $f_c \sim 1.5-2$ because of Compton scattering (Pavlov et al. 1991). This qualitative picture is similar in the case of Compton scattering in a strong magnetic field (Lyubarsky 1986), so the observed color temperature probably corresponds to a critical effective temperature at the neutron star surface. Another strong argument that an accretion column of significant height (i.e. comparable with the radius of the neutron star) does indeed exist in GX 301-2, is that the pulsed fraction in this source significantly decreases with the increase in luminosity and hence column height (Lutovinov & Tsygankov 2009).

The height of the accretion column may be estimated from very basic considerations. Because the magnetic field funnels the matter onto the poles of the neutron star the accretion column base radius can be estimated from the neutron star magnetic moment $r \approx R_{\text{NS}}(R_{\text{NS}}/R_{\text{H}})^{1/2}$ (Lipunov 1987). The magnetospheric radius is $\approx (3-30) \times 10^8 \text{ cm}$ for a magnetic field in the range $10^{12} - 10^{14} \text{ G}$, and the corresponding radius of the column base is 200-500 m. The accretion column height may then be estimated using a cylindrical geometry approximation, and the critical effective temperature from the observed luminosity $L \approx 10^{37} \text{ erg s}^{-1} \approx 2 \sigma_{\text{SB}} T_{\text{Edd}}^4 2\pi r H$. This simple estimate gives $H \approx 8-20 \text{ km}$ for GX 301-2 ($B = 10^{12} - 10^{14} \text{ G}$ and $\dot{M} = 1.2 \times 10^{17} \text{ g s}^{-1}$), and 3-7 km for Vela X-1 (same B and $\dot{M} = 4 \times 10^{16} \text{ g s}^{-1}$).

A more refined estimate was provided by Lyubarsky & Sunyaev (1988):

$$H \simeq \dot{m} R_{\text{NS}} \ln \left(\eta \frac{1 + \dot{m}}{\dot{m}^{5/4}} \right). \quad (7.2)$$

Here κ is opacity and d is the characteristic size of the polar cap, while

$$\dot{m} = \frac{GM}{R} \frac{\dot{M}}{L^{**}}, \quad \eta = \left(\frac{B^2 d^2 \kappa}{7\pi c \sqrt{2GM}} \right)^{1/4} \quad (7.3)$$

are the dimensionless accretion rate and a function characterizing the geometry of the column. The latter depends on the mass of the neutron star M , its radius R and magnetic field B , and on the diameter of the accretion column $d \sim \sqrt{\frac{R}{R_M}}$. Here

$$R_M = \left(\frac{B^2 R^6}{2\dot{M} \sqrt{2GM}} \right)^{2/7} \quad (7.4)$$

is the magnetospheric radius (Lipunov 1987). The height of the column estimated with (7.2) is $H \simeq 4$ km for Vela X-1 and $H \simeq 10$ km for GX 301-2, in agreement with the estimates above. As mentioned above, the estimated accretion column height $H \sim R_{\text{ns}}$ allows to reconcile the observed CRSF energy with the surface magnetic field of $B \sim 10^{13} - 10^{14}$ G obtained from timing considerations if the CRSF forms in the upper parts of the column.

Moreover, the CRSF may in principle form even higher in the accretion stream above the column or polar cap. Kraus et al. (2003) discussed that the up-scattering of the continuum emission in the accretion stream above the accretion column (where matter falls with nearly free-fall velocity $v \sim 0.7c$) may contribute a significant fraction of the total flux above the cutoff energy ($E_{\text{cut}} \sim 20$ keV for Vela X-1 and GX 301-2). This emission component was required to explain the observed pulse-profile shape and its evolution with energy in their analysis.

We argue that for a magnetic field at the surface of the neutron star in the range of $10^{13} - 10^{14}$ G, the cyclotron energy in the accretion stream at a height of several kilometers above the surface of the neutron star will be comparable to the typical energy of the photons of the continuum, and therefore the scattering in the stream can be resonant. Depending on the viewing geometry, this may lead either to the formation of an observable CRSF. Alternatively the overlapping of the continuum observed directly from the column with that up-scattered in the accretion stream could produce line-like features in the overall spectrum.

For the discussion below it is important to mention that the plasma within the accretion column is by definition Compton thick, otherwise the radiation would simply escape from the sides of the column and would not balance the ram pressure of the inflow. Part of the radiation obviously still escapes from the sides of the column and the parameters of the column are determined by the escape rate (Becker & Wolff 2005). A discussion of the accretion column models is beyond the scope of this work but it is important to note that the shape of the locally emerging spectrum

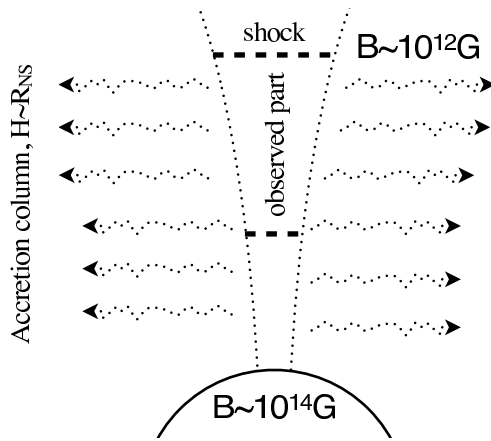


Figure 7.1: Sketch of a radiation-dominated accretion column. Temperature and magnetic field strength increase towards the neutron star surface.

at any given height in the column is expected to be the result of saturated thermal Comptonization (Lyubarsky 1986). The theoretically calculated spectra of the accretion column (Basko & Sunyaev 1976; Becker & Wolff 2005) describe the main properties of the observed continuum reasonably well.

As shown by Basko & Sunyaev (1976, see their Fig. 4 and accompanying discussion), the amount of energy released by a unit of height of the accretion column is almost constant, so a significant part of the emission comes from the upper parts of the column. In fact, the observed cutoff power-law shape of the spectra of accreting pulsars is interpreted by Basko & Sunyaev (1976) and Becker & Wolff (2005) as a superposition of the emission coming from the different parts of the column.

The whole column contributes both to the continuum and to the formation of the CRSF. The magnetic field changes by a factor of 10–100 within the column (i.e. in the line forming region) must be therefore taken into account. The impact of resonant scattering on spectrum formation in the accretion column was discussed by Nishimura (2008) who showed that a line-like CRSF is still predicted in this case. Although Nishimura (2008) considered smaller gradients (factor of 10) of physical parameters (i.e. temperature and magnetic field) across the column, he showed that the resonant scattering may still produce line-like absorption features. The resulting spectrum and particularly the energies of the emerging absorption features are, however, connected non-trivially with the maximal field strength within the line forming region making it difficult to estimate the field from the spectrum alone.

Note also that the observed continuum spectrum and the shape of the pulse profile

strongly depend on the viewing geometry. The understanding of their formation is an extremely complicated problem on itself. In most pulse phases a significant part of the columns at both poles is expected to be visible. This means that the contribution of different parts of the accretion column at any given pulse phase is not known a priori and must be reconstructed using some model of the emission region (see Kraus et al. (1995) for a possible approach).

The inner parts of the column are more likely to be obscured by the neutron star, so the relative contribution to the total spectrum of the upper and lower parts of the accretion column is expected to change with pulse phase. Since the magnetic field strength increases towards the neutron star and the observed CRSF is a superposition of features formed at different heights (Nishimura 2008), one can expect the centroid energy of the CRSF to shift to higher energies as the contribution of lower parts (where the field is stronger) increases. The correlation of the CRSF energy with temperature was indeed reported for GX 301–2 by Kreykenbohm et al. (2004, see Table 3) and is confirmed by our spectral analysis.

The contribution of the upper parts of a tall column is not expected to change significantly with pulse phase. Therefore in the pulse maximum one expects more contribution from the lower parts of the column and hence a higher CRSF centroid energy. This is the case for GX 301–2 (see Chapter 5) and in fact a similar behavior was reported by La Barbera et al. (2003) for Vela X-1. The CRSF energy is also expected to be correlated with column temperature (which increases towards the neutron star surface) and such correlation was indeed reported for both GX 301–2 and Vela X-1 (Kreykenbohm et al. 2004; La Barbera et al. 2003).

Also the pulse fraction is expected to increase with energy (that is with the temperature in the column). This behavior is a known common feature of X-ray pulsars, and Vela X-1 and GX 301–2 follow it as well.

Another feature of the CRSF phase dependence that may be predicted is the “line width - line energy” correlation. When the vertical span of the observed part of the column is short (which is when only the upper parts of the column are visible), the line width is expected to be smaller. In contrast, the line becomes wider when a larger part of the column is observed as the magnetic field increases by an order of magnitude from the column top to the bottom. This “line width” - “line energy” correlation was found in the pulse phase resolved spectrum of GX 301–2 (see Fig. 7.2). It was also reported by La Barbera et al. (2003) for Vela X-1 (see Fig. 7.2).

Note that the discussion above is *very* qualitative and in reality the situation is probably much more complicated. For instance Lyubarsky (1986) predicts that the emission of the column will be strongly beamed towards the neutron star because the outer layer of the plasma at the sides of the column is not supported by the radiation field and thus falls with nearly free-fall velocity. Lyubarsky (1986) provide an estimate for the angular distribution of the emission emerging from the sides of

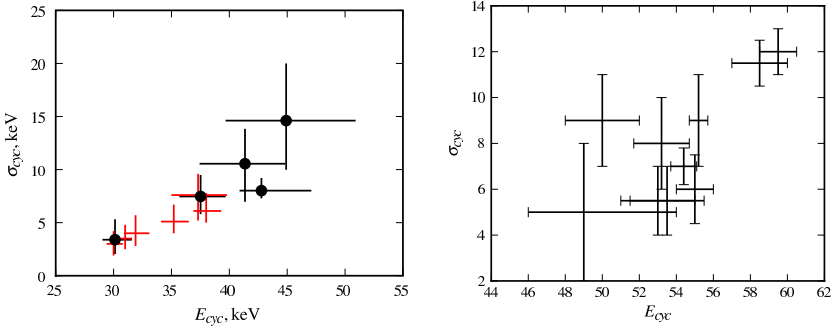


Figure 7.2: The “line width” - “line energy” correlation for the CRSF in the pulse phase resolved spectrum of GX 301–2 (left panel) and Vela X-1 (right panel). For GX 301–2 the correlation was found by Kreykenbohm et al. (2004) in *RXTE* data (red crosses) and was confirmed by my phase-resolved analysis (black points). For Vela X-1 the results reported by La Barbera et al. (2003) with *BeppoSax* data are plotted. The same correlation was reported by Coburn et al. (2002) for a number of other sources observed by *RXTE*.

the column:

$$I \sim \frac{1 - v \cos \theta / c + 2 \sqrt{1 - v^2 / c^2} \sin \theta}{(1 - v \cos \theta / c)^5} \quad (7.5)$$

Here θ is the angle between the emission direction and the plasma velocity v (see Fig. 7.3). Assuming that the plasma of the outer layer falls with free-fall velocity $v \simeq \sqrt{\frac{2GM}{r}}$ one may estimate that for a column lower than ~ 10 km most of the emission is intercepted by the neutron star (see Fig. 7.3).

One can predict that the beamed emission from the column will heat the atmosphere of the neutron star and produce a soft thermal component in spectrum, which has been indeed identified (Ferrigno et al. 2009). Hard emission will be mostly reflected (Lyubarsky 1986). Note that there is a gradient in magnetic field strength across the surface of the neutron star as it is $B \propto \sin \theta$ proportional to latitude. Taking into account the enormous resonant cross-section one may expect that resonant scattering will be also important for the reprocessed emission. The observed spectrum will be therefore a pulse-phase dependent sum of the spectra emerging directly from the two accretion columns and the component reprocessed in the atmosphere of the neutron star.

The main message here is that the usual assumption that the energy of a CRSF allows to estimate the magnetic field of the neutron star is only justified if we observe emission from a small polar cap. Note that even in this case the reprocessing in

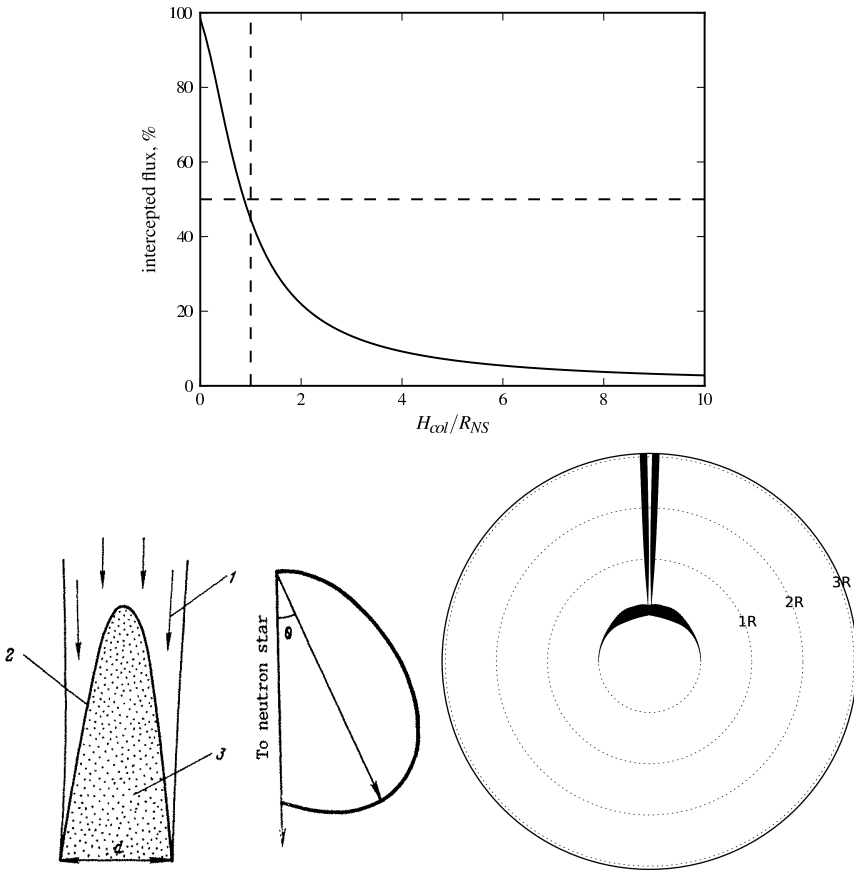


Figure 7.3: Fraction of total flux from the column intercepted by the neutron star as a function of height is shown in the top panel. The left panel at the bottom shows the sketch of the accretion column structure and the beaming pattern as presented by Lyubarsky & Sunyaev (1988) (1–free-falling plasma, 2–deceleration zone, 3–gradual settling). The right panel shows graphically how much light actually escapes from the column and gets scattered by the neutron star (thickness characterizes how much energy can be observed from outside of the system from a given point from all directions for illustrative purposes).

the accretion stream may change the emerging spectrum considerably (particularly contributing to its hard part where cyclotron lines are typically observed).

I wish to emphasize that the discussion above may well be relevant also for other

accreting pulsars. Indeed, the majority of pulsars which exhibit a CRSF in their spectra are luminous and therefore an accretion column is likely to form in these sources. One may argue that the luminosity estimates and the criteria for the formation of accretion columns are somewhat uncertain (for instance, the configuration of the magnetic field is important for the formation of the column), and therefore high luminosities do not imply that the accretion column will indeed form. This issue was discussed by Karino (2007), who investigated how the pulse-profiles of accreting pulsars change with energy.

Using a sample of all pulsars in the Galaxy and Magellanic Clouds for which pulse-profiles in several energy ranges were available, Karino (2007) found that the sample may be divided in two groups: pulsars where the pulse profile does not change significantly with energy (“regular” pulsars), and pulsars for which it does change significantly (“irregular” pulsars). Karino (2007) noticed that the “regular” pulsars typically have luminosities below $\sim 5 \times 10^{36}$ ergs $s^{-1} \simeq L^*$ defined by (7.1), while “irregular” ones are more luminous (see Figure 7.4).¹ Taking into account that an accretion column is expected to form for higher luminosity pulsars and also that it is difficult to explain the “irregular” pulse profiles if the emission comes from a polar cap, Karino (2007) concluded that the change in pulse profile behavior is associated with the formation of accretion column at high luminosities. Note that a relatively tall column (comparable to the radius of the neutron star) is required to explain significant changes of the pulse-profile shape (Karino 2007).

While Karino (2007) did not discuss CRSFs, it is important to note that the majority of the pulsars which exhibit a CRSF in their spectra are not only luminous but also fall into the “irregular” group (see Figure 7.4). I consider this as an independent strong argument that these sources do indeed host an accretion column. One definitively has to keep this in mind when estimating the magnetic field of neutron stars using the observed CRSF energy. I wish to conclude that until the structure of emission region, the formation of the spectrum and particularly of the CRSF in accreting pulsars are really understood, it is dangerous to rely only on the observed energy of the CRSF to estimate the magnetic fields of the neutron stars.

¹Note that this was also a case for pulsars in Magellanic clouds where the uncertainty in luminosity is negligible.

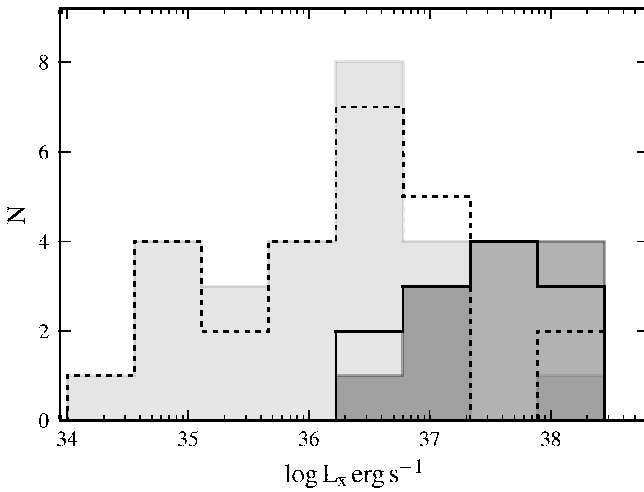


Figure 7.4: Distribution of Galactic X-ray pulsars with regular (light shaded) and irregular (shaded) pulse profiles by luminosities. The same is shown for pulsars with (solid line) and without (dashed line) a CRSF in their spectrum.

Generalizing the torque model

In the previous chapter we discussed a possible scenario to reconcile the estimates of the magnetic field obtained from the observed CRSF energy with the stronger field required by timing considerations. The estimate of the magnetic field in the latter case is obviously model-dependent. We should therefore discuss whether it is possible to explain the timing properties of long period pulsars with a model which does not require a strong magnetic field.

A brief review of all currently available torque models was given in Chapter 2. As already emphasized there, the torque balance is determined by the interaction between the magnetosphere and the plasma. As we have shown the pulse frequency evolution depends on the magnetosphere radius, accretion rate and the rotational frequency. Indeed, it is difficult to imagine, that the braking torque can be present in absence of matter. I would like to point out, however, that the only model which satisfies this requirement and has a correct functional dependence, is the one by Illarionov & Kompaneets (1990), and for this reason the estimates by Lipunov (1987) and Bisnovatyi-Kogan (1991) should be considered an approximation.

The Illarionov & Kompaneets (1990) model, on the other hand, requires an outflow of matter to be formed. At the moment there is no direct observational evidence for such an outflow. The criteria for the outflow formation formulated by the model authors are qualitative, and do not take factors like accretion geometry, plasma heating/cooling timescales and details of magnetosphere-plasma interaction.

In fact, this is a problem for the other models as well: our poor knowledge of the processes which lead to the angular momentum exchange between the neutron star and the accretion flow requires some qualitative assumptions in order to estimate the torques affecting the neutron star. We observe here, that these assumptions (i.e. the presence of an outflow in Illarionov & Kompaneets (1990) or of a shock in the Bisnovatyi-Kogan (1991) model) and the accompanying physical justifications answer mainly the question “how does the angular momentum exchange between the neutron star and the matter proceed?”. We here wish to focus on another ques-

tion: “what fraction of the orbital angular momentum of the matter gets eventually transferred to the neutron star?”, preferably on observational grounds.

As pointed out by Illarionov & Sunyaev (1975) and Bisnovatyi-Kogan (1991) the accretion from wind away from the magnetosphere boundary may be considered as a quasi-spherical adiabatic inflow. The orbital angular momentum of the accreting matter $L = k\Omega R_G^2$ is conserved and hence it spirals-down to the neutron star with angular frequency

$$\omega_m(r) = \Omega \left(\frac{R_G}{r} \right)^2, \quad (8.1)$$

and nearly free-fall velocity

$$v_{\text{ff}} = \sqrt{\frac{2GM}{r}}. \quad (8.2)$$

The matter falls down till the pressure of the magnetic field stops it at the magnetosphere boundary. Here the matter couples with the magnetic field lines and thus acquires angular velocity equal to that of the neutron star: a flux of angular momentum across the magnetospheric boundary must occur if the angular velocity of the in-falling matter ω_m differs from that of the neutron star. In other words a torque

$$K = I_m \dot{\omega}_m = A \dot{M} R_M^2 (\omega_m(R_M) - \omega) \quad (8.3)$$

is required to bring the matter in co-rotation with the neutron star. This is apparently also the torque exerted onto the magnetosphere by the accretion flow. Here A characterizes the moment of inertia of the plasma shell which interacts with the magnetosphere.

Once the matter penetrates the magnetosphere it continues to fall along the field lines and exerts a spin-up torque

$$K_+ = B \dot{M} R_M^2 \omega \quad (8.4)$$

onto the neutron star. Here B characterizes the moment of inertia of the plasma shell which *actually penetrates* the magnetosphere and reaches the surface of the neutron star. The dynamic equation for the neutron star may be therefore written as

$$I \dot{\omega} = A \dot{M} R_M^2 (\omega_m(R_M) - \omega) + B \dot{M} R_M^2 \omega \quad (8.5)$$

or, taking into account (8.1), as

$$I \dot{\omega} = A \dot{M} \Omega R_G^2 - (A - B) \dot{M} \omega R_M^2. \quad (8.6)$$

Here R_G and R_M are gravitational capture and magnetospheric radii defined by (2.7) and (2.8). We assume that A includes a factor $\sim \cos \theta$ which emerges if the ω and

Ω are not aligned. Apparently it is required (although not sufficient) that $A > B$ for the neutron star to spin down. The physical meaning of this requirement is really simple: the angular momentum flux through R_M must be less than that through R_G . This may happen either if some fraction of angular momentum is transported outwards from the magnetosphere boundary by convective motions, or if some kind of outflow forms within the magnetosphere which carries the angular momentum away as in the Illarionov & Kompaneets (1990) model. In some sense (8.6) is a generalization of the Illarionov & Kompaneets (1990) model, where we do not consider by which means the angular momentum gets transported. The physical meaning of $(A - B)/A$ is the fraction of angular momentum which is not transferred through the magnetospheric boundary, or equivalently gets expelled from the neutron star.

In the Illarionov & Kompaneets (1990) model the presence of a macro-scale outflow implies $(A - B) \simeq 0.1$. More than half of the angular momentum is not transferred to the neutron star but carried away by the outflow (the authors fix $A = 0.25$).

The convection-driven plasma motions may also carry the angular momentum away. Note, that in this case the presence of a stand-off shock above the magnetosphere is crucial. Below the shock the plasma falls with sub-sonic velocity and the angular momentum may be transported to a shock and then carried away by the surrounding wind. It is also required that at least some part of the shock lies outside R_G . Detailed modeling is needed in this case to estimate the numerical coefficients from physical considerations.

Assuming that A and B are constants (they may depend on the accretion rate but the assumption is justified if we consider a fixed accretion rate $\dot{M} \simeq \dot{M}_{\text{eq}}$ when $\dot{\omega} = 0$), we can derive the connection between the coefficients:

$$k_1 \Omega R_{G,\text{eq}}^2 = k_2 \omega R_{M,\text{eq}}^2 \quad (8.7)$$

here $k_1 = A \leq 1$, $0 \leq k_2 = (A - B) \leq 1$ ($k_1 = k_w$ and $k_2 = k_i$ in Illarionov & Kompaneets (1990) model), and ω , Ω are the spin and orbital frequencies of the neutron star. Note, that as we discussed in Chapter 6, the Eq. 6.3 allows to constrain $k_w = k_1$ from the observations assuming some reasonable wind parameters, and it turns out to be $k_1 \simeq 0.2$ for GX 301-2 and $k_1 \simeq 0.4$ for Vela X-1. For the case of Bondi accretion the accretion rate is proportional to the capture rate

$$\dot{M} \propto \pi R_G^2 \rho_w v \quad (8.8)$$

where ρ_w, v are the wind density and the relative velocity between wind and the neutron star. From (8.7) we can substitute k_2 into (8.6) and get

$$I \dot{\omega} = k_2 \omega_{\text{eq}} R_{M,\text{eq}}^2 \dot{M} \left(\frac{R_G^2}{R_{G,\text{eq}}^2} - \frac{v}{v_{\text{eq}}} \frac{R_M^2}{R_{M,\text{eq}}^2} \right). \quad (8.9)$$

It is usually assumed that the accreting pulsars spin at nearly equilibrium frequency, so $\omega \simeq \omega_{\text{eq}}$. The accretion rate varies either because of the variations of the wind density or of the wind velocity. If the accretion rate changes only due to changes in the wind density, $R_G = R_{G,\text{eq}}$ and taking into account Eq. (8.8) the dynamical equation may be rewritten as

$$I\dot{\omega} = k_2\omega_{\text{eq}}R_{M,\text{eq}}^2\dot{M}\left(1 - \frac{\dot{M}_{\text{eq}}^{4/7}}{\dot{M}^{4/7}}\right). \quad (8.10)$$

We can now differentiate it with respect to \dot{M} to find out how the spin of the neutron star is affected by changes in accretion rate, so we can compare the results with the observed “flux”–“frequency derivative” correlation:

$$I\frac{\partial\dot{\omega}}{\partial\dot{M}} = k_2\omega_{\text{eq}}R_{M,\text{eq}}^2\left(1 - \frac{3}{7}\frac{\dot{M}_{\text{eq}}^{4/7}}{\dot{M}^{4/7}}\right), \quad (8.11)$$

or, at the equilibrium

$$I\left(\frac{\partial\dot{\omega}}{\partial\dot{M}}\right)_{\text{eq}} = \frac{4}{7}k_2\omega_{\text{eq}}R_{M,\text{eq}}^2. \quad (8.12)$$

If on the other hand we assume that the variations of flux are caused only by the variations of the relative velocity of wind, the R_G will be a function of \dot{M}

$$R_G^2 = \frac{\dot{M}^{4/3}}{(\pi\rho_w)^{4/3}(2GM)^{2/3}}. \quad (8.13)$$

The dynamic equation then takes form

$$I\dot{\omega} = k_2\omega_{\text{eq}}R_{M,\text{eq}}^2\dot{M}\frac{\dot{M}^{4/3}}{\dot{M}_{\text{eq}}^{4/3}}\left(1 - \frac{\dot{M}_{\text{eq}}^{40/21}}{\dot{M}^{40/21}}\right), \quad (8.14)$$

and the partial derivative over \dot{M} will be at equilibrium point

$$I\left(\frac{\partial\dot{\omega}}{\partial\dot{M}}\right)_{\text{eq}} = \frac{40}{21}k_2\omega_{\text{eq}}R_{M,\text{eq}}^2. \quad (8.15)$$

The dependence of the spin frequency derivative on the accretion rate is therefore the same in both cases

$$I\left(\frac{\partial\dot{\omega}}{\partial\dot{M}}\right)_{\text{eq}} = C \times k_2\omega_{\text{eq}}R_{M,\text{eq}}^2 \quad (8.16)$$

and only the constant C is different. It is natural to assume that in reality the accretion rate depends both on variations in wind density and in relative wind-neutron star velocity and C shall lie between the extreme values (i.e. $C \in [0.5, 2]$).

An important feature of Eq. (8.16) is that the spin frequency derivative of the neutron star depends only on k_2 and on the magnetospheric radius, i.e. on the magnetic field. It does not depend on the accretion rate or on the relative velocity between wind and the neutron star. The problem is that we can not constrain the numerical coefficient k_2 from first principles. Still we can put a lower limit on magnetic field strength (since $k_2 \leq 1$ and $C \in [0.5, 2]$):

$$R_M \approx 1.26 \times 10^9 \sqrt{\frac{P_{100s}}{k_2 C} \left(\frac{\partial \dot{\omega}}{\partial \dot{M}} \right)_{\text{eq}}}. \quad (8.17)$$

Here P_{100s} is the pulse period in units of 100s, and $\left(\frac{\partial \dot{\omega}}{\partial \dot{M}} \right)_{\text{eq}}$ is in units of 10^{-12} s^{-2} per 10^{16} g s^{-1} . From the observed “flux”–“frequency derivative” correlations one immediately derives $\left(\frac{\partial \dot{\omega}}{\partial \dot{M}} \right)_{\text{eq}, \frac{-12}{16}} \approx 0.15, 0.5$ for GX 301–2 and Vela X-1 respectively.

This implies for $k_2 \leq 1$ magnetosphere radius of $R_M \geq 10^9 \text{ cm}$ and hence a magnetic fields of $B \geq 10^{13} \text{ G}$ for GX 301–2 and $B \geq 5 \times 10^{12} \text{ G}$ for Vela X-1, i.e. still a factor of two more than required to reconcile with the observed CRSF energy. Keep in mind also that this is a lower limit and if we consider the estimates of k_1 mentioned above and that $k_2 < k_1$, we will come up with significantly stronger fields as was shown in Chapter 6. Other means of estimation of the magnetospheric radius considered there for Vela X-1 also give larger values for R_M .

We conclude here that a lower limit on the magnetic field can be estimated from very general physical considerations, and for Vela X-1 and GX 301–2 this limit is not consistent with estimates obtained from the CRSF energy. We are aware that our result is not in line with the traditional view on the CRSFs as a direct probe of the magnetic field and believe that it may trigger important future work aimed to really understand the CRSF formation process in accreting pulsars.

CHAPTER 9

Summary and outlook

In this dissertation I studied the long-standing problem of the existence of accreting pulsars characterized by long spin periods. Accreting pulsars are neutron stars in binary systems powered by the accretion of matter from a normal star which due to the orbital motion possesses some angular momentum. This angular momentum (or a fraction of it) is transferred to the neutron star, which rapidly gains angular momentum while the accretion proceeds (spin-up torque). This appears to be the case also under the most conservative assumptions about the fraction of angular momentum transferred to the neutron star. Observations show (Liu et al. 2006), however, that the majority of known X-ray pulsars not only have long pulse periods, typically ≥ 100 s, significantly longer than the one neutron stars are believed to have at birth, but also that many of these systems exhibit long-term spin-down trends while accreting. This can only occur if some fraction of the angular momentum carried by the accreting matter is not transferred to the neutron star, but is removed from the system. Several models have been proposed to explain spin-down torques, and in all models the efficiency of braking depends on the size of the magnetosphere and therefore the magnetic field of the neutron star. A strong field is usually required to explain the observed long pulse periods.

On the other hand, the so-called cyclotron resonance scattering features (cyclotron lines), observed in spectra of many pulsars, provide an independent and direct estimate of the magnetic field in the line forming region. These estimates turn out to be incompatible with the ones from timing studies for most pulsars with periods longer than about 100 s. Magnetic field estimates based on the torque theory are of course strongly model dependent, so the observation of cyclotron lines has become the “universally” accepted method to estimate the magnetic fields of accreting pulsars, leaving the question of long periods open and often forgotten.

In my thesis I have conducted a detailed observational study of three accreting pulsars, namely 1A 1118-61, GX 301-2 and Vela X-1 using the data from *RXTE*, *INTEGRAL* and *Suzaku* observatories.

Using the *RXTE* observations of 1A 1118-61 during the January 2009 outburst

of the source, I have discovered a cyclotron line at ~ 55 keV, which was later confirmed by *Suzaku* observations. I have also determined the timing properties of the source, including the estimate of the up to now unknown orbital period. The *RXTE* observations revealed also a complicated pulse-profile energy dependence, while the pulse phase-resolved spectral analysis showed no obvious dependence of the CRSF parameters on pulse phase. These findings have been published in Doroshenko et al. (2010b); Staubert et al. (2011); Suchy et al. (2011).

To study the properties of GX 301–2 I firstly used the data obtained in a dedicated observation obtained with *INTEGRAL* of the so-called “pre-periastron” flare. I also used *INTEGRAL* public archival data to extend my analysis to other orbital phases. The search for a CRSF harmonic in the *INTEGRAL* spectrum was unsuccessful and the results of the spectral analysis (including pulse-phase resolved spectroscopic) confirmed earlier published findings (Kreykenbohm et al. 2004). I therefore focused on the timing properties of the source first improving the orbital ephemeris of the system. To study in detail the secular timing behavior of GX 301–2, I needed to use *CGRO BATSE* archival data, given the limited time span of the available *INTEGRAL* data. A correlation between the X-ray pulse-frequency derivative and the flux (hence the accretion rate) was indeed found for GX 301–2. This came out to be a key finding of my research. In fact, first, this correlation unambiguously shows that the accelerating and braking torques of the system are balanced, which is the essential condition required for a sound estimate of the magnetic field based on the torque theory. Second, the measured spin-up rate at high accretion rates provides evidence for a strong accelerating torque and consequently a similarly strong braking torque is required to explain the observed equilibrium. Moreover, the modeling of the discovered correlation, on the base of the state of the art torque theory, has unambiguously clarified that a magnetar-like, $B \sim 10^{14}$ G is required to explain the timing behavior of the source. This was a surprising and key result. This part of my work was published in Doroshenko et al. (2010a).

Following this result, I searched for a similar correlation in the *BATSE* observations of other accreting pulsars. Such a correlation was found for Vela X-1. Also in this case, the timing behavior of the source suggested a magnetic field of $\geq 10^{13}$ G. With the aim of obtaining an independent evidence of such a strong field, I also reviewed other observational properties of Vela X-1. As I show in Chapter 6, (1) the distribution of the so-called “off-states” (when the source “switches off” for several pulse periods) with the orbital phase; (2) the frequency of the quasi-periodic oscillations reported by Staubert et al. (2004); Kreykenbohm et al. (2008b); (3) the power-density spectrum of the X-ray emission can be naturally explained in the ultra-strong field scenario. These findings were summarized in Doroshenko et al. (2011b).

To study the properties and the origin of the “off-states”, I extensively searched the public archival data on Vela X-1 of various missions. Three such episodes were indeed observed by *Suzaku*. The low background level and the high sensitivity of *Suzaku* allowed for the first time the detection of pulsations and the study of the spectral properties of the source during the “off-state”. The observation of pulsed emission suggests that accretion still proceeds, which implies that matter still leaks through the magnetospheric boundary. In my thesis I interpret this result in the context of the scenario proposed by Burnard et al. (1983) where the KHI instability is responsible for the leakage of the plasma. I also conclude that this scenario favors a strong magnetic field.

The X-ray spectrum of Vela X-1 during the “off-states” changes drastically and provides matter for future elaborations. While the cutoff power-law spectrum in normal state can be interpreted as emerging from the accretion column, during the “off-states” the cutoff in spectrum is not observed anymore which can be naturally interpreted as a signature for bulk comptonization in the accretion stream. A similar scenario was proposed by Trümper et al. (2010) for AXPs. Note that low-luminosity persistent sources like X Per also show similar spectra. The results discussed above are reported in Doroshenko et al. (2011a).

To reconcile the values of the magnetic field estimated from torque models with the ones obtained from the detection of CRSFs in the spectra of GX 301–2 and Vela X-1, I carefully investigated a generalized torque model in Chapter 8. I conclude that, based on very general angular momentum conservation arguments it is not possible to significantly reduce the required field taking into account the observed “pulse frequency derivative” – “flux” correlation, and a different scenario should be invoked to solve the discrepancy.

So why a field of $B \sim 10^{13} - 10^{14}$ G is obtained from timing arguments and the observed CRSF energy (20-50 keV) gives us a magnetic field of $2 - 5 \times 10^{12}$ G? I argue in my thesis that this could be the case if the line forms high above the neutron star, i.e. in the accretion column or the accretion stream above the polar caps. I estimate that a column height of several kilometers (for both GX 301–2 and Vela X-1) well explains the observed CRSF energy if this forms close to the top of the column. I wish also to observe that the top parts of the column must definitively contribute both to the observed continuum and to the CRSF (Basko & Sunyaev 1976). On the other hand, the resonant scattering in regions with stronger magnetic field (i.e. inner part of the column) might well remain unnoticed since the spectra of accreting pulsars are relatively soft and it would be difficult to detect a CRSF at high energies.

I stress in my thesis that one has to be very cautious in interpreting the spectra of luminous accreting pulsars directly relating the observed features to precise emission regions. In fact, no detailed modeling of the emission from luminous accreting

pulsars has been carried out so far. This might be surprising 40 years after their discovery, but it's a fact. Even the most recent physical models of the intrinsic spectrum from an accretion column (Becker & Wolff 2007), do not take into account important effects like resonant scattering and the relativistic beaming towards the neutron star (Lyubarsky & Sunyaev 1988). Moreover, due to the complicated geometrical effects (including gravitational light bending) the observed spectrum may differ considerably from the intrinsic spectrum of the column (Kraus et al. 2003). It is also worth to note that recent studies of CRSF formation in magnetized accretion columns (Nishimura 2008), concluded that line-like absorption features are expected to form even if there is a substantial gradient in the value of physical parameters across the line-formation region. The observed CRSF energy is therefore non-trivially related to the surface field. In conclusion, I believe that there are too many open questions regarding the formation of the CRSFs, to rely on their observed energies as the only estimate of the magnetic field of the star. All possible ways to estimate the magnetic field shall be explored instead.

Such an "exploration" has only been started in this thesis. More can be certainly done to clarify the intriguing question of the field of "slow" pulsars:

- The *BATSE* archive may be reanalyzed and complemented with *Swift* BAT, *Fermi* GBM and *INTEGRAL* data to determine long-term pulse frequency evolution and to search for the correlation between pulse frequency derivative and flux in other accreting pulsars.
- There is certainly room for improvement in torque theory. Particularly future work should also take advantage of simulation. A full 3D MHD simulations of wind accretion onto strongly magnetized neutron could be carried out to study numerically the behavior of matter at the magnetospheric boundary.
- The light-curves of other pulsars can be searched for previously unnoticed "off-states". We expect more of these and even a quick inspection of the GX 301–2 light-curve has indeed revealed new ones. Besides the observed luminosity in "off-state" it is important to understand the criteria for switching "off" and "on" again, which can only be done as the sample of the observed off-states grows.
- If the "off-states" are interpreted in terms of the "gated accretion" scenario as proposed in this work, new interpretation of the quiescent state of accreting pulsars could open. Quiescence could be a low-luminosity state in which accretion proceeds via KHI instability. In fact, at luminosities similar to the ones of the "off-states", pulsations were detected in quiescence from 3 sources, namely 1A 0535+262, 4U 1145–619 and 1A 1118-61. I actually

proposed to observe these sources in quiescence to study this state in greater detail with XMM Newton. An observation of 50 ks was awarded to observe 1A 0535+262.

- I anticipate that in the “gated accretion” scenario one also expects to observe “anti-off-states” from a source in quiescence. These are short flares with luminosity close to that in normal state, which onset once the plasma breaches the magnetosphere and probably last just several pulse periods. Such events would not trigger any TOO and may be too short to be detected by monitors like *RXTE ASM*. They could be detected by *INTEGRAL* or *Swift* BAT, but a careful inspection of mission-long light-curves is required. The frequency of occurrence, the luminosity of the flares as well as the flux before/after the flare may also help to constrain the magnetic field. This scenario was discussed by Bozzo et al. (2008) in the context of super-fast X-ray transients, but similar activity may be observed also in normal pulsars.
- Magnetospheric flares similar to those observed in SGRs and now in AXPs could be also searched for. Note that to find this type of activity in AXPs many hundreds of kilo-seconds of pointed *RXTE* observations were required (Gavriil 2006), so it could pass unnoticed in ordinary accreting pulsars. Note also that the burst monitoring systems like GCN (including BAT and IBAS on *INTEGRAL*) blacklist known accreting pulsars. On the other hand, there is no reason to believe that this activity does not take place (even the Sun exhibits it!), and the fluence of the magnetospheric flares is believed to be related to the strength of the magnetic field providing yet another, independent estimate of the field.
- Last, but not least, a full modeling of the emission from the accreting pulsars, including the formation of the CRSF is required. Even toy models like the ones discussed by Kraus et al. (2003) are of great value. In fact, the modeling of the pulse-profiles shall be considered integral part of this problem.

What are the magnetic fields of the neutron stars in accreting binary pulsars? Do we have evidence of magnetar-like sources in binary systems? Are CRSF tracing the field of the neutron stars in binary systems? Is the transport/leakage of the plasma from the boundaries of the magnetosphere to the surface of the neutron star understood? Are the current models of the torque theory adequate? Do we have evidence of short flaring activity from these systems? And by the way do we have evidence of the two regime of accretion accretion columns/mounds in accreting pulsars?

Some of the points above are already being addressed. While at the moment I have started the search for new “off-states”, and for the detection of SFXT type ac-

tivity and for magnetospheric flashes in accreting pulsars, our group also continues to work on pulse profiles modeling, on the formation of the CRSF, and of the spectrum of accretion column. We also collaborate with a group in Moscow (K. Postnov and N. Shakura) to further refine the torque theory. I sincerely hope that at the end of this journey, we will understand much more on the physics of accreting pulsars. Although discovered more than forty years ago they remain fascinating objects and may be the key to some unification theory of magnetic field of magnetized neutron star systems.

Bibliography

- Araya, R. A. & Harding, A. K. 1996, A&AS, 120, C183
Araya, R. A. & Harding, A. K. 1999, ApJ, 517, 334
Araya-Góchez, R. A. & Harding, A. K. 2000, ApJ, 544, 1067
Arons, J. & Lea, S. M. 1980, ApJ, 235, 1016
Bagot, P. 1996, A&A, 314, 576
Basko, M. M. & Sunyaev, R. A. 1976, MNRAS, 175, 395
Becker, P. A. & Wolff, M. T. 2005, ApJ, 621, L45
Becker, P. A. & Wolff, M. T. 2007, ApJ, 654, 435
Bildsten, L., Chakrabarty, D., Chiu, J., et al. 1997, ApJS, 113, 367
Bisnovatyi-Kogan, G. S. 1991, A&A, 245, 528
Blondin, J. M., Kallman, T. R., Fryxell, B. A., & Taam, R. E. 1990, ApJ, 356, 591
Bondi, H. & Hoyle, F. 1944, MNRAS, 104, 273
Bozzo, E., Falanga, M., & Stella, L. 2008, ApJ, 683, 1031
Burke, B. E., Mountain, R. W., Daniels, P. J., Cooper, M. J., & Dolat, V. S. 1994, IEEE Transactions on Nuclear Science, 41, 375
Burnard, D. J., Arons, J., & Lea, S. M. 1983, ApJ, 266, 175
Castor, J. I., Abbott, D. C., & Klein, R. I. 1975, ApJ, 195, 157
Chen, K. & Ruderman, M. 1993, ApJ, 402, 264
Chevalier, C. & Ilovaisky, S. A. 1975, IAU Circ., 2778, 1
Clark, G. W., Woo, J. W., Nagase, F., Makishima, K., & Sakao, T. 1990, ApJ, 353, 274
Clayton, D. D. 1968, Principles of stellar evolution and nucleosynthesis (McGraw-Hill, New York)
Coburn, W., Heindl, W. A., Gruber, D. E., et al. 2001, ApJ, 552, 738
Coburn, W., Heindl, W. A., Rothschild, R. E., et al. 2002, ApJ, 580, 394
Coe, M. J. & Payne, B. J. 1985, A&AS, 109, 175
Coe, M. J., Roche, P., Everall, C., et al. 1994, A&A, 289, 784
Corbet, R. H. D. 1986, MNRAS, 220, 1047
Cordes, J. M. & Chernoff, D. F. 1997, ApJ, 482, 971
Cui, W. 1997, ApJ, 482, L163
dal Fiume, D., Orlandini, M., Cusumano, G., et al. 1998, A&A, 329, L41
Davidson, K. & Ostriker, J. P. 1973, ApJ, 179, 585
Davies, R. E., Fabian, A. C., & Pringle, J. E. 1979, MNRAS, 186, 779
de Kool, M. & Anzer, U. 1993, MNRAS, 262, 726

- DeCesar, M. E., Boyd, P. T., Markwardt, C. B., et al. 2009, in *Bulletin of the American Astronomical Society*, Vol. 41, 299
- Doroshenko, V., Santangelo, A., & Suleimanov, V. 2011a, *A&A*, 529, A52
- Doroshenko, V., Santangelo, A., Suleimanov, V., et al. 2010a, *A&A*, 515, A10
- Doroshenko, V., Staubert, R., Kreykenbohm, I., Santangelo, A., & Ferrigno, C. 2008, in *PoS(Integral08) 115*, 7th INTEGRAL Workshop
- Doroshenko, V., Suchy, S., Santangelo, A., et al. 2010b, *A&A*, 515, L1
- Doroshenko, V., V., S., & Santangelo, A. 2011b, submitted to *A&A*
- Duncan, R. C. & Thompson, C. 1992, *ApJ*, 392, L9
- Eyles, C. J., Skinner, G. K., Willmore, A. P., & Rosenberg, F. D. 1975, *Nature*, 254, 577
- Fabian, A. C., Pringle, J. E., & Webbink, R. F. 1975, *Nature*, 255, 208
- Ferrigno, C., Becker, P. A., Segreto, A., Mineo, T., & Santangelo, A. 2009, *A&A*, 498, 825
- Frank, J., King, A., & Raine, D. 1992, *Accretion Power in Astrophysics* (Cambridge University Press)
- Fürst, F., Kreykenbohm, I., Pottschmidt, K., et al. 2010, *A&A*, 519, A37
- Gavriil, F. P. 2006, PhD thesis, McGill University, Montreal Canada
- Ghosh, P. & Lamb, F. K. 1978, in *BAAS*, Vol. 10, *BAAS*, 507
- Ghosh, P. & Lamb, F. K. 1979, *ApJ*, 234, 296
- Giacconi, R., Gursky, H., Paolini, F. R., & Rossi, B. B. 1962, *Physical Review Letters*, 9, 439
- Ginzburg, V. L. 1964, *Soviet Physics Doklady*, 9, 329
- Gnedin, I. N. & Sunyaev, R. A. 1974, *A&A*, 36, 379
- Gold, T. 1968, *Nature*, 218, 731
- Göğüş, E., Kreykenbohm, I., & Belloni, T. M. 2011, *A&A*, 525, L6
- Göğüş, E., Woods, P. M., Kouveliotou, C., et al. 2000, *ApJ*, 532, L121
- Grebenev, S. A. 2010, in *PoS(extremesky2009) 060*, *The Extreme sky: Sampling the Universe above 10 keV*
- Grimm, H., Gilfanov, M., & Sunyaev, R. 2003, *Chinese Journal of Astronomy and Astrophysics Supplement*, 3, 257
- Güdel, M. 2004, *Astronomy and Astrophysics Review*, 12, 71, 10.1007/s00159-004-0023-2
- Harding, A. K. & Lai, D. 2006, *Reports on Progress in Physics*, 69, 2631
- Heindl, W., Coburn, W., Kreykenbohm, I., & Wilms, J. 2003, *The Astronomer's Telegram*, 200, 1
- Heindl, W. A. & Chakrabarty, D. 1999, in *Highlights in X-ray Astronomy*, ed. B. Aschenbach & M. J. Freyberg, 25
- Heindl, W. A., Coburn, W., Gruber, D. E., et al. 2001, *ApJ*, 563, L35
- Heindl, W. A., Rothschild, R. E., Coburn, W., et al. 2004, in *American Institute of Physics Conference Series*, Vol. 714, *X-ray Timing 2003: Rossi and Beyond*, ed. P. Kaaret, F. K. Lamb, & J. H. Swank, 323–330
- Herold, H. & Ruder, H. 1979, *Mitteilungen der Astronomischen Gesellschaft Hamburg*, 45, 25
- Hertzprung, E. 1911, *Publikationen des Astrophysikalischen Observatoriums zu Potsdam*, 63

- Hewish, A., Bell, S. J., Pilkington, J. D. H., Scott, P. F., & Collins, R. A. 1968, *Nature*, 217, 709
- Hewish, A. & Okoye, S. E. 1965, *Nature*, 207, 59
- Hilditch, R. W. 2001, *An Introduction to Close Binary Stars* (Cambridge University Press)
- Hillebrandt, W. & Niemeyer, J. C. 2000, *ARA&A*, 38, 191
- Ho, C. 1989, *MNRAS*, 236, 299
- Hoshino, M. & Takeshima, T. 1993, *ApJ*, 411, L79
- Hurley, K., Boggs, S. E., Smith, D. M., et al. 2005, *Nature*, 434, 1098
- Ikhsanov, N. R. 2007, *MNRAS*, 375, 698
- Illarionov, A. F. & Kompaneets, D. A. 1990, *MNRAS*, 247, 219
- Illarionov, A. F. & Sunyaev, R. A. 1975, *A&A*, 39, 185
- İnam, S. Ç. & Baykal, A. 2000, *A&A*, 353, 617
- Inoue, H., Ogawara, Y., Waki, I., et al. 1984, *PASJ*, 36, 709
- Isenberg, M., Lamb, D. Q., & Wang, J. C. L. 1998, *ApJ*, 505, 688
- Ives, J. C., Sanford, P. W., & Burnell, S. J. B. 1975, *Nature*, 254, 578
- Jahoda, K., Swank, J. H., Giles, A. B., et al. 1996, in *SPIE Conference proceedings*, Vol. 2808, 59–70
- Janot-Pacheco, E., Ilovaisky, S. A., & Chevalier, C. 1981, *A&A*, 99, 274
- Kaper, L., Lamers, H. J. G. L. M., Ruymaekers, E., van den Heuvel, E. P. J., & Zuidervijk, E. J. 1995, *A&A*, 300, 446
- Kaper, L., van der Meer, A., & Najarro, F. 2006, *A&A*, 457, 595
- Karino, S. 2007, *PASJ*, 59, 961
- Kendziorra, E., Mony, B., Kretschmar, P., et al. 1992, in *NASA Conference Publication*, Vol. 3137, *NASA Conference Publication*, ed. C. R. Shrader, N. Gehrels, & B. Dennis, 217
- Klochkov, D., Santangelo, A., Staubert, R., & Ferrigno, C. 2008, *A&A*, 491, 833
- Klochkov, D., Staubert, R., Postnov, K., Shakura, N., & Santangelo, A. 2009, *A&A*, 506, 1261
- Koh, D. T., Bildsten, L., Chakrabarty, D., et al. 1997, *ApJ*, 479, 933
- Kouveliotou, C., Dieters, S., Strohmayer, T., et al. 1998, *Nature*, 393, 235
- Koyama, K., Tsunemi, H., Dotani, T., et al. 2007, *PASJ*, 59, 23
- Kraus, U., Nollert, H.-P., Ruder, H., & Riffert, H. 1995, *ApJ*, 450, 763
- Kraus, U., Zahn, C., Weth, C., & Ruder, H. 2003, *ApJ*, 590, 424
- Kretschmar, P. 2004, PhD dissertation, Eberhard-Karls-Universität Tübingen
- Kreykenbohm, I. 2004, PhD dissertation, Eberhard-Karls-Universität Tübingen
- Kreykenbohm, I., Kretschmar, P., Wilms, J., et al. 1999, *A&A*, 341, 141
- Kreykenbohm, I., Wilms, J., Coburn, W., et al. 2004, *A&A*, 427, 975
- Kreykenbohm, I., Wilms, J., Kretschmar, P., et al. 2008a, *A&A*, 492, 511
- Kreykenbohm, I., Wilms, J., Kretschmar, P., et al. 2008b, *A&A*, 492, 511
- La Barbera, A., Burderi, L., Di Salvo, T., Iaria, R., & Robba, N. R. 2001, *ApJ*, 553, 375
- La Barbera, A., Santangelo, A., Orlandini, M., & Segreto, A. 2003, *A&A*, 400, 993
- La Barbera, A., Segreto, A., Santangelo, A., Kreykenbohm, I., & Orlandini, M. 2005, *A&A*, 438, 617
- Lapshov, I. Y., Syunyaev, R. A., Chichkov, M. A., et al. 1992, *Soviet Astronomy Letters*, 18

- Larsson, S. 1996, *A&AS*, 117, 197
- Latal, H. G. 1986, *ApJ*, 309, 372
- Lattimer, J. M. & Prakash, M. 2007, *Phys. Rep.*, 442, 109
- Layton, J. T., Blondin, J. M., Owen, M. P., & Stevens, I. R. 1998, *New Astronomy*, 3, 111
- Leahy, D. A. & Kostka, M. 2008, *MNRAS*, 384, 747
- Levine, A. M., Bradt, H., Cui, W., et al. 1996, *ApJ*, 469, L33
- Lewin, W. H. G., van Paradijs, J., & van den Heuvel, E. P. J. 1995, *Cambridge Astrophysics Series*, 26
- Lewin, W. H. G., van Paradijs, J., & van den Heuvel, E. P. J. 1997, *X-ray Binaries* (Cambridge University Press)
- Leyder, J., Walter, R., & Lubinski, P. 2009, *ATEL*, 1949, 1
- Lipunov, V. M. 1982, *AZh*, 59, 888
- Lipunov, V. M. 1987, *The astrophysics of neutron stars* (*Astronomische Nachrichten Supplement*)
- Liu, Q. Z., van Paradijs, J., & van den Heuvel, E. P. J. 2006, *A&A*, 455, 1165
- Liu, Q. Z., van Paradijs, J., & van den Heuvel, E. P. J. 2007, *A&A*, 469, 807
- Lovelace, R. V. E., Romanova, M. M., & Bisnovatyi-Kogan, G. S. 1995, *MNRAS*, 275, 244
- Lovelace, R. V. E., Romanova, M. M., & Bisnovatyi-Kogan, G. S. 1999, *ApJ*, 514, 368
- Lund, N., Budtz-Jørgensen, C., Westergaard, N. J., et al. 2003, *A&A*, 411, L231
- Lutovinov, A. A. & Tsygankov, S. S. 2009, *Astronomy Letters*, 35, 433
- Lyubarskii, Y. E. 1997, *MNRAS*, 292, 679
- Lyubarsky, Y. E. 1986, *Astrophysics*, 25, 577
- Lyubarsky, Y. E. & Sunyaev, R. A. 1988, *Pis'ma Astron. Zh.*, 14, 920
- MacQueen, J. 1967, Some methods for classification and analysis of multivariate observations., *Proc. 5th Berkeley Symp. Math. Stat. Probab.*, Univ. Calif. 1965/66, 1, 281-297 (1967).
- Makishima, K. & Mihara, T. 1992, in *Frontiers Science Series*, ed. Y. Tanaka & K. Koyama, 23
- Makishima, K., Mihara, T., Ishida, M., et al. 1990, *ApJ*, 365, L59
- Makishima, K., Mihara, T., Nagase, F., & Tanaka, Y. 1999, *ApJ*, 525, 978
- Manchester, R. N., Hobbs, G. B., Teoh, A., & Hobbs, M. 2005, *AJ*, 129, 1993
- Mangano, V. 2009, *ATEL*, 1896, 1
- Mangano, V., Baumgartner, W. H., Gehrels, N., et al. 2009, *GCN*, 8777, 1
- Maraschi, L., Huckle, H. E., Ives, J. C., & Sanford, P. W. 1976, *Nature*, 263, 34
- Markwardt, C. B., Swank, J. H., & Corbet, R. 2007, *The Astronomer's Telegram*, 1176
- Mazets, E. P., Golentskii, S. V., Ilinskii, V. N., Aptekar, R. L., & Guryan, I. A. 1979, *Nature*, 282, 587
- McLaughlin, M. A., Stairs, I. H., Kaspi, V. M., et al. 2003, *The Astrophysical Journal Letters*, 591, L135
- Mereghetti, S. 2008, *A&A Rev.*, 15, 225
- Meszaros, P. & Nagel, W. 1985a, *ApJ*, 298, 147
- Meszaros, P. & Nagel, W. 1985b, *ApJ*, 299, 138
- Mihara, T. 1995, PhD thesis, Dept. of Physics, Univ. of Tokyo

- Mihara, T., Makishima, K., Kamijo, S., et al. 1991, *ApJ*, 379, L61
- Mihara, T., Makishima, K., Ohashi, T., Sakao, T., & Tashiro, M. 1990, *Nature*, 346, 250
- Mihara, T., Yamamoto, T., Sugizaki, M., & Yamaoka, K. 2010, *The Astronomer's Telegram*, 2796, 1
- Nagase, F. 1989, *PASJ*, 41, 1
- Nagase, F., Hayakawa, S., Kunieda, H., et al. 1982, *ApJ*, 263, 814
- Nagase, F., Hayakawa, S., Sato, N., Masai, K., & Inoue, H. 1986, *PASJ*, 38, 547
- Nagel, W. 1980, *ApJ*, 236, 904
- Negueruela, I. 2004, *ArXiv Astrophysics e-prints:0411758*
- Nishimura, O. 2008, *ApJ*, 672, 1127
- Oppenheimer, J. R. & Volkoff, G. M. 1939, *Physical Review*, 55, 374
- Orlandini, M. 2006, *Advances in Space Research*, 38, 2742
- Orlandini, M., dal Fiume, D., del Sordo, S., et al. 1999, *A&A*, 349, L9
- Orlandini, M., dal Fiume, D., Frontera, F., et al. 1998, in *The Active X-ray Sky: Results from BeppoSAX and RXTE*, ed. L. Scarsi, H. Bradt, P. Giommi, & F. Fiore, 158
- Orlandini, M., dal Fiume, D., Frontera, F., et al. 2000, *Advances in Space Research*, 25, 417
- Parkes, G. E., Culhane, J. L., Mason, K. O., & Murdin, P. G. 1980, *MNRAS*, 191, 547
- Pavlov, G. G., Shibano, I. A., & Zavlin, V. E. 1991, *MNRAS*, 253, 193
- Pravdo, S. H. & Ghosh, P. 2001, *ApJ*, 554, 383
- Pringle, J. E. 1981, *ARA&A*, 19, 137
- Protassov, R., van Dyk, D. A., Connors, A., Kashyap, V. L., & Siemiginowska, A. 2002, *ApJ*, 571, 545
- Quaintrell, H., Norton, A. J., Ash, T. D. C., et al. 2003, *A&A*, 401, 313
- Rappaport, S. 1975, *IAU Circ.*, 2869, 2
- Revnitsev, M., Churazov, E., Postnov, K., & Tsygankov, S. 2009, *A&A*, 507, 1211
- Rodes-Roca, J. J., Torrejón, J. M., Kreykenbohm, I., et al. 2009, *A&A*, 508, 395
- Rose, W. K. 1998, *Advanced Stellar Astrophysics* (Cambridge University Press)
- Rothschild, R. E., Blanco, P. R., Gruber, D. E., et al. 1998, *ApJ*, 496, 538
- Rothschild, R. E., Wilms, J., Tomsick, J., et al. 2006, *ApJ*, 641, 801
- Ruffert, M. 1997, *A&A*, 317, 793
- Ruffert, M., Arnett, D., & Shankar, A. 1992, in *BAAS*, Vol. 24, *BAAS*, 1258
- Runacres, M. C. & Owocki, S. P. 2005, *A&A*, 429, 323
- Rutledge, R. E., Bildsten, L., Brown, E. F., et al. 2007, *ApJ*, 658, 514
- Santangelo, A., del Sordo, S., Segreto, A., et al. 1998, *A&A*, 340, L55
- Santangelo, A., Segreto, A., Giarrusso, S., et al. 1999, *ApJ*, 523, L85
- Sato, N., Nagase, F., Kawai, N., et al. 1986, *ApJ*, 304, 241
- Schönherr, G., Wilms, J., Kretschmar, P., et al. 2007, *A&A*, 472, 353
- Schwarzschild, M. 1958, *Structure and evolution of the stars.* (Princeton University Press)
- Shakura, N. I. 1975, *Soviet Astronomy Letters*, 1, 223
- Shakura, N. I. & Syunyaev, R. A. 1973, *A&A*, 24, 337
- Shklovsky, I. S. 1967, *ApJ*, 148, L1
- Shrader, C. R., Sutaria, F. K., Singh, K. P., & Macomb, D. J. 1999, *ApJ*, 512, 920
- Staubert, R., Klochkov, D., & Wilms, J. 2009, *A&A*, 500, 883

- Staubert, R., Kreykenbohm, I., Kretschmar, P., et al. 2004, in *ESA Special Publication*, Vol. 552, 5th INTEGRAL Workshop on the INTEGRAL Universe, ed. V. Schoenfelder, G. Lichti, & C. Winkler, 259
- Staubert, R., Pottschmidt, K., Doroshenko, V., et al. 2011, *A&A*, 527, A7
- Strohmayer, T. E. 1999, *ArXiv Astrophysics e-prints*
- Strüder, L., Briel, U., Dennerl, K., et al. 2001, *A&A*, 365, L18
- Suchy, S., Pottschmidt, K., Rothschild, R. E., et al. 2011, *ApJ*, 733, 15
- Sunyaev, R. A. & Titarchuk, L. G. 1980, *A&A*, 86, 121
- Takahashi, T., Abe, K., Endo, M., et al. 2007, *PASJ*, 59, 35
- Titarchuk, L. & Lyubarskij, Y. 1995, *ApJ*, 450, 876
- Titarchuk, L., Mastichiadis, A., & Kylafis, N. D. 1996, *A&AS*, 120, C171
- Tokovinin, A. A. 1997, *A&AS*, 124, 75
- Truemper, J., Pietsch, W., Reppin, C., et al. 1978, *ApJ*, 219, L105
- Trümper, J., Pietsch, W., Reppin, C., & Sacco, B. 1977, in *New York Academy Sciences Annals*, Vol. 302, Eighth Texas Symposium on Relativistic Astrophysics, ed. M. D. Papa-
giannis, 538
- Trümper, J. E., Zezas, A., Ertan, Ü., & Kylafis, N. D. 2010, *A&A*, 518, A46
- Ubertini, P., Lebrun, F., Di Cocco, G., et al. 2003, *A&A*, 411, L131
- ud-Doula, A. & Owocki, S. P. 2002, *ApJ*, 576, 413
- van den Heuvel, E. P. J. & Habets, G. M. H. J. 1984, *Nature*, 309, 598
- van Kerkwijk, M. H., van Paradijs, J., Zuiderwijk, E. J., et al. 1995, *A&A*, 303, 483
- Voges, W., Pietsch, W., Reppin, C., et al. 1982, *ApJ*, 263, 803
- Walter, R. & Zurita Heras, J. 2007, *A&A*, 476, 335
- Wang, Y. & Frank, J. 1981, *A&A*, 93, 255
- Wang, Y.-M. 1995, *ApJ*, 449, L153
- Warner, B. 2003, *Cataclysmic Variable Stars* (Cambridge University Press)
- Watanabe, S., Sako, M., Ishida, M., et al. 2003, *ApJ*, 597, L37
- Watanabe, S., Sako, M., Ishida, M., et al. 2006, *ApJ*, 651, 421
- Weisskopf, M. C., Brinkman, B., Canizares, C., et al. 2002, *PASP*, 114, 1
- Wheaton, W. A., Doty, J. P., Primi, F. A., et al. 1979, *Nature*, 282, 240
- White, N. E., Mason, K. O., Huckle, H. E., Charles, P. A., & Sanford, P. W. 1976, *ApJ*, 209, L119
- White, N. E. & Swank, J. H. 1984, *ApJ*, 287, 856
- White, N. E., Swank, J. H., & Holt, S. S. 1983, *ApJ*, 270, 711
- Wilson, C. A., Finger, M. H., & Camero-Arranz, A. 2008, *ApJ*, 678, 1263
- Yahel, R. Z. 1979, *ApJ*, 229, L73

Acknowledgements

Many people have contributed to this work and I wish to thank them all for making this thesis possible and joyful to work on. First of all, I would like to thank Prof. Dr. Andrea Santangelo for inviting me to Tübingen and wise supervision during all these years. I wish to thank also Dr. Ingo Kreykenbohm, my co-supervisor who was always open to my inquires. I am also very grateful to Prof. Dr. Konstantin Postnov, my diploma thesis supervisor, who convinced me to stay in science despite all obstacles, and was always open for discussions during my stay in Tübingen.

This thesis is based on several published papers and would not be possible without the contribution of my co-authors: Prof. Dr. Andrea Santangelo, Dr. Ingo Kreykenbohm, Dr. Dmitry Klochkov, Prof. Dr. Rüdiger Staubert, Dr. Carlo Ferrigno, Slawo Suchy, Dr. Richard E. Rothschild, Dr. Katja Pottschmidt, Prof. Dr. Jörn Wilms, and, especially, Dr. Valery Suleimanov who was always open for discussions and always supported me. Particularly his contribution to Chapter 8 can not be overestimated. I wish to sincerely thank Benjamin Mück for help with translation of the abstract into German, and Dr. Patrick Kavanagh for his help with proofreading of the thesis. Once again, I wish to thank Prof. Dr. Konstantin Postnov and Prof. Dr. Nikolai Shakura for very useful discussions regarding the torques affecting neutron stars in accreting pulsars.

I wish also to thank the members of the institute for the friendly and open working environment at IAAT. I can not forget to express my gratitude to Dr. Eckhard Kendziorra for all his help and his attitude to all IAAT newcomers. I also wish to thank my office-mate Davide Vasco for sharing the ups and downs of PhD work and many scientific discussions we shared during it.

Finally I wish to thank my parents, my small daughter Olesya and my wife Alya have always supported and believed in me. I wish also to thank Alya for patience throughout all these years and for the scientific contribution from her side. Without her help I would not have been able to do this thesis at all.

Curriculum vitae

- 25.05.1983 born in Stavropol, Russia
 09.1989 – 07.2000 School, Stavropol
 09.2001 – 02.2007 Moscow State University
 major: Astrophysics, M.S. equivalent.
 Diploma-Thesis “Observation of accreting pulsars with *INTEGRAL*”
 under supervision of Prof. Dr. K. Postnov at Sternberg
 Astronomical Institute (MSU SAI)
 02.2007 – 06.2007 SAP/MM Consultant at Hewlett-Packard Russia,
 Moscow.
 08.2007 – Scientific employee at the IAAT
 08.2007 – Preparation of this thesis entitled “Magnetic fields
 of accreting pulsars” under the supervision of
 Prof. Dr. A. Santangelo at the IAAT

Lebenslauf

- 25.05.1983 geboren in Stavropol, Russia
 09.1989 – 07.2000 Schule, Stavropol
 09.2001 – 02.2007 Moscow State University
 Studiengang: Diplom Physik
 Diplomarbeit “Observation of accreting pulsars with *INTEGRAL*”
 unter Anleitung von Prof. Dr. K. Postnov, Sternberg
 Astronomical Institute (MSU SAI)
 02.2007 – 06.2007 SAP/MM Consultant am Hewlett-Packard Russland,
 Moskau.
 08.2007 – Wissenschaftlicher Angestellter am IAAT
 08.2007 – Anfertigung der Dissertation “Magnetic fields of ac-
 creting pulsars” unter Anleitung von Prof. Dr. A. San-
 tangelo am IAAT

List of publications:

Doroshenko, V.; Doroshenko, R.; Postnov, K. A.: “*INTEGRAL Observations of X-Ray Pulsars X 1845-024 and XTE J1858+034*” 2007, Proc. of the 6th INTEGRAL workshop.

Doroshenko, V.; Doroshenko, R.; Postnov, K. A.; Cherepashchuk, A. M.; Tsygankov, S.: “*A study of the X-ray pulsars X1845-024 and XTE J1858+034 based on INTEGRAL observations.*” 2008, Astronomy Reports, 52, 138-151

Doroshenko, V.; Staubert, R.; Kreykenbom, I.; Santangelo, A.; Ferrigno, C.: “*GX 301-2 with INTEGRAL.*” 2008, Proc. of the 7th INTEGRAL Workshop

Doroshenko, V.; Santangelo, A.; Suleimanov, V.; Staubert, R.; Kreykenbohm, I.; Ferrigno, C.; Klochkov, D.: “*Highly magnetized neutron star in GX 301-2.*” 2010, AIP Conference Series, 1248, 155-156

Doroshenko, V.; Santangelo, A.; Suleimanov, V.; Kreykenbohm, I.; Staubert, R.; Ferrigno, C.; Klochkov, D.: “*Is there a highly magnetized neutron star in GX 301-2?*” 2010, A&A, 515

Doroshenko, V.; Suchy, S.; Santangelo, A.; Staubert, R.; Kreykenbohm, I.; Rothschild, R.; Pottschmidt, K.; Wilms, J.: “*RXTE observations of the 1A 1118-61 in an outburst, and the discovery of a cyclotron line*” 2010, A&A, 515

Staubert, R. and Pottschmidt, K. and Doroshenko, V. and Wilms, J. and Suchy, S. and Rothschild, R. and Santangelo, A.: “*Finding a 24-day orbital period for the X-ray binary 1A 1118-616*” 2010, A&A, 527

Doroshenko, V.; Suleimanov V.; Santangelo, A.: “*Witnessing the magnetospheric boundary at work in Vela X-1.*” 2011, A&A, 529

Suchy, S.; Pottschmidt, K.; Rothschild, R.E.; Wilms, J; Fürst, F; Barragan, L.; Caballero, I.; Grinberg, V.; Kreykenbohm, I.; Doroshenko, V.; Santangelo, A.; Staubert, R. : “*Suzaku observations of the HMXB 1A 1118-61.*” 2011, ApJ, 733

Doroshenko, V.; Suleimanov V.; Santangelo, A.: “*Vela X-1: another magnetar hidden in a binary system?*” 2011, submitted to A&A

